UNIVERSITY OF CALIFORNIA
RIVERSIDE

Theory of Relaxor Ferroelectrics

A Dissertation submitted in partial satisfaction
of the requirements for the degree of

Doctor of Philosophy

in

Physics

by

Gian Giacomo Guzmán Verri

September 2012

Dissertation Committee:

Professor Chandra M. Varma, Chairperson
Professor Shan-Wen Tsai
Professor Roland Kawakami

The Dissertation of Gian Giacomo Guzmán Verri is approved:

Committee Chairperson

University of California, Riverside

Acknowledgments

I would like to express my deep and sincere gratitude to my supervisor, Professor Chandra Varma. He introduced me to the fascinating problem of relaxor ferroelectricity and his profound physics insight provided me with great guidance in the course of my PhD studies.

My sincere thanks are due to the committee members, Prof. Roland Kawakami and Prof. Shan-Wen Tsai, for the interesting points they raised during the preparation of this dissertation.

Throughout this work, I collaborated and had discussions with the group of Dr. Alexandra Navrotsky at UC Davis, the group of Dr. Albert Migliori at Los Alamos National Laboratory, and the group of Dr. Frances Hellman at UC Berkeley. I wish to extend my warmest thanks to them.

I also acknowledge useful discussions with professors, postdoctoral scholars, and fellow graduate students for whom I have great regard: Dr. Arcady Shekhter, Professor Vivek Aji, Dr. Yan He, Dr. Yafis Barlas, Dr. Shomeek Mukhopadhyay and Jarred Wong.

I am indebted to my wife, Silvia Masís Sanabria, who has made enormous sacrifices so I could pursue doctoral studies. I am grateful to my mother, Anita Verri Arbizzani, my sisters, Caterina Guzmán Verri, Loredana Guzmán Verri, and Valeria Guzmán Verri, and parents-in-law, María Sanabria Fernández and Carlos Masís Acosta. Their love and support have always been very well received.

This work partially funded by the UC Lab Fees Research Program 09-LR-01-118286-HELF and the Dean's Distinguished Fellowship Award from UC Riverside.

To Silvia

ABSTRACT OF THE DISSERTATION

Theory of Relaxor Ferroelectrics

by

Gian Giacomo Guzmán Verri

Doctor of Philosophy, Graduate Program in Physics
University of California, Riverside, September 2012
Professor Chandra M. Varma, Chairperson

Relaxor ferroelectric crystals are characterized by a broad region of critical fluctuations of polarization: the observed dielectric constants and elastic diffuse scattering extend over a wide region of temperatures and have unusual line shapes. Despite more than 50 years since the synthesis of the first relaxors, a satisfactory theory of relaxor ferroelectricity that accounts for this broad region of fluctuations remains elusive, partly because of the various energy scales: the deviation from Curie-Weiss law, the onset of the elastic diffuse scattering and the maximum in the dielectric susceptibility. We present a theory of the fluctuations of relaxors with a model of polarizable unit cells with dipolar forces, local anharmonic forces, and local random fields. The usual Lorentz field approximation to the local dipolar field fails to account for the critical fluctuations of polarization at any temperature since it violates the fluctuation-dissipation theorem of statistical mechanics. Thus, thermodynamic functions and temperature dependencies of the phonon frequencies are computed self-consistently using the Onsager field, which is the simplest necessary correction to the Lorentz field that guarantees the fluctuation-dissipation theorem. Compositional disorder is treated by a self-consistent method that relates the local polarization to the local ran-

dom fields and to the susceptibility averaged over compositional disorder. Local anharmonic forces are treated within a quasi-harmonic approximation. We find that (i) arbitrarily small compositional disorder together with dipolar forces extend the region of critical fluctuations down to absolute zero temperature; (ii) the correlation functions of polarization are highly anisotropic and slowly varying with a power law component. We compare our results to the observed elastic diffuse scattering and dynamic dielectric constant.

Contents

List of Figures

List of Tables

Chapter 1

Introduction

Relaxor ferroelectrics are interesting because they exhibit new physics. Typical relaxors show a broad region of fluctuations with several temperature scales and unusual line shapes, as illustrated in Fig. 1.1. For high temperatures, the behavior of the relaxors is similar to that of conventional ferroelectrics, i.e., their dielectric constants follow the Curie-Weiss law with large Curie-Weiss constants. As temperature decreases, the behavior of the relaxors differs from that of conventional ferroelectrics: their dielectric constants deviate from the Curie-Weiss law and reach a broad maximum at a temperature $T_{\max}$ without any signature of a global broken symmetry. At low temperatures, no phase changes are observed unless large electric fields are applied. [1] The broadening of the dielectric response in the relaxors is known as diffuse phase transition and the temperature at which relaxors deviate from Curie-Weiss behavior is known as the Burns temperature T_B.

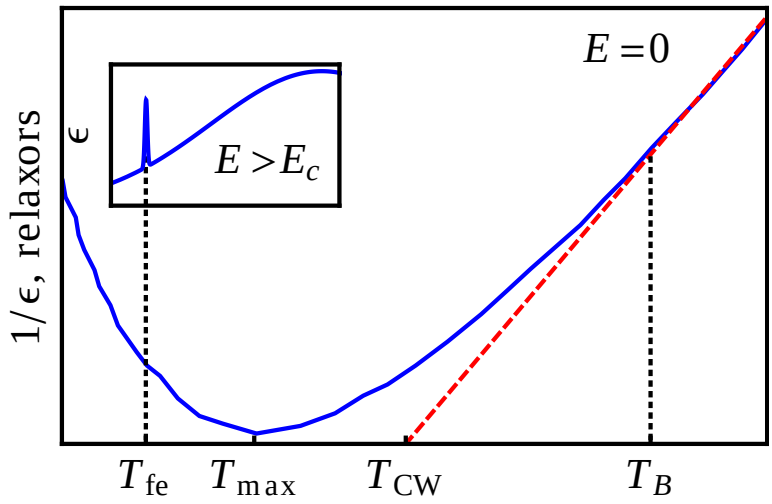

Figure 1.1: Schematic of the inverse dielectric constant ϵ of a typical relaxor ferroelectric in the absence of large static electric fields. Inset: schematic of the dielectric constant of the relaxors around the ferroelectric transition in the presence of large static electric fields.

Relaxors are technologically important materials. They are widely used in capacitors since their dielectric constants are large ($10^3 - 10^4$) over a broad temperature range of operation (few hundred Kelvin degrees). [2] Solid solutions of relaxors with conventional ferroelectrics, e.g., $PbMn_{1/3}Nb_{2/3}O_3$-$PbTiO_3$, or $PbZn_{1/3}Nb_{2/3}O_3$-$PbTiO_3$, exhibit large piezo-electric coefficients (2500 pC/N), which makes them a material of choice in the industry of electromechanical transducers. [3]

Compositional disorder is strong in the relaxors and it is essential for their unusual behavior. Typical relaxors belong to the complex perovskite family with chemical formula ABO_3 where the B-site is disordered. For example, consider the prototypical relaxor ferroelectric lead magnesium niobate, $PbMg_{1/3}Nb_{2/3}O_3$ (PMN). In PMN, Mg^{+2}, Nb^{+4} are randomly distributed on the B-site in a 1:2 ratio to preserve charge neutrality. The difference in the ionic radii and electronic valencies of Mg^{+2} and Nb^{+4} are sources of random fields and random bonds. In the absence of compositional disorder, no diffuse phase transition is

observed and relaxors behave like conventional ferroelectrics. [4]

Despite the first relaxors were synthesized more than 50 years ago [5, 6], understanding of their broad region of fluctuations together with its several special temperatures has proved difficult. A major challenge has been the characterization of the relaxor state and the identification of its transition temperature to any of the special temperatures ($T_B, T_{CW}, T_{\max}$, and T_{fe}). [7] For instance, a model by Westphal et al. [8] associated the relaxor state to that of a random field state and the transition temperature was assigned to the ferroelectric transition temperature T_{fe} under the presence of large static fields. Another model by Pirc and Blinc associated the relaxor state to that of a random-field-random-bond state but did not assign the transition point to any special temperature. [9, 10]

Only recently neutron scattering experiments have identified the onset temperature of critical fluctuations in the relaxors. [11, 12] Neutron scattering experiments observe the onset of elastic diffuse scattering at a temperature close to T_{CW}. The temperature dependence and wave-vector distribution of these fluctuations differ from those of conventional ferroelectrics and are suggestive of a transition to a random field state similar to that observed in magnets with quenched random fields. [13, 14, 15, 16]

The purpose of this work is to present a theory for relaxor ferroelectric crystals that accounts for the broad region of fluctuations. We consider a model of polarizable unit cells with local anharmonic forces, dipolar forces, and quenched random fields. Thermodynamic functions and the temperature dependence of the phonon frequencies are computed within the Onsager field approximation to the local dipolar field. The choice of the Onsager field over the Lorentz (mean) field is essential: it guarantees the fluctuation-dissipation theorem at all temperatures. Compositional disorder is treated by a self-consistent method that

relates the local polarization to the local quenched random fields and to the susceptibility averaged over disorder. To handle the local anharmonic forces, we adhere to a quasi-harmonic approximation: we linearize the equations of motion to reduce the problem to that of a harmonic oscillator with a renormalized phonon frequency. The phonon frequencies are then determined self-consistently.

The organization of this work is the following: in Chapter 1 we review basic definitions and concepts in ferroelectricity and compare conventional ferroelectrics to relaxor ferroelectrics. In Chapter 2 we review the standard model of conventional ferroelectrics We describe the Lorentz and Onsager field approximations in the context of this model. We study the thermodynamics of this model and describe the onset of the ferroelectric transition in terms of lattice dynamics. In Chapter 3 we present our model for relaxor ferroelectricity together with our results, discussion and comparison to experiments. In Chapter 4 we summarize our work, present the main conclusions, and discuss some of the assumptions in our model.

1.1 Ferroelectricity

Ferroelectricity is the appearance of a spontaneous reversible polarization. [17] The appearance of a spontaneous reversible polarization is manifested by well defined hysteresis loops and polar domain structures below a critical point. Fig. 1.2 shows an schematic view of a hysteresis loop for a typical ferroelectric where P is the polarization and E is the macroscopic field. At the origin of the PE diagram, Fig. 1.2, there are equal number of domain walls pointing up and down so the net polarization is zero. By applying a small positive field E, the polarization grows linearly with E: the field is not large enough to

switch the polarization of any domain. By increasing the strength of the field, some of domains switch over in the direction of the applied field increasing the polarization (AB). Upon further increasing E, the polarization saturates: all domains are aligned with the field. By decreasing the field strength, P does not follow the previous path (OABC). Instead, the polarization decreases by following the CBD path and there is a remnant polarization at $E = 0$: some of the polar domains remain with a polarization aligned in the direction of the field. Extrapolation of the linear path BC to the vertical axis (dashed line BE) gives the spontaneous polarization P_s The polarization of the crystal is set back to zero by applying a field in the opposite direction (DF path). The coercive field is the field required to set the polarization back to zero. By increasing the field strength in the opposite direction, the polarization of the domains aligns with the field. The loop is completed by reversing the field (GHC). Typical values of the spontaneous polarization are given in Table 1.1.

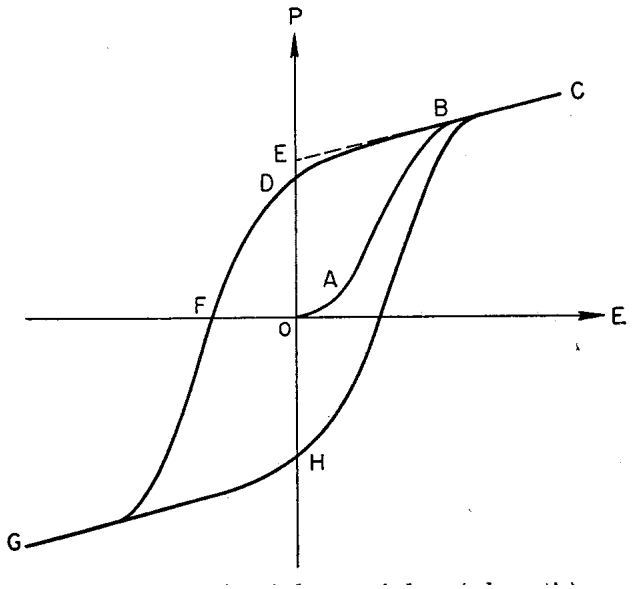

Figure 1.2: Hysteresis loop of ferroelectrics. Figure taken from Ref. [17].

Conventional ferroelectric crystals are broadly classified in two groups depending

Table 1.1: Spontaneous polarization P_s, Curie-Weiss constant C_{CW}, and critical temperature T_c for various ferroelectrics. Data taken from Ref. [17]

Name	Formula	P_s $[10^{-6}\mathrm{C/cm^2}]$	C_{CW} [K]	T_c [K]
Potassium di-hydrogen phosphate	KH_2PO_4 (KDP)	4.75 (96 K)	3.3×10^3	123
Sodium potassium tartrate tetrahydrate (Rochelle Salt)	$NaKC_4H_4O_64H_2O$	0.25 (278 K)	2.2×10^3	297
Lead titanate	$PbTiO_3$ (PTO)	> 50 (296 K)	5.0×10^5	763
Barium titanate	$BaTiO_3$ (BTO)	26 (296 K)	1.5×10^5	393

on the values of their Curie-Weiss constant, C_{CW} (see Table 1.1). The first group shows Curie-Weiss constants of the order of 10^3 K and includes hydrogen-bonded crystals such as KH_2PO_4 (KDP) and Rochelle salt together with related compounds. This group is called order-disorder ferroelectrics. This order of magnitude of C_{CW} is expected from models with permanent dipoles that have two equilibrium positions corresponding to opposite orientations or from an ion moving in a double-well local potential (see Figure 1.3). The dielectric constant from systems with permanent dipoles or ions in a double-well potential is given as follows, [17]

$$\epsilon = \frac{C_{CW}}{T - T_c}, \quad C_{CW} = \frac{4\pi}{4\pi/3} T_c, \quad \text{(order-disorder ferroelectrics)} \tag{1.1}$$

where T_c is the critical temperature. The factor of $4\pi/3$ comes from the expression of the Lorentz local field $\boldsymbol{E} + (4\pi/3)\boldsymbol{P}$ where $\boldsymbol{E}$ is the macroscopic field and $\boldsymbol{P}$ is the polarization. Typical critical temperatures for order-disorder ferroelectrics are of the order of 100 K (see Table 1.1), thus, $C_{CW} = 3\,T_c \sim 10^3$ K.

The second group shows Curie-Weiss constants of the order of 10^5 K (see Table 1.1). and includes the perovskite oxides BTO and PTO. This group is called displacive ferroelectrics. This order of magnitude of C_{CW} is expected from models with induced dipoles, i.e., models with oscillating ions with instantaneous electric moment z^*u, where u is the displacement coordinate from the equilibrium lattice point and z^* is the effective charge. For

local potentials with a quadratic term and quartic anharmonicity, $(\kappa/2)u^2 + (\gamma/4)u^4$, (see Fig. 1.3 (b)) the dielectric constant is given as follows, [17]

$$\epsilon = \frac{C_{CW}}{T - T_c}, \quad C_{CW} = \frac{4\pi n z^{*2}}{3k_B}\,\frac{\kappa}{\gamma}, \quad \text{(displacive ferroelectrics)} \tag{1.2}$$

where n is the number of dipoles per unit volume and k_B is the Boltzmann constant. According to this equation, C_{CW} is large if γ is small. For displacive ferroelectrics, the anharmonic coefficient γ is of the order of the coefficients of volumetric thermal expansion of ferroelectrics ($\sim 10^{-5}\,\mathrm{K}$). [18, 19] This explains the large Curie-Weiss constant of displacive ferroelectrics.

The order-disorder and displacive classification presented above represents limiting behavior. Experience shows that the local potentials in conventional ferroelectrics are neither double-deep wells (see Fig. 1.3 (a)) nor slightly anharmonic (see Fig. 1.3 (b)) but somewhere in-between. [20] The values of the Curie-Weiss constants manifest whether a ferroelectric is closer to the order-disorder or the displacive-type.

In the present work we make the assumption that relaxors are of the displacive type: the observed Curie-Weiss constants are large, e.g., $1.25 \times 10^5\,\mathrm{K}$ for PMN [21]. Additional evidence is provided by neutron diffraction experiments, which are discussed in Sec. 1.2.

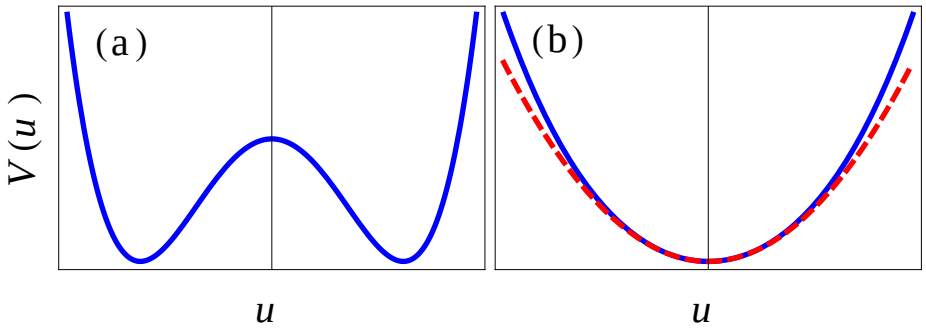

Figure 1.3: Schematic of the local potential function V plotted against the displacement coordinate u of the ion for an order-disorder (a) and a displacive (b) ferroelectric. The harmonic potential is shown for comparison (red, dashed line).

The current understanding of the onset of the ferroelectric transition in conventional ferroelectrics is from the works of Anderson [18] and Cochran [22, 23, 23]. Anderson and Cochran proposed that the of the onset of the ferroelectric transition is due to lattice instabilities. Crystal lattices are unstable against small deformations if one or more normal phonon mode frequencies are imaginary. [24]. Anderson and Cochran showed that in ionic systems such as conventional ferroelectrics there are two contributions to the harmonic phonon frequencies which are opposite in sign tend to cancel each other, i.e, tend to soften the mode. The positive contribution is from local forces: short-range repulsions between ions; and the negative contribution is from dipole forces: the displacements of the ions in the unit cell together with their charges generate induced dipoles which interact via dipole forces. For temperatures well above the critical point, the phonon mode is stabilized by local anharmonic forces. In addition, the crystal lattice has no permanent dipole moment since it has an inversion point. As the temperature approaches the critical point, the phonon mode becomes unstable inversion symmetry is lost. The new lattice structure has no inversion point and allows for a net polarization in the unit cell.

The soft mode concept explains the divergence of the dielectric constant in ferro-

electrics. The dielectric constant and the optic mode frequencies in ionic systems are related by the Lyddane-Sachs-Teller (LST) relation,

$$\frac{\epsilon_0(0)}{\epsilon_0(\infty)} = \frac{\Omega_{\mathrm{LO}}^2}{\Omega_{\mathrm{TO}}^2}. \tag{1.3}$$

Here, $\epsilon_0(0)$ is the static ($\omega = 0$) dielectric constant in the long-wavelength limit ($\boldsymbol{q}$=0); $\epsilon_0(\infty)$ is the dielectric constant at optical frequencies ($\sim \omega = \infty$) in the long-wavelength limit; and Ω_{TO}^2 and Ω_{TO} are the transverse and longitudinal optical mode frequencies. Eq. (1.3), shows that $\epsilon_0 \to \infty$ as $\Omega_{\mathrm{LO}}^2 \to 0$. In Chapter 2, the onset of the ferroelectric transition and its relation to the soft modes is discussed in more detail.

1.2 Unit cell of Relaxor Ferroelectrics with perovskite Structure

In this section, we describe the unit cell of a typical relaxor ferroelectric: PMN. The unit cell of PMN is well described by the cubic perovskite structure with chemical formula ABO_3. The A-site is at $(0, 0, 0)$, the B-site at $(0.5, 0.5, 0.5)$ and the oxygen at $(0.5, 0.5, 0)$ and symmetry related positions (see Fig. 1.4). [7, 25] The B-site is disordered since it is randomly occupied by Mg^{+2} or Nb^{+5} in a 1 : 2 ratio, respectively. The lattice constant a is of about 4.0 Å.

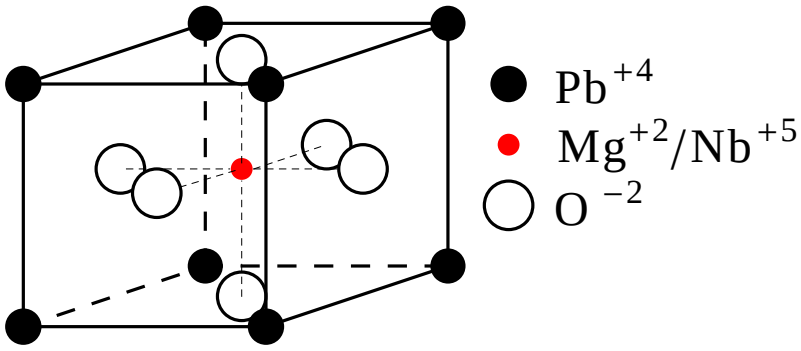

Figure 1.4: PMN unit cell

The precise location of the Pb^{+4} ions is temperature dependent. Fig. 1.5 shows the probability density function (PDF) of the of the Pb^{+4} ions determined from neutron diffraction experiments. For temperatures above the Burns temperature $T_B \simeq 620\,\mathrm{K}$, the PDF is a single peaked Gaussian, i.e, the Pb^{+4} ions are close to the A site of the perovskite unit cell. Upon cooling below T_B, the PDF shows a double peak centered at about 0.3 Å. at 293 K, i.e, the Pb^{+4} ions are uniformly distributed over a spherical layer of radius of about 0.3 Å. The fits to the neutron diffraction data do not improve if a displacement of Mg^{+2} or Nb^{+5} from the B-site is assumed. This suggests that the displacements of Mg^{+2} and Nb^{+5} are significantly smaller than those of Pb^{+4}. [7]. Similar results were obtained for the relaxor $PbMg_{1/3}Ta_{2/3}O_3$. [26]

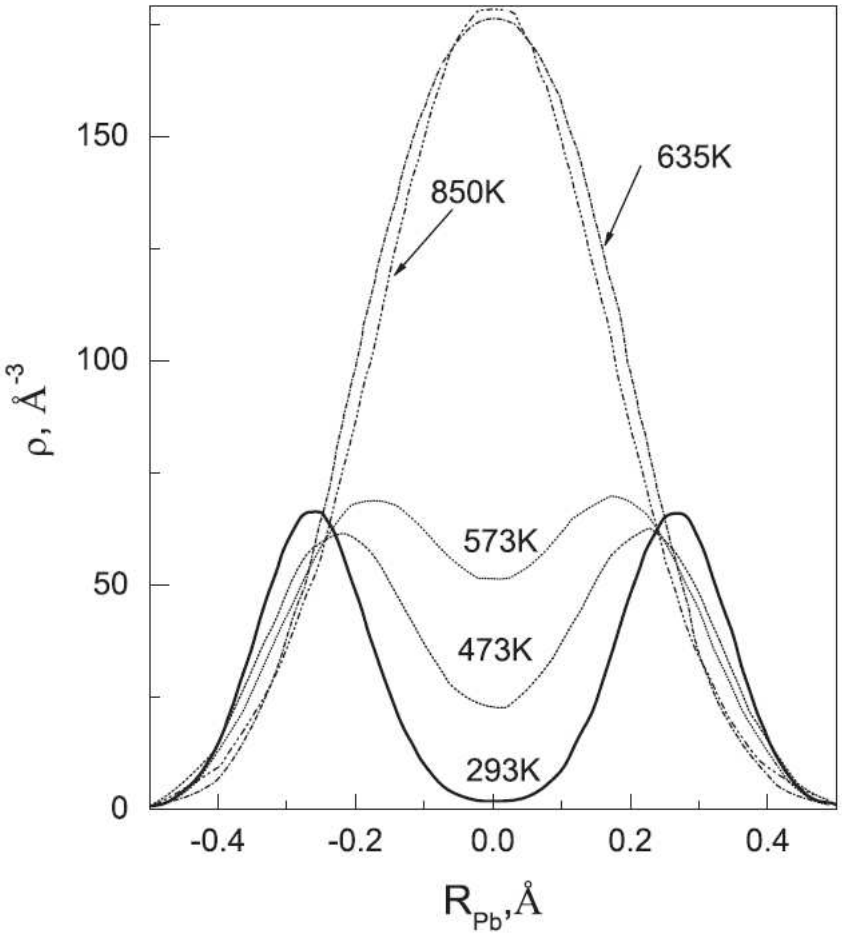

Figure 1.5: Probability density function of the Pb^{+4} ions in PMN. R_{Pb} is the displacement from the $(0, 0, 0)$ position. Reprinted with permission from S.B. Vakhrushev and N.M. Okuneva, AIP Conference Proceedings **626**, 117 (2002). [27] Copyright (2002) by the American Institute of Physics.

In the non-polar phase, the unit cell of displacive ferroelectrics such as PTO and BTO is well described by a perovskite cubic structure as that of Fig. 1.4 except the B-site is not disordered.

1.3 Review of Experimental Work: Comparison between Conventional and Relaxor Ferroelectrics

The purpose of this section is four-fold: (i) to contrast the physical properties of conventional and relaxor ferroelectrics; (ii) to provide evidence that compositional disorder in the relaxors extends the critical region of fluctuations down to low temperatures; (iii) to show that relaxor ferroelectrics exhibit several special temperatures; (iv) to introduce the concept of polar nanoregions. We focus our attention on measurements that probe the fluctuations of polarization throughout the diffuse phase transition of the relaxors: dielectric constant, diffuse scattering, and soft transverse optic phonon modes.

1.3.1 Dielectric Constant

Phase transitions are identified by divergences in the response functions $\chi_0(\omega)$. The temperature dependence of the response functions around the critical point T_c provides information about the behavior of the fluctuations of the system in the critical region. Here, we contrast the dielectric constant, $\epsilon_0(\omega) = 1 + 4\pi\chi_0(\omega)$ of conventional displacive ferroelectrics to that of the relaxors

We first consider the dielectric constant of conventional ferroelectrics. Fig. 1.6 (a) shows the dielectric constant ϵ_0 of a typical ferroelectric, PTO. For temperatures close to $T_c \simeq 770\,\mathrm{K}$, ϵ_0 follows the Curie-Weiss law (see black, solid line) with a large Curie-Weiss constant ($C_{CW} \simeq 5.0\times10^5\,\mathrm{K}$) and a Curie-Weiss constant $T_{CW} \simeq 715\,\mathrm{K}$. PTO is paraelectric well above 770 K, with a cubic lattice structure. For temperatures well below and close to the critical point 770 K, ϵ_0 follows the Curie-Weiss law (not shown in figure) with a slightly different Curie-Weiss constant and critical point $T_c^- \simeq 770\,\mathrm{K}$. PTO is ferroelectric well

below $T_c^+ \simeq 715\,\mathrm{K}$ with a tetragonal lattice structure. For temperatures slightly above and below 770 K, ϵ_0 is large and sharp. The width of the sharp peak is of a few tenths of Kelvin degrees. The phase transition is of first order, although rather weak since the region of coexistence between the paraelectric and ferroelectric phases is of a few tenths of Kelvin degrees. The dielectric constant of PTO and most conventional ferroelectrics varies little with frequency below the optical range ($\sim 10^{12}$ Hz). [4, 28]

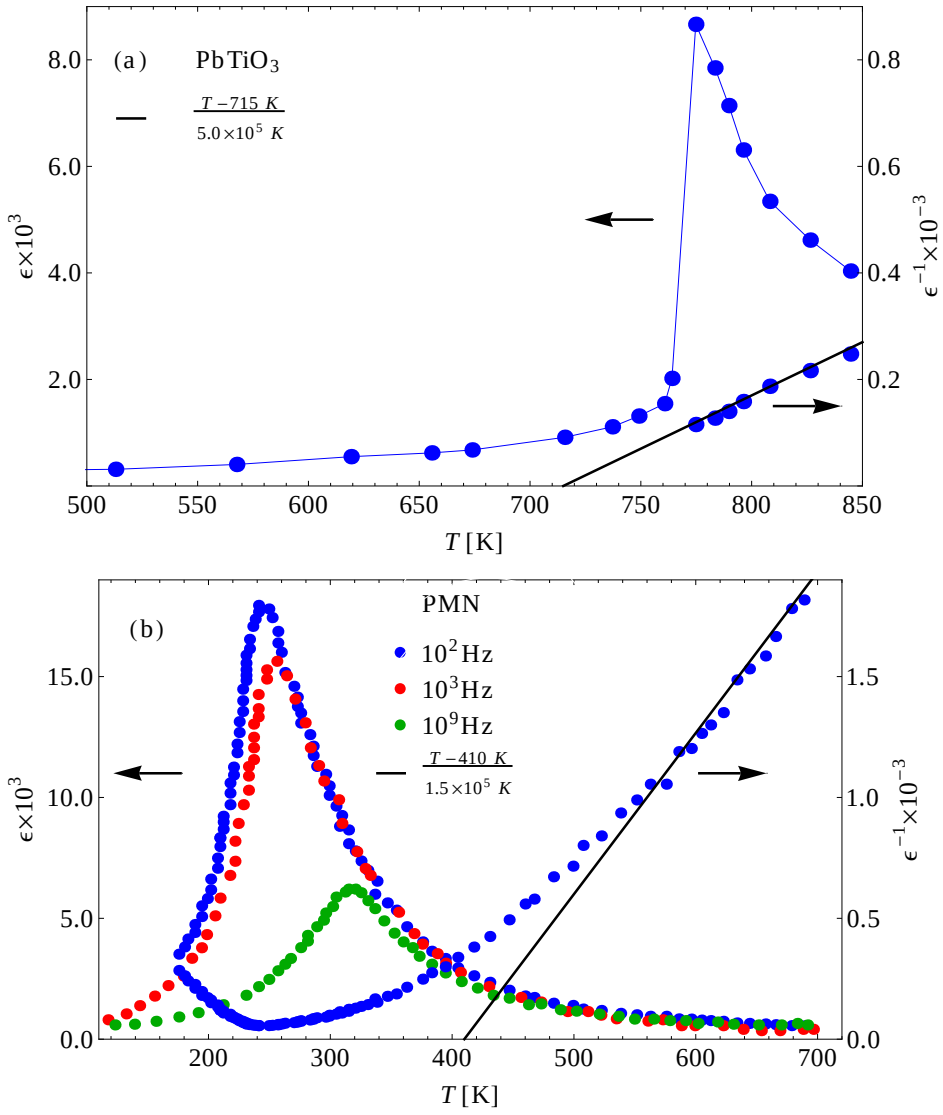

Figure 1.6: Dielectric constants for PTO (a) and PMN (b). Data taken from Refs. [29, 30].

In conventional ferroelectrics, the divergence of the dielectric constant occurs because of a lattice instability: the transverse optic mode $\Omega_{\rm TO}$ softens and the non-polar cubic lattice is unstable below T_c. The phase change is accompanied by the formation of macroscopic polar domains, as described in Sec. (1.1). The divergence of the response functions χ_0 indicates a change in the behavior of the correlation functions. For systems with isotropic short-ranged forces such as magnets, it is well known the correlation functions change from exponential to power-law behavior at T_c. [31] For systems with anisotropic long-ranged forces, the correlation functions change from a power-law to a distinct power-law behavior (see Sec. 2.4.2).

We now consider the dielectric constant of the relaxors. The behavior of the dielectric response in the relaxors differs depending on whether large static fields are applied: in the absence of large static fields there is no ferroelectric transition at any temperature; in the presence of large fields ($> 1.7\,{\rm kV/cm}$ for PMN), there is a first order ferroelectric transition. We first describe the dielectric constant without large static fields.

Fig. 1.6 (b) shows the dielectric constant ϵ of a typical relaxor ferroelectric, PMN, in the absence of large static fields ($> 1.7\,{\rm kV/cm}$) . For temperatures above the Burns temperature $T_B \simeq 620\,{\rm K}$, ϵ follows the Curie-Weiss law (see, black, solid line), with a large Curie-Weiss constant ($C_{CW} \simeq 1.5 \times 10^5\,{\rm K}$) and a Curie-Weiss temperature of $T_c \simeq 410\,{\rm K}$. For $T < T_B$, the ϵ deviates from the Curie-Weiss law behavior and grows as temperature decreases. ϵ reaches a maximum $\epsilon_{\rm max}$ at a temperature $T_{\rm max}$ and then decreases upon further cooling. $T_{\rm max} \simeq 240\,{\rm K}$ in the mHz range and $T_{\rm max} \simeq 380\,{\rm K}$ in the GHz range (not shown in figure). [7, 32] The peak in ϵ is very broad in temperature compared to that of PTO: it extends over a few hundred Kelvin degrees. ϵ is strongly dependent on the frequency of the

applied field: $\epsilon_{\max}$ decreases and shifts towards higher temperatures as frequency increases. The lattice structure remains cubic at all temperatures with no long-range ferroelectric order.

The behavior of the relaxor dielectric constant is fairly well described by a Debye formula with a broad distribution of relaxation times, [32]

$$\epsilon_0(\omega) = \epsilon_0(\infty) + \frac{\epsilon_0(0) - \epsilon_0(\infty)}{1 + i\omega\tau}. \tag{1.4}$$

Here, $\epsilon_0(0)$ is the static ($\omega = 0$) dielectric constant in the long-wavelength limit; $\epsilon_0(\infty)$ is the dielectric constant at optical frequencies in the long-wavelength limit; and τ is the relaxation time.

The distribution of relaxation times is approximately described by the Vogel-Fulcher law,

$$\frac{1}{\tau} = \begin{cases} \omega_0 \exp\left[-\frac{E_a}{k_B(T-T_f)}\right], & T \geq T_f \\ \infty, & T \leq T_f. \end{cases} \tag{1.5}$$

Here, ω_0 is a characteristic hopping frequency, E_a is the activation energy; and T_f is a freezing temperature. For PMN, $\tau_0 \equiv (2\pi\omega_0)^{-1} \sim 10^{-11}\,\mathrm{s}$, $T_f \sim 225\,\mathrm{K}$, and $E_a/k_B \sim 750\,\mathrm{K}$. [33]. A distribution of relaxation times of the Arrhenius form ($T_f = 0$ in Eq. (1.5)) gives unphysical large hopping frequencies and activation energies. [7] The long relaxation times implied by (1.5) indicates that the thermally activated reorientations of dipoles responsible for polarization slow down with decreasing temperature and freeze at $T = T_f$. [34]

Similar temperature dependencies and relaxation times with Vogel-Fulcher distributions have been observed in spin glasses, i.e., magnetic systems with random exchange interactions that result in long-time spin correlations rather than long-spatial correlations. [35] This lead to the proposal that the observed deviations from the Curie-Weiss law in $\epsilon_0(\omega)$

are due to the formation of polar nanoregions (PNRs): domains of strong correlations of the size of a few nanometers. [21] It is believed that for temperatures well above the Burns temperature T_B, there are no PNRs and relaxors are similar to conventional ferroelectrics, i.e., follow the Curie-Weiss law with large Curie-Weiss constants ($\sim 10^5\,\mathrm{K}$) and a Curie-Weiss temperature T_{CW}. At about T_B PNRs nucleate with a random distribution of polarizations such the overall polarization of the crystal is zero and no long-range ferroelectric order is established. For temperatures below T_B but above T_{CW}, the PNRs are dynamic and weakly interacting. For temperatures below T_{CW}, their dynamics slow down and become strongly interacting. Upon passing through the temperature $T_{\max}$, the dielectric constant peaks but the PNRs do not form macroscopic polar domains and there is no ferroelectric phase transition, instead the PNRs form a glassy phase. [7]

Despite the behavior of the dielectric constant supports the picture described above, there are important objections. First, the description is only qualitative and it is incomplete, e.g., nothing is said about the mechanism by which PNRs form. Second, and most importantly, the observed fluctuations by neutron scattering strongly suggest a transition to a random-field state and not to a glassy state (see Sec. 1.3.2). A random-field state does not exclude PNRs: systems with isotropic short-range forces with quenched random fields lower their free energy with respect to the ordered state by breaking up into domain structures with short range correlations.

We now describe the dielectric constant of the relaxors in the presence of large static fields. A ferroelectric phase transition occurs at a temperature T_{fe} if a large static field is applied (> 1.7 kV/cm for PMN). [1] Fig. 1.7 shows the dielectric constant of PMN along the $[001], [011], [111]$ directions at $1.0\,\mathrm{kHz}$. The measurements were done in zero

field heating after cooling in field of about 10 kV/cm. The peak around 270 K ($\lesssim 0\,^{\circ}$C) is typical of the relaxors: it is broad in temperature and it shifts towards higher temperatures as the frequency the probing field increases (not shown in figure). [36] A narrow peak is observed around $T_{fe} \sim 200$ K ($\sim 73\,^{\circ}$C). T_{fe} is independent of the frequency of the probing field (not shown in figure). [36] The narrow peak corresponds to a ferroelectric phase transition, although very different from that of conventional ferroelectrics. Fig. 1.8, shows the temperature dependence of the polarization in PMN. [37] Below 210 K, the polarization slightly decreases with increasing temperature and then drops abruptly close to 210 K, as expected from a phase transition. However, a finite polarization persists for temperatures above T_f with well defined hysteresis loops (see Fig. 1.9) The lattice structure is most likely rhombohedral in the ferroelectric phase: for fields applied along the [111], [110], [100] directions, the polarization is largest along the [111] direction and the values of those along [110], [100] are close to its projection. (see Fig. 1.8). [1, 7, 37]

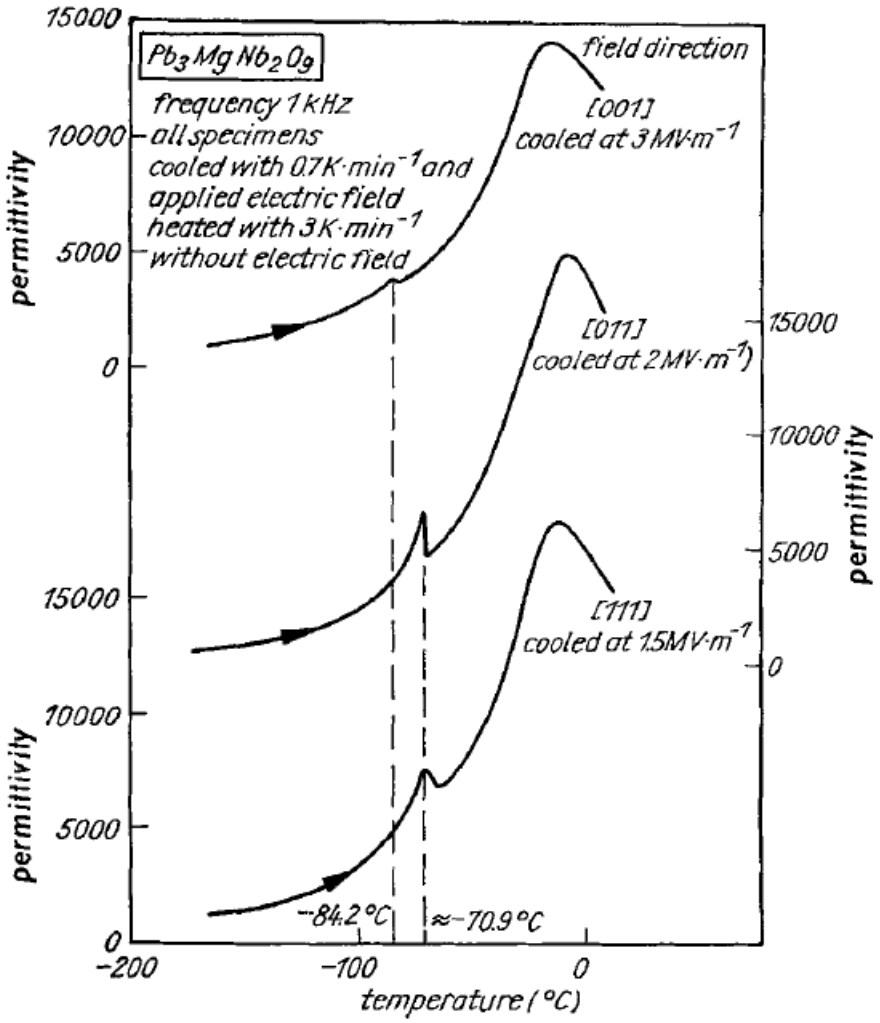

Figure 1.7: Dielectric constant of PMN along the [001], [011], [111] directions Measurements were done in a zero field heating after a cooling with the indicated fields. The peak around 270 K ($\lesssim 0\,^{\circ}$C) is typical of the relaxors. The narrow peak at about $T_{fe} \sim 200$ K ($\sim 73\,^{\circ}$C) indicates a ferroelectric phase transition. Reprinted with permission from G. Schmidt, H. Arndt, J. Voncieminski, T. Petzsche, H. Voigt, and N.N. Krainik, Krist. Tech. **15**, 1415 (1980). [1] Copyright (1980) by John Wiley and Sons.

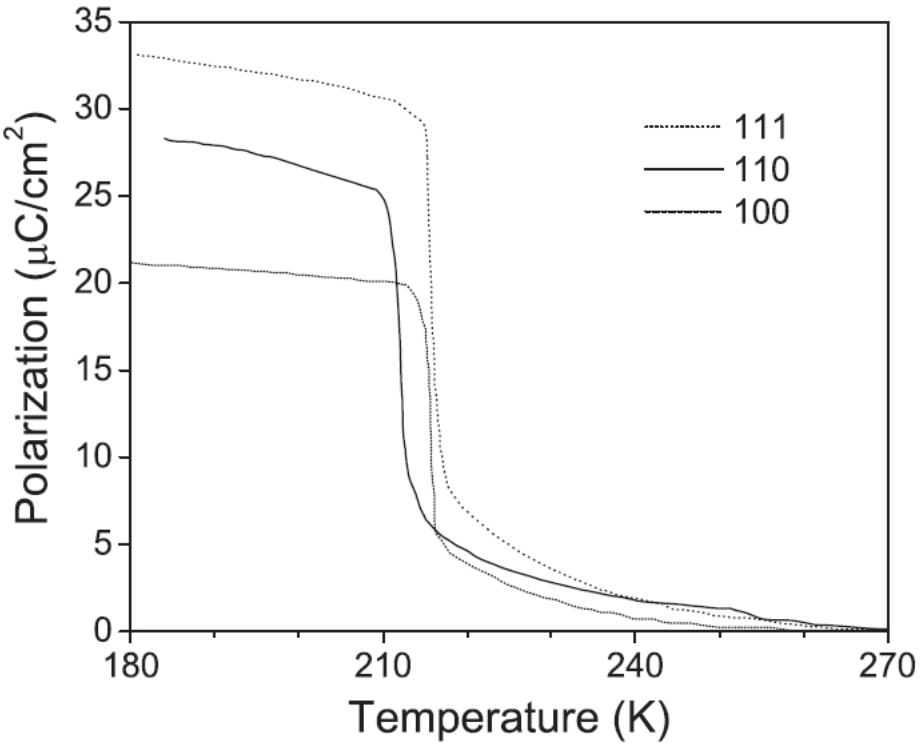

Figure 1.8: Temperature dependence of the polarization in PMN along different directions. Measurements were done in zero field heating after a 10 kV/cm cooling. Note a finite polarization persists above the temperature $T_{fe} \sim 200$ K where the dielectric constant peaks. Reprinted with permission from X. Zhao, W. Qu, X. Tan, A. A. Bokov, and Z.G. Ye, Phys. Rev. B **75**, 104106 (2007). . [37] Copyright (2007) by the American Physical Society.

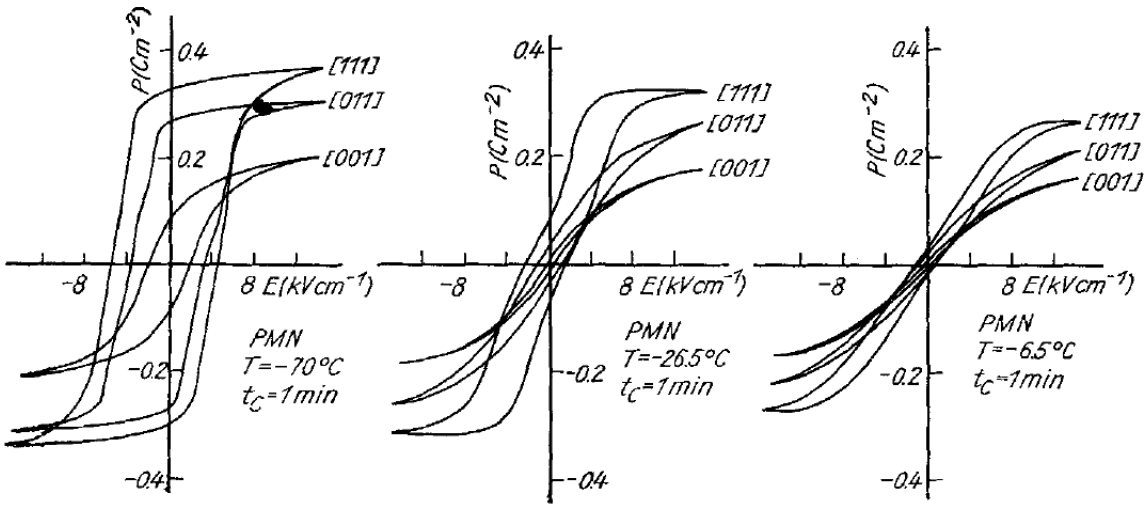

Figure 1.9: Hysteresis loops in PMN below the ferroelectric transition temperature. Well defined hysteresis loops are present below the transition temperature $T_{fe} \sim 200\,\mathrm{K}$ ($\sim 73\,^{\circ}\mathrm{C}$) where the dielectric constant peaks. Reprinted with permission from G. Schmidt, H. Arndt, J. Voncieminski, T. Petzsche, H. Voigt, and N.N. Krainik, Krist. Tech. **15**, 1415 (1980). [1] Copyright (1980) by John Wiley and Sons.

Summarizing, the fluctuations of polarization in the relaxors are broad in temperature and exhibit several special temperatures, as manifested by the dielectric response: the Burns temperature T_B, at which the relaxor dielectric constant deviates from the Curie-Weiss law; the temperature $T_{\max}$, at which the dielectric constant peaks; and T_{fe}, the temperature at which a first-order ferroelectric transition occurs for large enough electric fields. It is the purpose of the present work to provide a model that describes the temperature and frequency dependencies of the dielectric constant in the relaxors. We will compute the correlation functions of polarization and discuss their relation to the PNRs (see Chap. 3)

1.3.2 Phonon Dynamics and Soft Modes

The paraelectric-to-ferroelectric transition in conventional ferroelectrics is the result of a lattice structural change. According to Landau's theory of phase transitions,

symmetries must break spontaneously for a phase change to occur. The lattice structure of typical ferroelectrics is centrosymmetric (has an inversion point), above the critical point T_c (see Fig. 1.14 (a)). Therefore, no permanent dipole moment is allowed in the unit cell. For a permanent dipole to occur, a structural phase change to a non-centrosymmetric lattice must occur (see Fig. 1.14 (b)). Lattice instabilities occur when at least one phonon mode is unstable, i.e., its frequency becomes imaginary. [24]. These vibrational modes are called soft modes and correspond to zone-center transverse optic modes in ferroelectrics. Lattice anharmonicities stabilize these soft modes at temperatures above T_c.

For temperatures above the Burns temperature T_B, relaxor ferroelectrics behave as conventional displacive ferroelectrics in the non-polar phase: they (i) are well described by a perovskite lattice with cubic unit cell (see Sec. 1.2); and (ii) the dielectric susceptibility follows the Curie-Weiss law with large Curie-Weiss constants (see Sec. 1.3.1). These suggests that the behavior of the relaxors above and below the Burns temperature could be understood in terms of lattice dynamics and soft modes in the presence of strong compositional disorder. In this section, we contrast the lattice dynamics of conventional displacive ferroelectrics to that of the relaxors.

We focus our attention in results obtained from neutron scattering experiments: (i) constant $\boldsymbol{Q}$ scans and (ii) constant energy scans. Constant $\boldsymbol{Q}$ scans are performed by holding the momentum transfer $\boldsymbol{Q} = \boldsymbol{k}_i - \boldsymbol{k}_f$ fixed while varying the energy transfer $\Delta E = E_i - E_f$. Here, $E_i, \boldsymbol{k}_i$ are the energy and wavevector of the incident neutron and $E_f, \boldsymbol{k}_f$ are the energy and wavevector of the scattered neutron. Constant energy scans are performed by holding ΔE fixed while varying the momentum transfer $\boldsymbol{Q}$. From the conservation laws of of momentum (wavevector) and energy, it follows that $\boldsymbol{k}_i - \boldsymbol{k}_f = \boldsymbol{Q} = \boldsymbol{\tau} + \boldsymbol{q}$ and $E_i - E_f = \hbar\Omega_{\boldsymbol{q}}$,

where $\boldsymbol{\tau}$ is a reciprocal lattice vector; $\boldsymbol{q}$ is a wavevector within the Brillouin zone; and $\Omega_{\boldsymbol{q}}$ is the frequency of the phonon at $\boldsymbol{q}$. In the experiments described below, $\boldsymbol{Q}$ and $\boldsymbol{q}$ are measured in reciprocal lattice units (rlu), where $1\,\mathrm{rlu} = 2\pi/a$ where a is the lattice constant.

We first consider PTO, a typical ferroelectric. Figure 1.10 shows the dispersion curves for the phonons observed by neutron scattering along the [001] direction at $T = 510\,^{\circ}\mathrm{C}$ (783 K). [38] The dip in the transverse acoustic mode at about 0.1 rlu is due to its interaction with the transverse optic mode. The soft optic mode was observed at the zone-center of the Brillouin zone ($\boldsymbol{q} = 0$) with increasing energy with increasing $\boldsymbol{q}$. For PTO, the soft mode is well defined (undamped) away from its critical point, $T_c = 440\,^{\circ}\mathrm{C}$ (766 K) (see Fig. 1.11)). Close to T_c, the soft optic mode broadens and it is difficult to directly measure its frequency at $\boldsymbol{q} = 0$ since it must be distinguished from acoustic phonons and Bragg reflections. An extrapolation method is used to find the soft optic mode frequency $\Omega_{\mathbf{0}}$ at $\boldsymbol{q} = 0$. The phonon dispersion $\Omega_{\boldsymbol{q}}$ is approximated in the vicinity of $\boldsymbol{q} = 0$ by the relation, $(\hbar\Omega_{\boldsymbol{q}})^2 = (\hbar\Omega_0)^2 + \alpha|\boldsymbol{q}|^2$, where α is a temperature independent constant. The temperature dependence of the energy $\hbar\Omega_{\boldsymbol{q}}$ is determined by constant energy scanning in the vicinity of the zone center ($0.2\,\mathrm{rlu} < \boldsymbol{q} < 0.8\,\mathrm{rlu}$). The results are shown in Figure 1.12. The vertical lines indicate the result of this extrapolation. For temperatures above T_c, Ω_0^2 decreases linearly with temperature, [38]

$$\hbar^2\Omega_0^2 = A_f(T - T_c), \quad A_f = 0.13\ (\pm 0.03)\,\mathrm{meV}^2/^{\circ}\ \mathrm{C}, \quad T_c = 440\,^{\circ}\ \mathrm{C}. \tag{1.6}$$

This is precisely the temperature dependence predicted by the theory of W. Cochran for the frequency of the transverse optic mode. [22, 23].

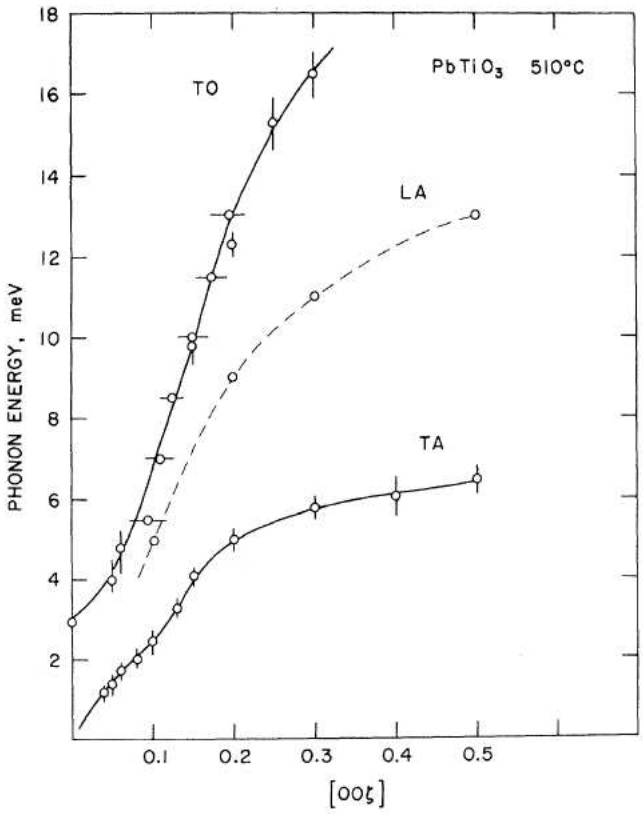

Figure 1.10: Three lowest phonon branches in PTO at $T = 510\,^{\circ}\mathrm{C}$ (783 K). Here, $|\boldsymbol{q}| = (2\pi/a)\zeta$, where $a = 3.97\,\text{Å}$ is the lattice constant in the non-polar phase. Reprinted figure with permission from G. Shirane, J. D. Axe, J. Harada, and J. P. Remeika, Phys. Rev. B **2**, 155 (1970). [38] Copyright (2008) by the American Physical Society.

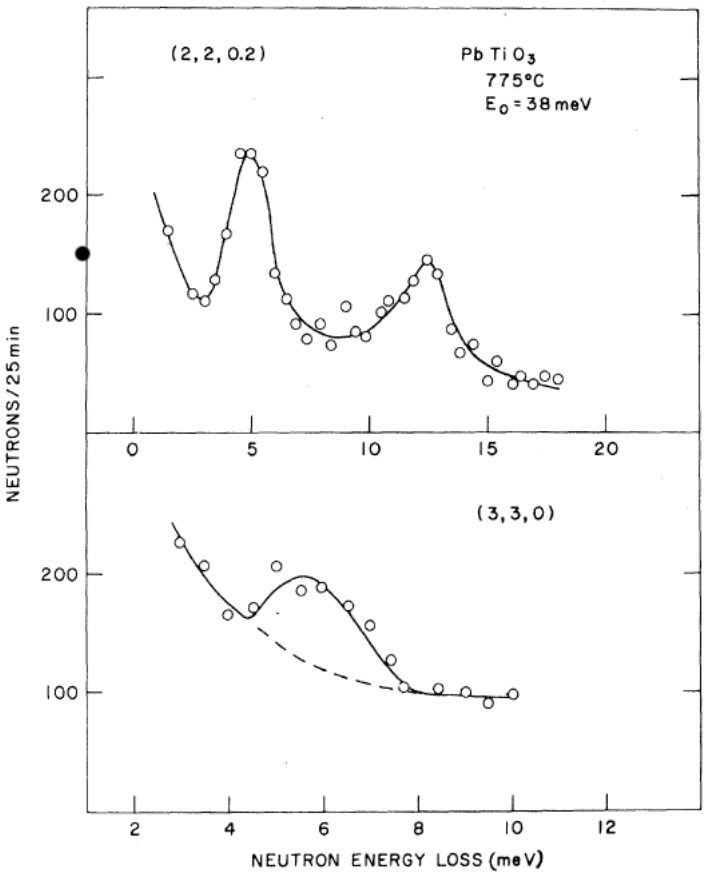

Figure 1.11: Constant-$\boldsymbol{Q}$ scans for PTO measured at $\boldsymbol{Q} = (2, 2, 0.2)$ and $\boldsymbol{Q} = (3, 3, 0)$ at $T = 775\,^{\circ}\mathrm{C}$ (1048 K). G. Shirane, J. D. Axe, J. Harada, and J. P. Remeika, Phys. Rev. B **2**, 155 (1970). [38] Copyright (2008) by the American Physical Society.

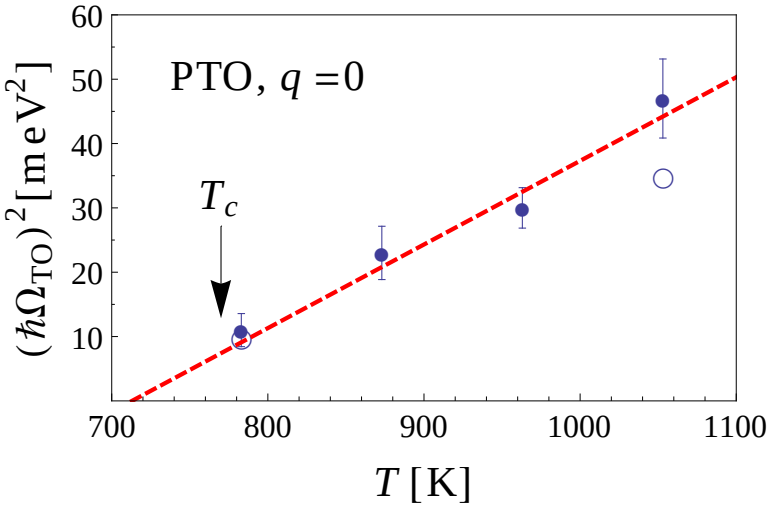

Figure 1.12: The frequency squared of the zone-center transverse optic mode for PTO. Filled and empty circles are obtained by the extrapolation method (see text) and by direct measurements, respectively. Data taken from Ref. [38].

The displacements of the ions associated with the soft transverse optic modes are determined from neutron scattering. [39] A symmetry analysis of the PTO unit cell at the zone center ($\boldsymbol{q} = 0$) shows that the frequency of the mode is 3-fold degenerate: the Slater mode, the Last mode, and the Axe mode (see Fig. 1.13). In the Slater mode, the oxygen and the Ti ion vibrate in opposition while the Pb ions remain stationary. The Last mode corresponds to opposing motions of the TiO_6 octahedron and the Pb ions. In both modes, the three oxygen atoms in the unit cell move as a rigid unit. In the Axe mode, the Pb and Ti ions are at rest while the oxygen octahedron bends. The actual displacements of the ions in the unit cell are a linear combination of Slater, Last and Axe modes. The relative intensities of these vibrational modes are determined by measuring the intensity of the inelastic scattering for a one phonon process. For the perovskite ferroelectric PTO, the two dominant modes are the Slater and Last modes and the resulting displacements are shown in Fig. 1.14 (b). [40]

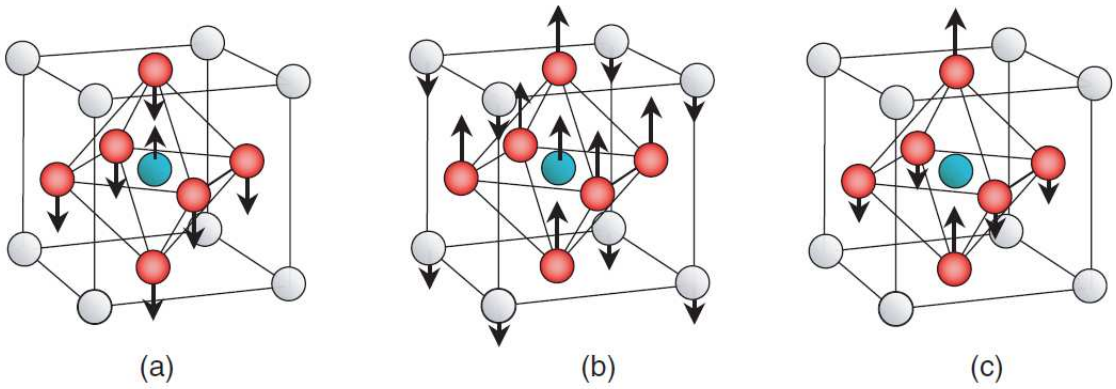

Figure 1.13: Zone-center transverse optic modes in PTO: (a) Slater, (b) Last, and (c) Axe modes. Grey, blue, and red spheres are the Pb^{+4}, Ti^{+2}, and O^{-2} ions, respectively. Reprinted with permission from J. Hlinka, J. Petzelt, S. Kamba, D. Noujni, and T. Ostapchuk, Phase Transitions **79**, 41 (2006). [41] Copyright (2006) by Taylor & Francis.

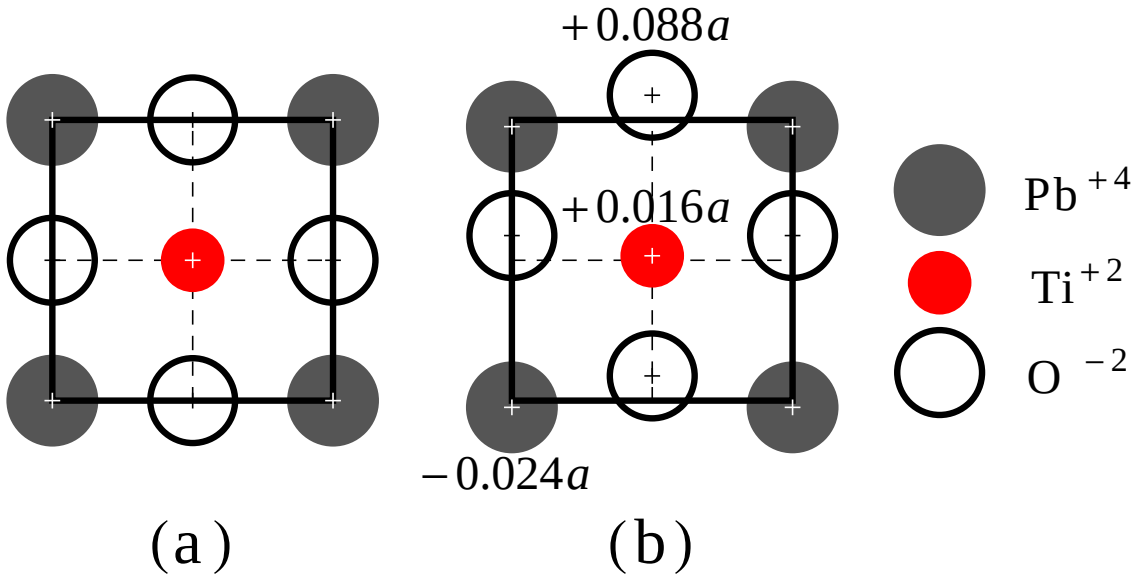

Figure 1.14: Cubic (a) and tetragonal (b) unit cells of PTO. The cubic unit cell is centrosymmetric, thus, no permanent dipole moment is allowed. Below T_c, the tetragonal unit cell is non-centrosymmetric and a permanent dipole moment is allowed. $a = 3.97\,\text{Å}$ is the lattice constant in the non-polar phase. Data taken from Ref. [38]

We now discuss the lattice dynamics in the relaxors. As opposed to conventional ferroelectrics, the transverse optic modes that soften have not been fully identified in the relaxors. For temperatures well above the Burns temperature T_B, a soft mode has been

identified and behaves similarly to that of conventional ferroelectrics. For temperatures below T_B and above the temperature T_{fe} in which a ferroelectric transition is induced by large fields (see Sec. 1.3.1), the experimental identification of the soft mode has been difficult because (i) the optic mode becomes strongly overdamped and (ii) it exhibits the waterfall effect: a nearly vertical drop of the transverse optic branch into the acoustic branch observed in the vicinity of some Bragg peaks. The wavevector for which this drop is observed is called the waterfall wavevector $|\boldsymbol{q}_{wf}|$.

Consider the typical relaxor PMN. Figure (1.15) shows the transverse optic and transverse acoustic modes for PMN close to the (200) Bragg peak at $T = 1100\,\mathrm{K}$, well above $T_B \simeq 620\,\mathrm{K}$ and $T_{fe} \simeq 210\,\mathrm{K}$. [42] The modes are underdamped (see Fig. 1.15 (a)-(b)) and exhibit conventional phonon dispersions along the $[20q]$ direction, i.e., the acoustic and optic frequencies are, respectively, proportional to $|\boldsymbol{q}|$ and $|\boldsymbol{q}|^2$ in the long-wavelength limit and increase with increasing wavevector $|\boldsymbol{q}|$ (see inset in Fig. 1.15).

Figure 1.16 shows the transverse optic and transverse acoustic modes close to the (200) Bragg peak at $(T_{fe} <)T = 550\,\mathrm{K}$ $(< T_B)$. The transverse optic mode is strongly damped at $\boldsymbol{Q} = (2, 0, 0.08)$ (see Fig. 1.16 (a)). The transverse acoustic mode is not observed since its energy is $< 3\,\mathrm{meV}$. At $\boldsymbol{Q} = (2, 0, 0.16)$ the transverse optic and transverse acoustic modes are undamped (see Fig. 1.16 (b)). The solid lines in the inset of Fig. 1.16 (a) show the dispersion relations of the transverse acoustic and transverse optic phonons at 550 K along the $[20|\boldsymbol{q}|]$ direction determined from constant-$\boldsymbol{Q}$ scattering. The transverse acoustic dispersion follows conventional behavior for all $|\boldsymbol{q}|$. The transverse optic dispersion follows conventional behavior for $|\boldsymbol{q}| > |\boldsymbol{q}_{wf}| \simeq 0.12\,\mathrm{rlu}$, For $q < |\boldsymbol{q}_{wf}|$, the transverse optic frequencies cannot be determined from constant-$\boldsymbol{Q}$ scans since the mode is damped.

Constant-energy scans are then performed and the positions of the maxima are plotted on a dispersion curve. It is found that the wavevector positions of the maxima are independent of the energy over a considerable range in the energy. This is shown by the dashed line in the inset of Fig. 1.16 (a) in which the optic dispersion exhibits an almost vertical drop at $\boldsymbol{q} = |\boldsymbol{q}_{wf}|$, i.e., the waterfall effect. For temperatures below about $T_{fe} \simeq 210\,\mathrm{K}$ no waterfall effect is observed and the transverse optic mode is undamped. [43]

It was initially proposed the waterfall effect was the result of the interaction between transverse optic modes and PNRs (short range polar correlations of nanoscale size, see Sec. 1.3.1). [42] In addition to the waterfall effect, it was observed that for $T_{fe} < T < T_B$ the frequency of the transverse acoustic mode for $|\boldsymbol{q}| \simeq |\boldsymbol{q}_{wf}|$ has a stronger temperature dependence than that for $|\boldsymbol{q}| < |\boldsymbol{q}_{wf}|$. [42] This observation lead to the simple picture in which phonon modes with wavelengths comparable to the size of the PNRs are damped by the PNRs themselves, while those with longer wavelengths are not affected. This explanation was later challenged by (i) the experimental observation of the waterfall effect in solid solutions of PMN with 60%PTO (PMN-60%PT) where there is no evidence of PNRs [44]; and (ii) a similar effect is observed already in conventional ferroelectrics such as BTO. [45] An alternative explanation for the waterfall effect has been provided by a model of coupled transverse acoustic and transverse optic phonons without invoking the concept of PNRs. [45, 46] The model was applied to PZN-8%PT with good qualitative and quantitative agreement. [45, 46] It is also important to restate here the point of Cowley et al. [7] and Gehring et al. [44]: there is no justification for plotting the maxima of the intensity from constant energy scans as points on a dispersion curve, as done in Fig. 1.16), since the mode is overdamped in the first place.

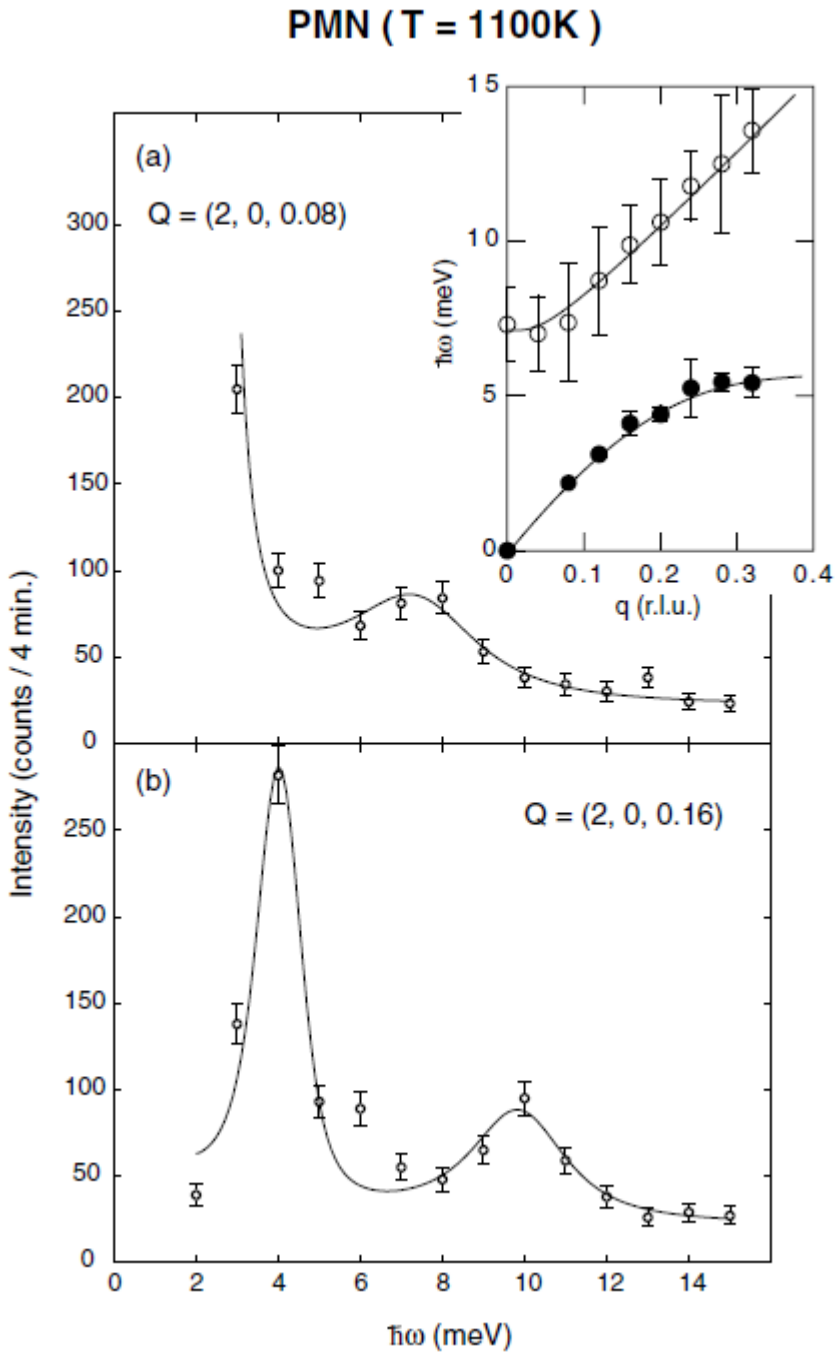

Figure 1.15: Constant-$\boldsymbol{Q}$ scans for PMN at (a) $\boldsymbol{Q} = (2, 0, 0.08)$ and (b) $\boldsymbol{Q} = (2, 0, 0.16)$ at $T = 1100\,\mathrm{K}$. The inset shows the dispersion relation of the transverse acoustic and transverse optic phonons at the same temperature. Reprinted with permission from P. M. Gehring, S. Wakimoto, Z.-G. Ye, and G. Shirane, Phys. Rev. Lett. **87**, 277601 (2001). [42] Copyright (2001) by the American Physical Society.

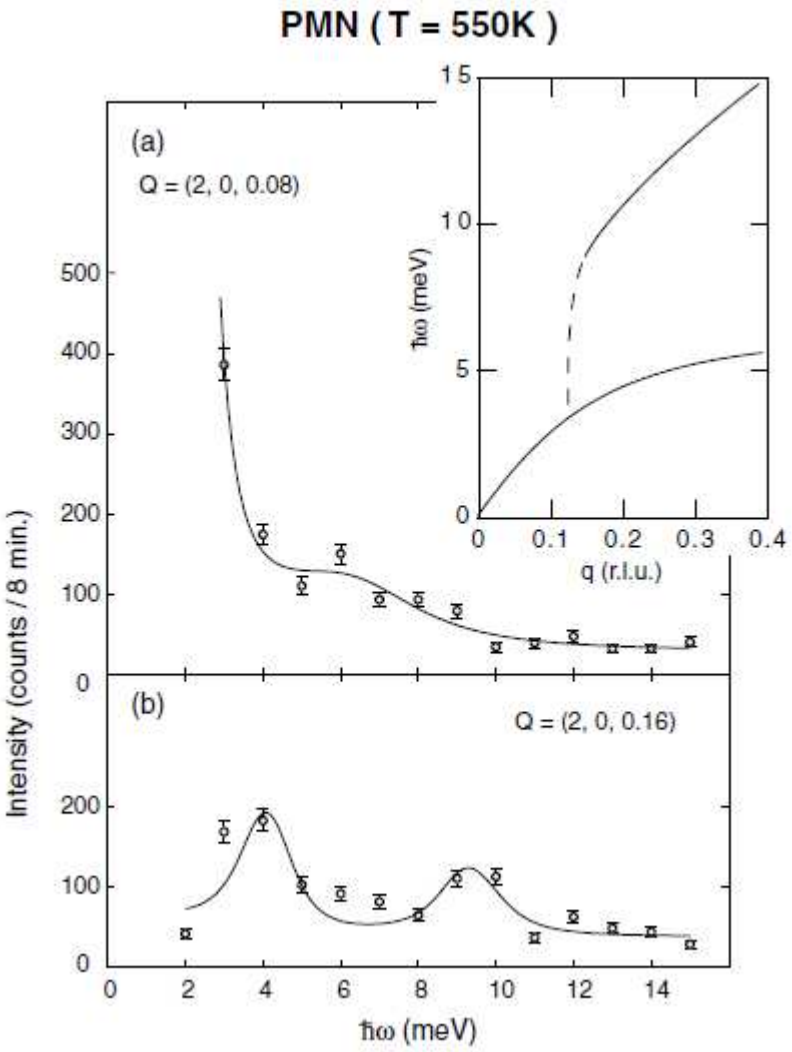

Figure 1.16: Constant-$\boldsymbol{Q}$ scans for PMN at (a) $\boldsymbol{Q} = (2, 0, 0.08)$ and (b) $\boldsymbol{Q} = (2, 0, 0.16)$ at $T = 550\,\mathrm{K}$. The inset shows the dispersion relation of the transverse acoustic and transverse optic phonons at the same temperature. Solid lines are obtained from constant-$\boldsymbol{Q}$ scans and dashed lines from constant energy scans. Reprinted with permission from P. M. Gehring, S. Wakimoto, Z.-G. Ye, and G. Shirane, Phys. Rev. Lett. **87**, 277601 (2001). [42] Copyright (2001) by the American Physical Society.

Figure 1.17 shows the temperature dependence of the frequency of the zone center transverse optic mode Ω_0 for the relaxor ferroelectric PMN. The empty circles correspond to direct measurements of Ω_0 at $\boldsymbol{q} = 0$ in the vicinity of the (200) Bragg reflection. [47] The filled circles correspond to measurements of Ω_0 at $\boldsymbol{q} = 0$ obtained by a similar extrapolation

method used for PTO (see above) in the vicinity of the (220) Bragg reflection. [43] For $T > T_B \simeq 620\,\mathrm{K}$, Ω_0 is well defined and it decreases linearly. For $400\,\mathrm{K} \lesssim T \lesssim T_B \simeq 620\,\mathrm{K}$, Ω_0^2 decreases linearly with temperature and reaches a minimum at a finite frequency at about 400 K. For $210\,\mathrm{K} \lesssim T \lesssim 400\,\mathrm{K}$, Ω_0^2 increases linearly with a greater slope that of $T \gtrsim 400\,\mathrm{K}$. For $T \lesssim 210\,\mathrm{K}$, Ω_0^2 is well defined (underdamped) and increases linearly with temperature with similar slope to that of $210\,\mathrm{K} \lesssim T \lesssim 400\,\mathrm{K}$. We point out that the minimum of Ω_0 at about 400 is close to the Curie-Weiss temperature determined from the observed dielectric constant (see Sec. 1.3.1). This temperature dependence of the soft mode in PMN provides evidence there is no structural lattice change in the absence of strong electric fields.

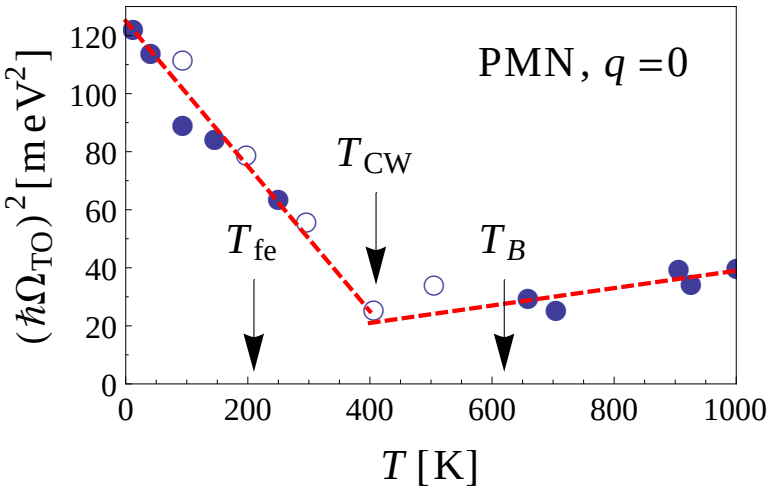

Figure 1.17: The frequency squared of the zone center transverse optic mode for PMN measured at (200) (empty circles) and (220) (filled circles). For $220 - 620\,\mathrm{K}$ the mode is strongly overdamped. The error bars are roughly of the size of the data points. Data taken from Refs. [43, 47].

1.3.3 Diffuse Scattering

Neutron scattering experiments provide a direct measure of the wave-vector distribution of the static fluctuations of polarization close to the critical point. The elastic cross-section is proportional to the static structure factor, i.e., the Fourier transform of the

static correlation functions of polarization. A typical cross section has two components: (i) a sharp and (ii) a broad peak in wave-vector space $\boldsymbol{q}$. Both peaks are centered at $\boldsymbol{q} = 0$. The sharp peak is resolution limited and it corresponds to the Bragg reflection. The broad peak is referred as diffuse scattering and it gives the wave-vector distribution of the correlation function. Here, we contrast the diffuse scattering of conventional ferroelectrics to that of the relaxors.

We first describe the diffuse scattering in conventional ferroelectrics. We consider a typical ferroelectric, BTO. BTO has a paraelectric-to-ferroelectric transition at about $T_c \simeq 320\,\mathrm{K}$. Figure 1.18 shows the elastic structure factor of BTO close to the (010) Bragg peak and close to T_c. For temperatures well above 393 K, only the sharp Bragg peak (green, dashed line) is observed. For temperatures slightly above 393 K there is diffuse scattering (red, solid line) with a small intensity around the Bragg reflection. As $T \to 393\,\mathrm{K}$, the intensity grows and becomes very narrow. For temperatures below 393 K, the intensity of the diffuse scattering decreases. The line shape of the diffuse scattering is well described by a Lorentzian. [48] Figure 1.19 shows the temperature dependence of the diffuse scattering close to $\boldsymbol{q} = 0$. For $T \to T_c$, the diffuse scattering increases as $(T - T_c)^{-1}$ (see solid line in Fig. 1.19).

In systems with isotropic short range forces, e.g., ferromagnets, the elastic magnetic diffuse scattering has similar behavior to that of conventional ferroelectrics: the intensity increases as the temperature approaches from above and below the critical point T_c; and the line shape is that of a Lorentzian. It is well known that for isotropic short range forces, diffuse scattering with Lorentzian line shapes, gives correlation functions that decay exponentially with a correlation length that increases in vicinity of the critical point and

diverges at T_c. It is not-so-well known, however, that for anisotropic long-ranged dipolar forces, diffuse scattering with Lorentzian line shapes, gives correlation functions that decay as power-laws. [49] We will discuss this point in more detail in Chapter 2.

We now describe the static diffuse scattering in relaxor ferroelectrics. We consider a typical relaxor ferroelectric, PMN. In the absence of large static fields, PMN does not have a ferroelectric transition (see Secs. 1.3.2 and 1.3.1). Figure 1.18 shows the elastic the structure factor of a typical relaxor, PMN close to the (110) Bragg peak. For temperatures well above 450 K, only the sharp Bragg peak (green, dashed line) is observed. For temperatures of about 450 K there is diffuse scattering (blue dots) with a small intensity around the Bragg reflection. As temperature decreases to 300 K the intensity grows and the width becomes narrower. Upon further cooling below 300 K, the intensity keeps growing and the width keeps narrowing down to 150 K. Both intensity and width vary little below 150 K. The line shape of the diffuse scattering is not described by that of a simple Lorentzian. [11, 12] Figure 1.20 shows the temperature dependence of the diffuse scattering close to $\boldsymbol{q} = 0$. For temperatures above below the Burns temperature $T_B \simeq 620\,\mathrm{K}$ to about 400 K, the intensity is very small. For temperatures below 400 K, the intensity increases rapidly and then saturates at about 200 K. Similar behavior has been observed in the complex relaxor $(1-x)\mathrm{PbZn}_{1/3}\mathrm{Nb}_{2/3}\mathrm{O}_3$-$x\mathrm{PbTiO}_3$. [50]

Non-Lorentzian line shapes in the elastic diffuse scattering are highly suggestive of random-field transitions. Theoretical and experimental studies in magnetic systems with quenched random fields show the static fluctuations have the shape of a Lorentzian squared in the long-wavelength limit ($\boldsymbol{q} \to 0$). [13, 14, 15, 16, 51, 52] In this work we will show the observed fluctuations in the relaxors (see Figs. 1.18 and 1.20) are indeed the onset of a

random-field transition.

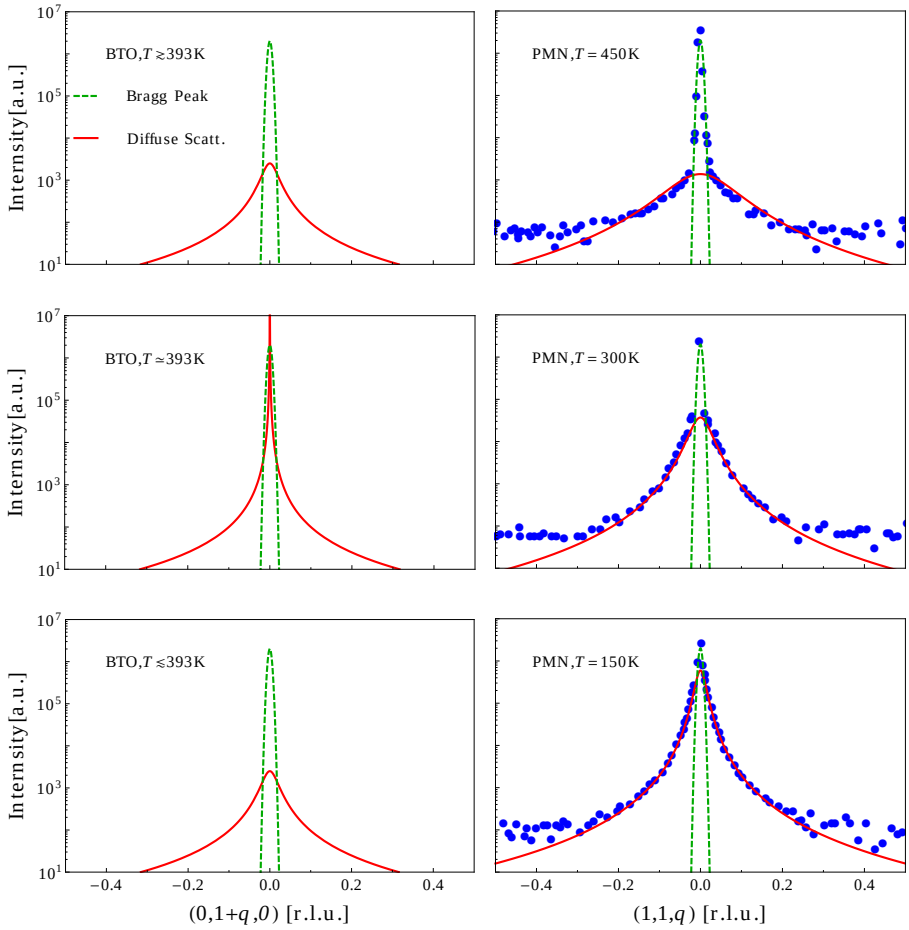

Figure 1.18: Log-linear plot of the diffuse scattering for BTO and PMN. Data taken from Refs. [11, 12, 48].

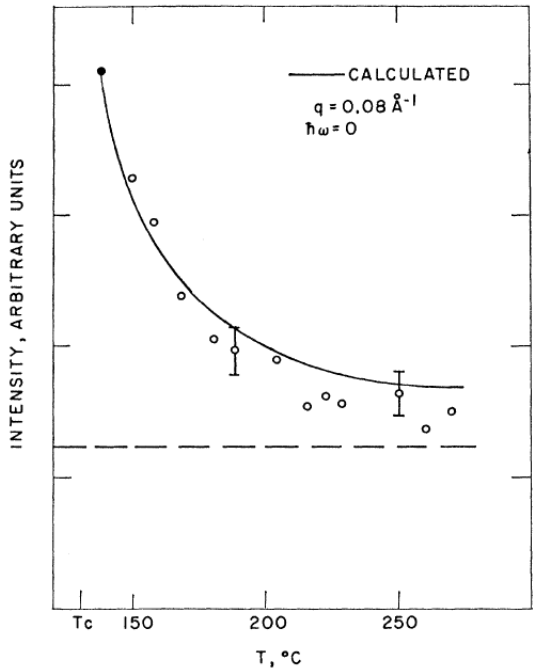

Figure 1.19: Temperature dependence of the elastic diffuse scattering in BTO close to the (010) Bragg peak. Solid line corresponds to a fit to a Lorentzian of width given by the susceptibility $\chi^{-1} \propto T - T_c$. Reprinted with permission from Y. Yamada, G. Shirane, and A. Linz, Phys. Rev. **177**, 848 (1969). [48] Copyright (1969) by the American Physical Society.

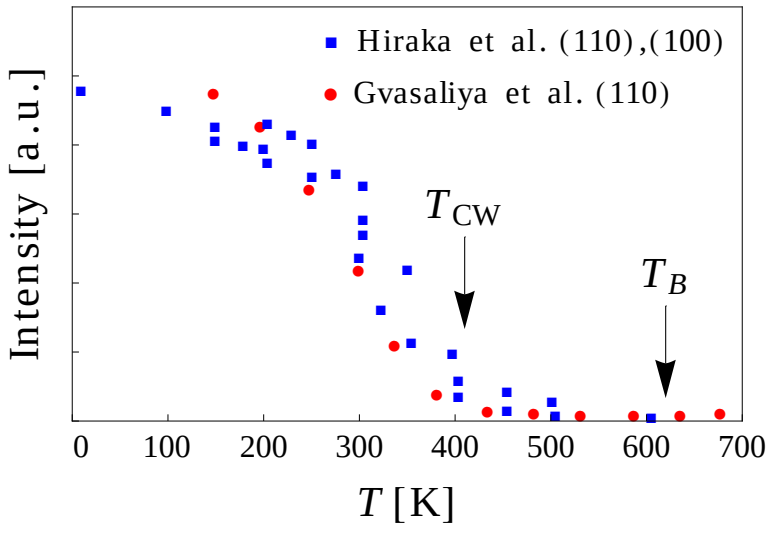

Figure 1.20: Temperature dependence of the elastic diffuse scattering in PMN close to the (110), (100) Bragg peaks. Intensity data from Hiraka et al. has been rescaled by an overall constant factor. Data taken from Ref. [11, 12, 53].

1.4 Review of Previous Theoretical Work in the Relaxors

In this section we review previous theoretical work done in the relaxors. We focus our attention in the so-called Spherical Random-Bond-Random-Field (SRBRF) model put forward by Pirc and Blinc. [9, 10]

The SRBRF model is a semimicroscopic description of the relaxors such as PMN: it consists of reorientable and interacting PNRs embedded in a random array of pinned domains. Pirc and Blinc considered PMN to be a structurally inhomogeneous material consisting of (i) chemically disordered regions rich of Nb ions and (ii) chemically ordered regions poor of Nb. [9, 54, 55] They assumed that PNRs are formed when two or more Nb ions in a chemically disordered region respond along with their surroundings as a single reorientable unit. The chemically ordered regions are static and are sources of random fields. The PNRs are subjected to these random local fields.

Consider n_i Nb-type unit cells in a PNR i, with $i = 1, .., N$ where N is the number of PNRs. The dipole moment of the PNR is $\boldsymbol{M}_i = \sum_l \boldsymbol{m}_i(l)$, where $\boldsymbol{m}_i(l)$ is the dipole moment of a unit cell l in the PNR i. Assuming all dipole moments within a PNR are identical, $\boldsymbol{m}_i = \boldsymbol{m}_i(l)$, then $\boldsymbol{M}_i = n_i \boldsymbol{m}_i$. By introducing the dimensionless pseudospin $\boldsymbol{S}_i \equiv \left(3/[m_i^2]_{av}\right)^{1/2} \boldsymbol{M}_i/n_i$, where $[m_i^2]_{av} \equiv (1/N)\sum_i m_i^2$, it is found that $\boldsymbol{S}_i$ satisfies the constrain,

$$\sum_i |\boldsymbol{S}_i|^2 = 3N. \tag{1.7}$$

Since the number of possible orientations of $\boldsymbol{S}_i$ is high, it is assumed that its components fluctuate continuously,

$$-\infty < S_{i\mu} < \infty, \ (\mu = x, y, z), \tag{1.8}$$

however, they must satisfy the constrain (1.7).

The Hamiltonian of a system of interacting PNRs is given as follows,

$$H = -\sum_{i,j} J_{ij} \boldsymbol{S}_i \cdot \boldsymbol{S}_j - \sum_i \boldsymbol{h}_i \cdot \boldsymbol{S}_i. \tag{1.9}$$

Here, J_{ij} is a random bond (interaction) between PNRs i, j; and $\boldsymbol{h}_i$ is a local random field on the PNR i. The bonds J_{ij} are infinitely ranged independent random variables with a Gaussian probability distribution of mean J_0/N and variance J^2/N. The fields $\boldsymbol{h}_i$ are assumed to be independent random variables with a Gaussian probability distribution of zero mean and of variance $\Delta\, \delta_{ij}\delta_{\mu\nu},\ (i, j = 1, ..., N),\ (\mu, \nu = x, y, z)$. Some of the quantities calculated by Pirc and Blinc are the polarization $P_\mu = (1/N) \sum_i \left\langle \langle S_{i\mu} \rangle_{th} \right\rangle_c$; the Edward-Anderson order parameter, $q_\mu = (1/N) \sum_i \left\langle \langle S_{i\mu} \rangle_{th}^2 \right\rangle_c$; and the linear susceptibility $\chi_1(\omega)$, where ω is the frequency of an external electric field. $\langle \ldots \rangle_{th}$ and $\langle \ldots \rangle_c$ are thermal and configurational average, respectively.

The phase diagram predicted by the SRBRF model is shown in the inset of Fig. 1.21. Here, an infinitesimal external field $\boldsymbol{E}^{ext}$ in the $(1, 1, 1)$ direction is applied so $P = P_x = P_y = P_z$ and $q = q_x = q_y = q_z$. In the absence of random fields ($\Delta = 0$) and for $J_0 > J$, the model predicts a paraelectric to ferroelectric transition at a finite temperature with a non-zero order parameter ($P \neq 0$). For $\Delta = 0$ and $J_0 < J$, the system goes through a sharp transition to a spherical glass phase with no long-range order ($P = 0$). The Edwards-Anderson order parameter q decreases linearly with increasing temperature and vanishes at $T = J$. For $T > J$, q remains zero. In the presence of random fields ($\Delta > 0$), there is long range ferroelectric order for $J_0 > \sqrt{J^2 + \Delta}$. For $\Delta > 0$ and $J_0 < \sqrt{J^2 + \Delta}$, long-range ferroelectric order is suppressed at all temperatures and there is no sharp transition to a spherical glass state: q is small well above $T = J$ and increases as temperature decreases (see Fig. 1.21). When compared to experiments, the SRBRF model describes

well the observed Edwards-Anderson order parameter with physically reasonable fitting parameters (see Fig. 1.22).

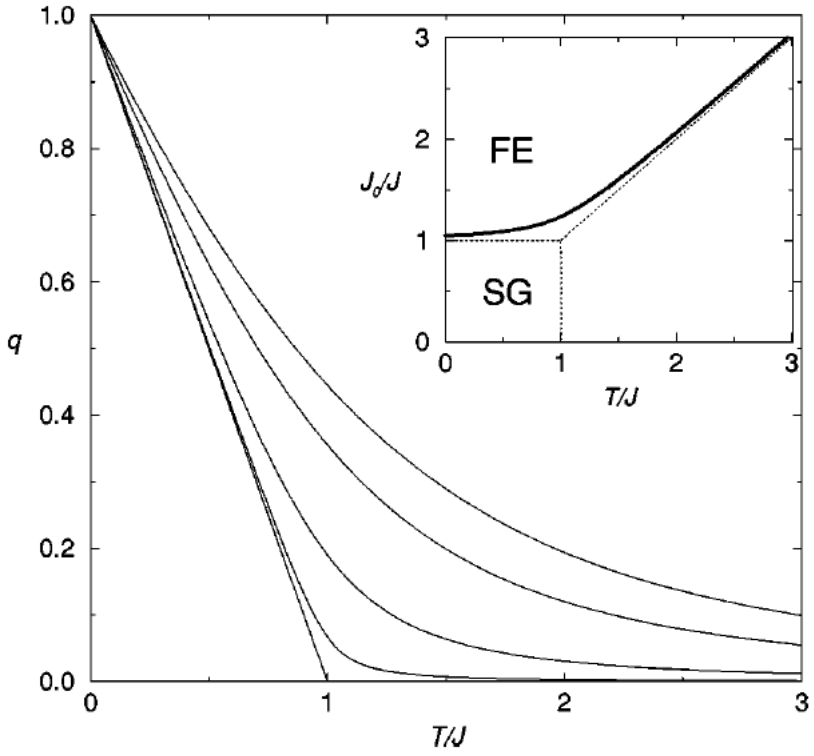

Figure 1.21: Temperature dependence of the Edwards-Anderson order parameter for the SRBRF model. Here $J_0 = 0$ and for (top-to-bottom) $\Delta/J^2 = 1.0, 0.5, 0.1, 0.01, 0.0$. The inset shows the phase diagram of the SRBRF model without random fields (dashed line, $\Delta = 0$) and with random fields (solid line, $\Delta/J^2 = 0.1$). There is no sharp transition to the spherical glass phase (SG) in the presence of random fields. Reprinted with permission from R. Pirc and R. Blinc, Phys. Rev. B **60**, 13470 (1999). [9] Copyright (1999) by the American Physical Society.

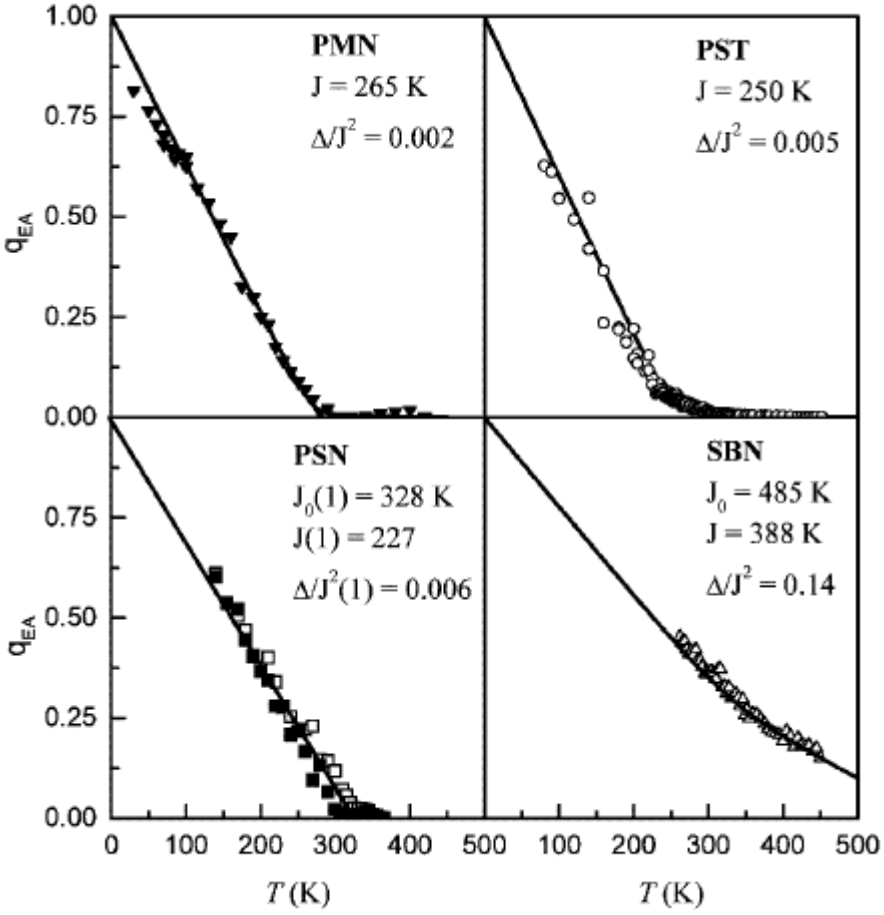

Figure 1.22: Temperature dependence of the Edwards-Anderson order parameter q for several relaxors. Solid line corresponds to the q from the SRBRF model and the circles, triangles, and squares to that of NMR experiments. For PMN and PST, $J_0 = 0$. For PSN, $J_0(1)$ and $J(1)$ are the pressure dependent mean and variance of the random bonds, respectively. The units of pressure are unspecified. Reprinted with permission from R. Blinc and R. Pirc and V. Bobnar and A. Gregovič, AIP Conference Proceedings: Fundamentals of Physics of Ferroelectrics **582**, 97 (2001). [56] Copyright (2001) by the American Institute of Physics.

The real and imaginary parts of the linear susceptibility $\chi_1(\omega) = \chi_1{}'(\omega) + i\chi_1{}''(\omega)$

are shown Fig. 1.23. Here, it is assumed the relaxation time τ is given by the Vogel-Fulcher

law,

$$\frac{1}{\tau} = \begin{cases} \frac{1}{\tau_0} \exp\left[-\frac{E_a}{k_B(T-T_f)}\right], & T \geq T_f \\ \infty, & T \leq T_f. \end{cases} \tag{1.10}$$

Here, τ_0 is a characteristic relaxation time, E_a is the activation energy; and T_f is a freezing temperature. There is no a priori relation between the freezing temperature T_f and the parameters of the SRBRF model. In the absence of compositional disorder, ${\chi_1}'(\omega = 0)$ diverges at $T_c = J_0$ (not shown in figure). In the presence of random bonds and random fields, the calculated ${\chi_1}'(\omega)$ has a broad peak and a maximum that shifts towards higher temperatures with increasing frequencies. Large values of ${\chi_1}'(\omega)$ are found if the mean J_0 of the random bonds is slightly smaller than their variance J. For $T < T_f$, $\chi_1(\omega)$ is strictly zero. The Burns temperature T_B and its dependence on the model parameters is not discussed in the SRBRF papers. [9, 10] No fits to experiments are provided.

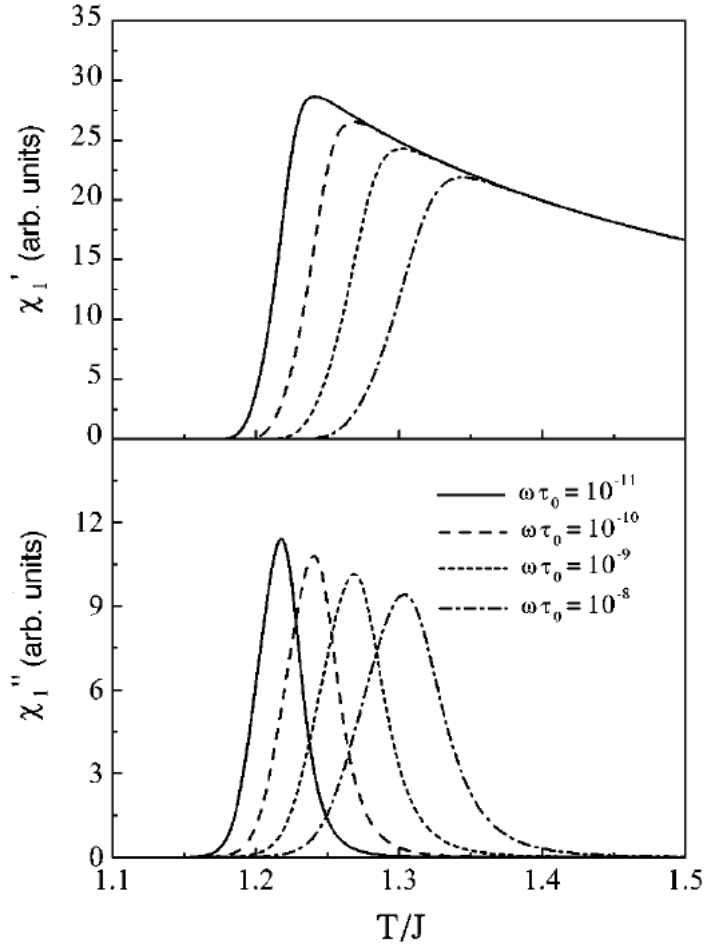

Figure 1.23: Temperature dependence of the real ($\chi_1'(\omega)$) and imaginary ($\chi_1''(\omega)$) parts of the liner susceptibility calculated from the SRBRF model. Here, $J_0 = 0.9J, \Delta/J^2 = 0.001, T_f = J$, and $E_a = 5.5J$ The response is strictly zero for $T < T_f = J$. Reprinted with permission from R. Pirc, R. Blinc, and V. Bobnar, Phys. Rev. B **63**, 054203 (2001). [10] Copyright (2001) by the American Physical Society.

The purpose of this work is to to provide a theory for the static and dynamic critical fluctuations of polarization of the relaxors together with their several special energy scales ($T_B, T_{CW}, T_{\max}$) in the absence of large static electric fields. The SRBRF model is not suitable for this purpose. First, the SRFRB model assumes the interactions are infinitely ranged. In the absence of compositional disorder, an infinitely ranged model is in qualitative and somewhat quantitative agreement with the behavior of conventional ferro-

electrics: there is a paraelectric-to-ferroelectric phase transition at a finite temperature and the critical exponents are of the mean field type. However, an infinite ranged model fails to predict the large-values of the Curie-Weiss constant and the LST relation (1.3) typical of ionic systems. [57] To obtain qualitative and quantitative agreement with the behavior of conventional ferroelectrics, dipolar and local anharmonic forces must be considered simultaneously. [18, 22, 23]. Second, it is difficult to assign the temperature for the onset of the diffuse phase transition to any of the various energy scales observed in the relaxors. [7] For weak disorder in the random fields, the Edwards-Anderson order parameter q of the SRBRF model increases from zero at temperatures of about the square root of the variance of the random bonds J ($\simeq 265\,\mathrm{K}$ for PMN, see Figs. 1.21 and 1.22). This is below the temperature for which the intensity of the static diffuse scattering is observed to increase from zero ($\simeq 400\,\mathrm{K}$ for PMN, see Fig. 1.20 and Fig. 8 in Ref. [44]). Third, the SRBRF model predicts a large susceptibility provided the mean value of the random bonds is close and slightly less than their variance ($J_0 \lesssim J$). When contrasted to experiments, this condition is not satisfied (see Fig. 1.22).

In this thesis, we will present a model for the relaxors which consists polarizable unit cells with local anharmonic forces, dipolar forces and random fields. We will show that these components are essential to calculate the observed static and dynamic fluctuations. The points raised above will be addressed in Chapter 3.

Chapter 2

Theory of Conventional Ferroelectrics

In this chapter, we present the theory of conventional ferroelectrics, i.e., a displacive ferroelectric without compositional disorder. There are two approaches to describe a ferroelectric transition in displacive ferroelectrics: (i) the phenomenological theory of Devonshire [58, 59, 60] and (ii) the lattice dynamical theory based on the ideas of P.W. Anderson [18] and W. Cochran [22, 23]. The basic idea of (i) is to expand the free energy in terms of the polarization and the coefficients of the expansion are arbitrary functions of temperature determined from experiments. This phenomenological approach is useful to compare with experimental data but no temperature dependencies are predicted and no mechanism of the ferroelectric transition if provided. On the other hand, (ii) starts from general lattice models and assumes at least one phonon mode is unstable. The modes are stabilized by anharmonic effects. The advantage of this approach is that temperature dependencies are predicted for thermodynamic quantities and the onset of the ferroelectric

transition is described in terms of lattice instabilities. Here, we adopt the dynamical lattice approach since it provides a useful framework to investigate the critical fluctuations in the relaxors discussed in Chapter (1).

We first introduce a model Hamiltonian in terms of polarizable unit cells with local and dipolar forces. Second, we discuss the Lorentz and Onsager field approximations to handle dipolar forces and derive an effective Hamiltonians within the Lorentz and Onsager approximations. Third, we study the thermodynamics of the model within these approximations and discuss the onset of the paraelectric-to-ferroelectric phase transition.

2.1 Model Hamiltonian

We consider a simplified model of an uniaxial ferroelectric without compositional disorder in which the displacements of the ions in the unit cell i are described by a local displacement field $\boldsymbol{u}_i$ along the polar axis (here, arbitrarily chosen to be the z-axis). $\boldsymbol{u}_i$ is a linear combination of the displacements of the individual ions taking part in the soft transverse optic mode, the condensation of which leads to the distorted structure. [61, 62, 63]

We consider the following model Hamiltonian,

$$H = \sum_i \left[\frac{\Pi_i^2}{2M} + V(u_i) \right] - \frac{1}{2} \sum_{i,j} v_{ij} u_i u_j - \sum_i E_i^{ext} u_i. \tag{2.1}$$

Here, z^* is an effective charge defined such that $z^* u_i$ is the dipole moment of the unit cell at site $\boldsymbol{R}_i$. $\Pi_i = M\dot{u}_i$ is the conjugate momentum of the displacement u_i; M is an effective mass; and E_i^{ext} is an external applied field.

$V(u_i)$ is an anharmonic potential,

$$V(u_i) = \frac{\kappa}{2} u_i^2 + \frac{\gamma}{4} u_i^4, \tag{2.2}$$

where $\kappa,\ \gamma$ are positive constants.

v_{ij} is the dipole interaction,

$$v_{ij}/z^{*2} = \begin{cases} 3\frac{(z_i-z_j)^2}{|\boldsymbol{R}_i-\boldsymbol{R}_j|^5} - \frac{1}{|\boldsymbol{R}_i-\boldsymbol{R}_j|^3}, & \boldsymbol{R}_i \neq \boldsymbol{R}_j \\ 0, & \boldsymbol{R}_i = \boldsymbol{R}_j, \end{cases} \tag{2.3}$$

where a is the lattice constant.

The Fourier transform of the dipole interaction,

$$v_{\boldsymbol{q}} = \sum_{i,j} v_{ij} e^{i\boldsymbol{q}\cdot(\boldsymbol{R}_i-\boldsymbol{R}_j)} \tag{2.4}$$

is non-analytic for $\boldsymbol{q} \to 0$, i.e., its value depends on the direction in which $\boldsymbol{q}$ approaches zero. For cubic lattices and $\boldsymbol{q} \to 0$, $v_{\boldsymbol{q}}$ has the form, [64, 65]

$$\lim_{\boldsymbol{q}\to 0} \frac{v_{\boldsymbol{q}}}{nz^{*2}} = \frac{4\pi}{3}\left(1 - 3\frac{q_z^2}{|\boldsymbol{q}|^2}\right) - \eta|\boldsymbol{q}a|^2 + 3\eta(q_z a)^2 \tag{2.5}$$

where n is the number of lattice points per unit volume and η is a dimensionless coefficient that depends on the structure of the lattice ($\eta \simeq 0.084$ for FCC lattices).

We will use the notation,

$$v_0 = \begin{cases} v_0^{\perp} = \frac{4\pi}{3} nz^{*2}, & \boldsymbol{q} \perp \hat{z} \text{ (transverse)} \\ v_0^{\parallel} = -\frac{8\pi}{3} nz^{*2}, & \boldsymbol{q} \parallel \hat{z} \text{ (longitudinal).} \end{cases} \tag{2.6}$$

The model parameters that specify $V(u_i)$ and v_{ij} are adjustable and will be fitted to experiments.

Several simplifications are made in writing the Hamiltonian (2.1): we ignore (i) the full cubic symmetry typical of perovskite ferroelectrics; (ii) coupling to strain; (iii) short-range interactions between unit cells. By ignoring the cubic symmetry of conventional perovskite ferroelectrics, the phonon dispersion relations differ since the the dynamical matrix are necessarily different and may lead to different temperature dependencies of the

soft modes. By ignoring strain we miss the first-order phase transition observed in most perovskite ferroelectrics. Numerical analysis shows that only second-order phase transitions arise from the Hamiltonian (2.1). [66] This, however, is not severe since the first-order transitions in conventional ferroelectrics tend to be rather weak. (see, for example, the cubic-to-tetragonal phase transition in PTO in Fig. 1.6 (a)). Inclusion of strain is also important to obtain the right sequence of structural phase transitions, e.g., the cubic-to-tetragonal phase transition in PTO or the cubic-to-tetragonal-to-orthorhombic-to-rhombohedral phase transitions in BTO. [63, 67, 68, 69, 70, 71] Finally, the short-range interactions arise from differences of the short-range repulsion and electronic hybridization between adjacent local modes and isolated local modes. [67] Nearest-neighbor short-range forces change the transition temperature and sometimes the ground state structure. Short-range forces beyond nearest-neighbor do not have a significant effect on the critical temperature and do not change the ground state. [67]

Despite the simplifications mentioned above, the importance of the Hamiltonian (2.1) is that it generates the most fundamental properties that characterize conventional ferroelectrics: (i) a spontaneous polarization at a finite temperature that results from a structural phase transition; (ii) a susceptibility that diverges with a phonon frequency that softens as it approaches the critical point; and (iii) a large Curie-Weiss constant.

It is impossible, however, to study the thermodynamics of the Hamiltonian (2.1) exactly. The difficulties arise because of (i) the anisotropic long ranged dipolar forces and (ii) the local anharmonic forces. Usually, the Lorentz field approximation is used to handle (i). Here, we will use instead the Onsager field approximation since it incorporates the fluctuations of polarization, which are important for the relaxors (see Sec. 1.3). The details

of the the Lorentz and Onsager approximations are given in the next section.

To handle the local anharmonic forces, we use a quasi-harmonic approximation. The basic idea is to assume that the local potential $V(u_i)$ of Eq. (2.2) is slightly anharmonic so the equations of motion can be linearized. This reduces the problem to that of a harmonic oscillator with a renormalized phonon frequency which is determined self-consistently. The quasi-harmonic assumption is justified by the large Curie-Weiss constant observed in perovskite ferroelectrics (see, for instance, Fig. 1.6 (a)). The details of the quasi-harmonic approximation are presented in Sec. 2.4.

2.2 Lorentz and Onsager Field Approximation

One of the major difficulties of studying the thermodynamics of the Hamiltonian (2.1) is the presence of long-ranged anisotropic dipolar forces. The Lorentz and Onsager field approximations provide a method to handle them. The crucial difference between these approaches is that the Onsager method incorporates the fluctuations of polarization and the Lorentz method does not (the Lorentz method is a mean field approximation). For conventional ferroelectrics, most of the thermodynamic properties, e.g., critical exponents, are of the mean field type. Therefore, the Lorentz field provides a good description of them and the Onsager field is almost always ignored. [49, 72, 73] This, however, is not the case of the relaxors. As discussed in Sec. 1.3, compositional disorder in the relaxors extends the region of critical fluctuations over a broad range of temperatures, which, together with the dipolar forces, become significant down to zero temperature. [74] It is then essential that any theory of relaxor ferroelectrics accounts for the fluctuations of polarization at all temperatures. The Lorentz field approximation violates the fluctuation dissipation theo-

rem of statistical mechanics [75, 76], consequently, it fails to account for such fluctuations. On the other hand, the Onsager approximation is the simplest necessary correction to the Lorentz field which accounts for the fluctuations and guarantees the fluctuation dissipation theorem. [75, 76]

In this section, we present the Onsager field approximation in the context of our model Hamiltonian 2.1. It is necessary, however, to discuss the Lorentz field approximation first.

Consider the equation of motion of the Hamiltonian (2.1),

$$M\ddot{u}_i = -\frac{dH}{du_i} = -\frac{dV(u_i)}{du_i} + E_i^{local} \tag{2.7}$$

where E_i^{local} is the local field,

$$E_i^{local} = \sum_j v_{ij} u_j + E_i^{ext}. \tag{2.8}$$

The physical meaning of (2.7) is clear: the dynamics of the dipole at site i is determined by the local forces $-dV/du_i$; and the local field E_i^{local}.

In the Lorentz approximation, E_i^{local} of Eq. (2.8) is approximated by the Lorentz field in which the instantaneous displacement u_j is replaced by its thermal average $\langle u_j \rangle_{th}$,

$$E_i^{local} \simeq E_i^{Lorentz} = \sum_j v_{ij} \langle u_j \rangle_{th} + E_i^{ext}. \tag{2.9}$$

I.e., the Lorentz field is a mean field approximation for which the fluctuations of polarization are ignored. We will see that by ignoring the fluctuations in systems of permanent dipoles, we overestimate the local field. This is the crucial point of Onsager. [74]

In systems of permanent dipoles ($V(u_i)$ of (2.7) is an infinite double-well potential), the Lorentz field approximation gives a paraelectric-to-ferroelectric phase transition at a

finite temperature and the dielectric constant is that of Clausius-Mossotti (see Appendix C),

$$\frac{\epsilon - 1}{\epsilon + 2} = \frac{4\pi}{3} \frac{np^2}{3k_B T} \tag{2.10}$$

where n is the number of dipoles per unit volume and p is the magnitude of the permanent dipole moment. In the vicinity of the paraelectric-to-ferroelectric transition, $\epsilon \to \infty$ and the transition temperature is given by $\frac{4\pi}{3} \frac{np^2}{k_B T} \to 1$. Eq. (2.10) agrees with experience for systems with a small concentration of dipoles. [74]

For systems with a large concentration of dipoles, e.g. polar liquids, the Lorentz approximation fails: it does not describe the absence of long-range order at any finite temperature. E.g., the Lorentz approximation predicts a paraelectric-to-ferroelectric phase transition for water at about 100° C. This is known as the polar catastrophe. Onsager showed that this failure occurs because the Lorentz field ignores the fluctuations of polarization. [74] In the Onsager field approximation, the fluctuations of polarization are incorporated and there is no polar catastrophe.

We now describe the Onsager approximation. First we enclose the dipole at site i in a cavity. The volume of the cavity is such that encloses only the dipole in question. Second, we write the local field E_i^{local}, as the sum of the reaction field $E_i^{reaction}$, and the cavity field E_i^{cavity},

$$E_i^{local} \simeq E_i^{Onsager} = E_i^{reaction} + E_i^{cavity}. \tag{2.11}$$

The reaction field $E_i^{reaction}$, is the response from the medium outside the cavity as u_i fluctuates. Onsager showed that $E_i^{reaction}$ is always parallel to the instantaneous orientation of the dipole u_i,

$$E_i^{reaction} = \lambda u_i \tag{2.12}$$

where λ is a temperature dependent parameter.

The cavity field E_i^{cavity}, is the field inside the cavity when the dipole u_i is absent. E_i^{cavity} is then independent of the instantaneous orientation of u_i. The main point of Onsager is that the cavity field is the only field that contributes to the polarization in systems with permanent dipoles. The reaction field $E_i^{reaction}$ does not contribute to the polarization since it has no torque: $E_i^{reaction}$ is always parallel to the instantaneous orientation of u_i. An expression for E_i^{cavity} is given below.

Unlike the cavity field, the Lorentz field is not independent of the orientation of u_i: $E_i^{Lorentz}$ has a component along $\langle u_i \rangle_{th}$, which in turn, is proportional to the thermal average of the reaction field, $\left\langle E_i^{reaction} \right\rangle_{th}$. This is precisely the reason the Lorentz approximation fails to describe the absence of long-range order at any finite temperature in systems with permanent dipoles: $E_i^{Lorentz}$ overestimates the local field by an amount given by the average reaction field, $\left\langle E_i^{reaction} \right\rangle_{th}$. [75, 76]

An expression for the cavity field is obtained by subtracting off the thermal average of the reaction field $\left\langle E_i^{reaction} \right\rangle_{th}$, from the Lorentz field, [75, 76]

$$E_i^{cavity} = E_i^{Lorentz} - \left\langle E_i^{reaction} \right\rangle_{th} \tag{2.13}$$

where $E_i^{Lorentz}$ and $E_i^{reaction}$ are given in Eqs. (2.9) and (2.12).

Substitution of (2.12) and (2.13) into (2.11) gives the local field E_i^{local} in the Onsager approximation,

$$E_i^{local} \simeq E_i^{Onsager} = E_i^{Lorentz} - \left\langle E_i^{reaction} \right\rangle_{th} + E_i^{reaction}. \tag{2.14}$$

According to this relation, the thermal average of the Onsager field is the Lorentz field, $\left\langle E_i^{Onsager} \right\rangle_{th} = E_i^{Lorentz}$. [75, 76]

When the Onsager field, Eq. (2.14), is applied to systems with permanent dipoles, there is no paraelectric-to-ferroelectric phase transition at any finite temperature and the

dielectric constant is that of Onsager (see Appendix C),

$$\epsilon - 1 = \frac{\epsilon}{2\epsilon + 1} \frac{4\pi n p^2}{k_B T}. \tag{2.15}$$

Simple inspection of (2.15) shows that $\epsilon \to \infty$ for $T \to 0$.

For conventional ferroelectrics in which most of the polarization is due to displacements of the ions with respect to their equilibrium points, the Onsager field approximation is almost always ignored. The thermodynamic properties are well described by the Lorentz field and most critical exponents are of the mean field type. [72] This is because the Lorentz field $E_i^{Lorentz}$ does not overestimate the local field E_i^{local} in conventional ferroelectrics: the reaction field $E_i^{reaction}$ is always parallel to the instantaneous displacement u_i, therefore, $E_i^{reaction}$ contributes to the polarization.

The Lorentz approximation, however, violates the fluctuation-dissipation theorem of statistical mechanics. This is not very severe in conventional ferroelectrics where the region of critical fluctuations is narrow in temperature (a few tenths of Kelvin degrees, see Fig. 1.6 (a)). It is severe in the relaxors, however, where the region of critical fluctuations is very broad (several hundreds of Kelvin degrees, see Fig. 1.6 (b)).

We now write the exact Hamiltonian (2.1) in the Onsager approximation. Substitution of Eqs. (2.11) and (2.12) into (2.7) gives the equation of motion,

$$\begin{aligned} M\frac{d^2 u_i}{dt^2} &= -\frac{dV(u_i)}{du_i} + E_i^{Onsager} \\ &= -\frac{dV(u_i)}{du_i} + \lambda u_i + E_i^{cavity}. \end{aligned} \tag{2.16}$$

where E_i^{cavity} is given in Eq. (2.13). Direct integration of (2.16) gives the the Hamiltonian in the Onsager field approximation,

$$H = \sum_i H_i^{Onsager} = \sum_i \left(H_i^0 - E_i^{cavity} u_i \right), \tag{2.17}$$

where,

$$H_i^0 = \frac{\Pi_i^2}{2M} + V(u_i) - \frac{\lambda}{2}u_i^2 \tag{2.18}$$

and E_i^{cavity} is the cavity field given in Eq. (2.13).

The Hamiltonian in the Onsager approximation, Eq. (2.17), is the sum of single cell Hamiltonians $H_i^{Onsager}$ in which a dipole experiences a a local potential $V(u_i)-(\lambda/2)u_i^2$ and a cavity field E_i^{cavity}. H_i^0 of Eq. (2.18) is a non-interacting Hamiltonian whereas $E_i^{cavity}u_i$ is the effective dipolar interaction.

The Hamiltonian (2.17) has several advantages: (i) it has reduced the many-body problem (2.1) to a single-body problem; and (ii) it incorporates fluctuations of polarization through the parameter λ, which are essential for the relaxors. Eq. (2.17) is the starting point of our calculations.

2.3 Model for Ferroelectrics without Random Fields in the Lorentz Approximation

The single-cell Hamiltonian in the Lorentz approximation is as follows (see Sec. 2.2),

$$H_i^{Lorentz} = H_i^0 - E_i^{Lorentz}u_i \tag{2.19}$$

where H_i^0 is the non-interacting Hamiltonian,

$$H_i^0 = \frac{\Pi_i^2}{2M} + V(u_i) \tag{2.20}$$

and $E_i^{Lorentz}$ is the Lorentz field,

$$E_i^{Lorentz} = \sum_j v_{ij} \langle u_j \rangle_{th} + E_i^{ext} \tag{2.21}$$

Here, u_i is the displacement along the z-axis of the unit cell at site $\boldsymbol{R}_i$; and $\langle u_i \rangle_{th}$ its thermal average. $\Pi_i = M\dot{u}_i$ is the conjugate momentum of the displacement associated with the the displacement u_i; M is an effective mass; and E_i^{ext} is an external applied field.

$V(u_i)$ is an anharmonic potential,

$$V(u_i) = \frac{\kappa}{2}u_i^2 + \frac{\gamma}{4}u_i^4, \tag{2.22}$$

where $\kappa,\ \gamma$ are positive constants.

v_{ij} is the dipole interaction,

$$v_{ij}/z^{*2} = \begin{cases} 3\frac{(z_i - z_j)^2}{|\boldsymbol{R}_i - \boldsymbol{R}_j|^5} - \frac{1}{|\boldsymbol{R}_i - \boldsymbol{R}_j|^3}, & \boldsymbol{R}_i \neq \boldsymbol{R}_j \\ 0, & \boldsymbol{R}_i = \boldsymbol{R}_j, \end{cases} \tag{2.23}$$

where z^* is the effective charge of the unit cell; a is the lattice constant.

The Fourier transform of the dipole interaction,

$$v_{\boldsymbol{q}} = \sum_{i,j} v_{ij} e^{i\boldsymbol{q}\cdot(\boldsymbol{R}_i - \boldsymbol{R}_j)} \tag{2.24}$$

is non-analytic for $\boldsymbol{q} \to 0$, i.e., its value depends on the direction in which $\boldsymbol{q}$ approaches zero. For cubic lattices and $\boldsymbol{q} \to 0$, $v_{\boldsymbol{q}}$ has the form, [64, 65]

$$\lim_{\boldsymbol{q}\to 0} \frac{v_{\boldsymbol{q}}}{nz^{*2}} = \frac{4\pi}{3}\left(1 - 3\frac{q_z^2}{|\boldsymbol{q}|^2}\right) - \eta|\boldsymbol{q}a|^2 + 3\eta(q_z a)^2 \tag{2.25}$$

where n is the number of lattice points per unit volume and η is a dimensionless coefficient that depends on the structure of the lattice ($\eta \simeq 0.084$ for FCC lattices).

We will use the notation,

$$v_0 = \begin{cases} v_0^{\perp} = \frac{4\pi}{3}nz^{*2}, & \boldsymbol{q} \perp \hat{z} \text{ (transverse)} \\ v_0^{\parallel} = -\frac{8\pi}{3}nz^{*2}, & \boldsymbol{q} \parallel \hat{z} \text{ (longitudinal)} \end{cases} \tag{2.26}$$

Our goal is to derive self-consistent equations for the phonon frequencies. These, in turn, will determine the susceptibility and the fluctuations of polarization. To do so, we use linear response theory,

$$\begin{aligned} \langle u_i \rangle_{th} &= \phi(\omega) E_i^{Lorentz} \\ &= \phi(\omega) \left[\sum_j v_{ij} \langle u_j \rangle_{th} + E_i^{ext}(t) \right] \end{aligned} \tag{2.27}$$

Here, $\phi(\omega)$ is the susceptibility of the non-interacting problem H_i^0, i.e, a dipole in a local potential $V(u_i)$.

By Fourier transforming (2.27), we obtain the susceptibility of the interacting problem,

$$\chi_{\boldsymbol{q}}(\omega) = \frac{u_{\boldsymbol{q}}}{E_{\boldsymbol{q}}} = \frac{1}{\phi(\omega)^{-1} - v_{\boldsymbol{q}}} \tag{2.28}$$

We now determine the polarizability of the non-interacting problem.

Equation of motion of a dipole in a local potential $V(u_i)$.

$$M\ddot{u}_i = -\frac{dV(u_i)}{du_i} + E_i^{ext}(t) - \Gamma \dot{u}_i \tag{2.29}$$

$$= -\kappa u_i + \lambda u_i - \gamma u_i^3 + E_i^{ext}(t) - \Gamma \dot{u}_i. \tag{2.30}$$

Here, $E_i^{ext}(t) = E_i^{ext} e^{i\omega t}$ is an infinitesimal external field. We have added a retarded force which gives rise to damping. The damping constant is Γ.

We now linearize the equation (2.29). We consider fluctuations around the expectation value of u_i,

$$u_i = \langle u_i \rangle_{th}^0 + \eta_i \tag{2.31}$$

Here, $\langle \ldots \rangle_{th}^0$ is the static thermal average with $E_i^{ext} = 0$. η_i are the fluctuations around $\langle u_i \rangle_{th}^0$ with zero average, $\langle \eta_i \rangle_{th}^0 = 0$.

Substitution of Eq. (2.31) into (2.29) gives,

$$M\ddot{\eta}_i = -\kappa\left(\langle u_i\rangle_{th}^0 + \eta_i\right) - \gamma\left(\langle u_i\rangle_{th}^{0\ 3} + 3\langle u_i\rangle_{th}^{0\ 2}\eta_i + 3\langle u_i\rangle_{th}^0\eta_i^2 + \eta_i^3\right) + E_i^{ext}(t) - \Gamma\dot{\eta}_i. \tag{2.32}$$

We now assume quasi-harmonic approximation in the absence of the external applied field, i.e, $\langle\ddot{u}_i\rangle_{th}^0 = 0, \langle\dot{u}_i\rangle_{th}^0 = 0$ for $E_i^{ext} = 0$

$$\left[\kappa + \gamma\langle u_i\rangle_{th}^{0\ 2} + 3\gamma\left\langle\eta_i^2\right\rangle_{th}^0\right]\langle u_i\rangle_{th}^0 = 0 \tag{2.33}$$

We used $\langle\eta_i\rangle_{th} = 0$ to derive the above result. We now subtract the above equation from (2.32),

$$M\ddot{\eta}_i = -\kappa\eta_i - \gamma\left[3\langle u_i\rangle_{th}^{0\ 2}\eta_i + 3\langle u_i\rangle_{th}^0\left[\eta_i^2 - \left\langle\eta_i^2\right\rangle_{th}^0\right] + \eta_i^3\right] - \Gamma\dot{\eta}_i \tag{2.34}$$

By approximating the fluctuations η_i^2 by their static thermal averages, i.e., $\eta_i^2 \simeq \left\langle\eta_i^2\right\rangle_{th}^0$, we obtain the equation of motion,

$$M\ddot{\eta}_i = -M\Omega'^2\eta_i + E_i^{ext}(t) - \Gamma\dot{\eta}_i \tag{2.35}$$

where Ω' is the frequency of the non-interacting problem,

$$M\Omega'^2 \equiv \kappa + 3\gamma\left(\left\langle\eta_i^2\right\rangle_{th}^0 + \langle u_i\rangle_{th}^{0\ 2}\right) \tag{2.36}$$

Eq. (2.35) is the equation of motion of a damped harmonic oscillator with frequency Ω' in a external field $E_i^{ext}(t)$ and damping constant Γ.

We now determine the fluctuations of the non-interacting system, $\left\langle\eta_i^2\right\rangle_{th}^0$. We fix the fluctuations $\left\langle\eta_i^2\right\rangle_{th}^0$ to those of a undamped quantum harmonic oscillator with frequency Ω',

$$\left\langle\eta_i^2\right\rangle_{th}^0 = \left\langle u_i^2\right\rangle_{th}^0 - \langle u_i\rangle_{th}^{0\ 2} = \frac{\hbar}{2M\Omega'}\coth\left(\frac{\beta\hbar\Omega'}{2}\right). \tag{2.37}$$

We are now ready to determine the susceptibility of the non-interacting system, $\phi(\omega)$. $\phi(\omega)$ is easily obtained from (2.35),

$$\phi(\omega) = \frac{1}{M\Omega'^2 - \omega^2 + i\omega\Gamma} \tag{2.38}$$

where Ω' is given in Eq. (2.36).

We have now determined the susceptibility of the non-interacting problem, $\phi(\omega)$.

Substitution of (2.38) into (2.28) gives the susceptibility of the interacting problem,

$$\chi_{\boldsymbol{q}}(\omega) = \frac{1}{M\Omega'^2 - M\omega^2 + i\omega\Gamma - v_{\boldsymbol{q}}} \tag{2.39}$$

We recast the susceptibility (2.39) as follows,

$$\chi_{\boldsymbol{q}}(\omega) = \frac{1}{M\Omega_{\boldsymbol{q}}^2 - M\omega^2 + i\omega\Gamma} \tag{2.40}$$

where $\Omega_{\boldsymbol{q}}$ is the phonon frequency of the interacting problem,

$$M\Omega_{\boldsymbol{q}}^2 = M\left(\Omega_0^{\perp}\right)^2 + \left(v_0^{\perp} - v_{\boldsymbol{q}}\right) \tag{2.41}$$

and $\Omega_0^{\perp}$ is the $\boldsymbol{q} = 0$ component of the phonon frequency in the direction perpendicular to the polar axis ($\boldsymbol{q} \perp \hat{\boldsymbol{z}}$),

$$M\left(\Omega_0^{\perp}\right)^2 = M\Omega'^2 - v_0^{\perp}. \tag{2.42}$$

Equations (2.33) (2.36), (2.37), (2.41), and (2.42) form a closed system of equations that determine the temperature dependence of $\langle u_i \rangle_{th}^0$, Ω', $\langle \eta^2 \rangle_{th}^0, \Omega_{\boldsymbol{q}}$, $\Omega_0^{\perp}$. Here, we will refer to these equations as Lorentz equations.

Our presentation of the model Hamiltonian for ferroelectrics in the Lorentz approximation concludes here. In the next section we discuss the onset of the paraelectric-to-ferroelectrics phase transition of conventional ferroelectrics in this approximation.

Paraelectric Phase and the Onset of the Paraelectric-to-Ferroelectric Transition in the Lorentz Approximation

We now discuss the paraelectric phase and the onset of the paraelectric-to-ferroelectric phase transition. Our discussion is done in the classical limit, $\hbar \to 0$. This is justified since transverse optic frequency that drives the ferroelectric transition in conventional ferroelectrics softens at temperatures well above ($\sim 10^2\,\mathrm{K}$) the temperatures where the zero-point fluctuations become important ($\sim 0\,\mathrm{K}$).

In the paraelectric phase, $\langle u \rangle_{th} = 0$, and in the classical limit we can eliminate Ω' from the Lorentz equations, Eqs. (2.33) (2.36), (2.37), (2.41), and (2.42). The resulting system of equations is given as follows,

$$M\Omega_{\boldsymbol{q}}^2 = M\left(\Omega_0^{\perp}\right)^2 + \left(v_0^{\perp} - v_{\boldsymbol{q}}\right), \tag{2.43a}$$

$$M\left(\Omega_0^{\perp}\right)^2 = \kappa + 3\gamma\left\langle \eta_i^2 \right\rangle_{th}^0 - v_0^{\perp}, \tag{2.43b}$$

$$\left\langle \eta_i^2 \right\rangle_{th}^0 = \frac{k_B T}{M\left(\Omega_0^{\perp}\right)^2 + v_0^{\perp}}. \tag{2.43c}$$

where,

$$\lim_{\boldsymbol{q}\to 0} \frac{v_0^{\perp} - v_{\boldsymbol{q}}}{nz^{*2}} = 4\pi \frac{q_z^2}{|\boldsymbol{q}|^2} + \eta|\boldsymbol{q}a|^2 - 3\eta(q_z a)^2. \tag{2.44}$$

Here, n is the number of dipoles per unit volume; a is the lattice constant; z^* is the effective charge of the unit cell; and η is a dimensionless coefficient that depends on the lattice structure ($\eta \simeq 0.084$ for FCC lattice).

Eqs. (2.43a)-(2.43c) are the Lorentz field equations for a ferroelectric without compositional disorder in the classical limit. Eqs. (2.43b)-(2.43c) determine the temperature dependence of $\boldsymbol{q} = 0$ component of the soft mode frequency $\Omega_0^{\perp}$. Eq. (2.43a) determines the temperature dependence of the $\boldsymbol{q} \neq 0$ component of the soft mode frequency, $\Omega_{\boldsymbol{q}}$.

We now consider the static susceptibility. The $\boldsymbol{q}$ component of the static susceptibility is given by Eq. (2.75),

$$\chi_{\boldsymbol{q}}^{-1} = M\Omega_{\boldsymbol{q}}^2 = M\left(\Omega_0^{\perp}\right)^2 + \left(v_0^{\perp} - v_{\boldsymbol{q}}\right), \tag{2.45}$$

$\chi_{\boldsymbol{q}}$ is non-analytic, i.e., its value depends on the direction in which $\boldsymbol{q}$ approaches zero,

$$\chi_{\boldsymbol{q}=0}^{-1} = \begin{cases} M\left(\Omega_0^{\perp}\right)^2, & \boldsymbol{q} \perp \hat{\boldsymbol{z}} \\ M\left(\Omega_0^{\perp}\right)^2 + 4\pi n z^{*2}, & \boldsymbol{q} \parallel \hat{\boldsymbol{z}} \end{cases} \tag{2.46}$$

This non-analicity is due to the dipole forces.

The susceptibility diverges in direction perpendicular to the polar axis provided there is a soft mode, i.e, $\Omega_0^{\perp} \to 0$ for $T \to T_c$, where T_c is a critical temperature. We will derive an expression for T_c below.

We now show that dipole forces produce a soft mode. The phonon frequency $\Omega_0^{\perp}$ is given by Eqs. (2.43b)-(2.43c). Dipole forces produce a lattice instability if the following condition is satisfied,

$$M\left(\Omega_0^{\perp}\right)^2 = \kappa + 3\gamma\left\langle\eta^2\right\rangle_{th}^0 - v_0^{\perp} = 0, \quad T = T_c. \tag{2.47}$$

For $T < T_c$, the lattice becomes unstable against the phonon mode, i.e, $\left(\Omega_0^{\perp}\right)^2 < 0$, and a structural phase transition must occur. For $T > T_c$, the fluctuations $\left\langle\eta^2\right\rangle_{th}^0$ increase and stabilize the mode, i.e, $\left(\Omega_0^{\perp}\right)^2 > 0$.

The limit of stability of the paraelectric phase is the critical temperature T_c. By setting $\Omega_0^{\perp} = 0$ and $T = T_c$ in Eqs. (2.43b)-(2.43c), we find an expression for T_c,

$$k_B T_c = \frac{v_0^{\perp} - \kappa}{3\gamma} \times v_0^{\perp}. \tag{2.48}$$

There is a finite critical temperature provided the $\boldsymbol{q} = 0$ component of the dipole force is greater than the stiffness of the lattice, i.e., there is a paraelectric-to-ferroelectric phase

transition provided

$$v_0^{\perp} - \kappa > 0. \tag{2.49}$$

From Eqs. (2.43b), (2.43c), and (2.48) we obtain the temperature dependence of $\Omega_0^{\perp}$ for $T \gtrsim T_c$,

$$M\left(\Omega_0^{\perp}\right)^2 = \frac{3\gamma k_B}{2v_0^{\perp} - \kappa} \times (T - T_c), \quad (T \gtrsim T_c). \tag{2.50}$$

Eq. (2.50) is known as Cochran's law. [22, 23]

The temperature dependence of the susceptibility in the Lorentz approximation is simply given by the inverse phonon frequency, Eq. (2.45). For $T \to T_c$, we obtain the result,

$$\chi_0^{\perp} = \frac{1}{M\left(\Omega_0^{\perp}\right)^2} = \frac{2v_0^{\perp} - \kappa}{3\gamma k_B} \times \frac{1}{T - T_c}, \quad (T \gtrsim T_c). \tag{2.51}$$

where $\chi_0^{\perp}$ is the $\boldsymbol{q} = 0$ component of the susceptibility in the direction perpendicular to the polar axis (see Eq. (2.45)). From (2.51) we identify the Curie-Weiss constant $C_{CW} = (2v_0^{\perp} - \kappa)/(3\gamma k_B)$. For displacive ferroelectrics, the anharmonic coefficient is of the order of the coefficients of volumetric thermal expansion of ferroelectrics ($\sim 10^{-5}\,\mathrm{K}$). [18, 19] This explains the large Curie-Weiss constant of displacive ferroelectrics.

Let us now consider the susceptibility at large temperatures ($T \gg T_c$). For $T \gg T_c$, Eqs. (2.43b), and (2.43c) give the following the temperature behavior for $\Omega_0^{\perp}$,

$$M\left(\Omega_0^{\perp}\right)^2 = \sqrt{3\gamma k_B T}, \quad (T \gg T_c). \tag{2.52}$$

For large temperatures, there is no distinction between the longitudinal and transverse components of the susceptibility (see Eq. 2.46)). Substitution of Eq. (2.52) into (2.46) gives,

$$\chi_0^{\parallel} \simeq \chi_0^{\perp} = \frac{1}{\sqrt{3\gamma k_B T}}, \quad (T \gg T_c). \tag{2.53}$$

The results (2.53) and (2.52) must be taken with caution: for large temperatures ($T \gg T_c$), the anharmonic effects may be more important and invalidate the quasi-harmonic approximation used here.

We conclude our discussion of the paraelectric and onset of the ferroelectric transition in the Lorentz approximation here. In the next section we present a model for conventional ferroelectrics within the Onsager approximation.

2.4 Model for Ferroelectrics without Random Fields in the Onsager Approximation

The single-cell Hamiltonian in the Onsager approximation is as follows (see Sec. 2.2),

$$H_i^{Onsager} = H_i^0 - E_i^{cavity} u_i \tag{2.54}$$

where H_i^0 is the non-interacting Hamiltonian,

$$H_i^0 = \frac{\Pi_i^2}{2M} + V(u_i) - \frac{\lambda}{2} u_i^2 \tag{2.55}$$

and E_i^{cavity} is Onsager's cavity field,

$$E_i^{cavity} = \sum_j v_{ij} \langle u_j \rangle_{th} - \lambda \langle u_i \rangle_{th} + E_i^{ext} \tag{2.56}$$

Here, u_i is the displacement along the z-axis of the unit cell at site $\boldsymbol{R}_i$; and $\langle u_i \rangle_{th}$ its thermal average. $\Pi_i = M\dot{u}_i$ is the conjugate momentum of the displacement associated with the the displacement u_i; M is an effective mass; and E_i^{ext} is an external applied field.

$V(u_i)$ is an anharmonic potential,

$$V(u_i) = \frac{\kappa}{2} u_i^2 + \frac{\gamma}{4} u_i^4, \tag{2.57}$$

where $\kappa,\ \gamma$ are positive constants.

v_{ij} is the dipole interaction,

$$v_{ij}/z^{*2} = \begin{cases} 3\frac{(z_i-z_j)^2}{|\boldsymbol{R}_i-\boldsymbol{R}_j|^5} - \frac{1}{|\boldsymbol{R}_i-\boldsymbol{R}_j|^3}, & \boldsymbol{R}_i \neq \boldsymbol{R}_j \\ 0, & \boldsymbol{R}_i = \boldsymbol{R}_j, \end{cases} \tag{2.58}$$

where z^* is the effective charge of the unit cell; a is the lattice constant.

The Fourier transform of the dipole interaction,

$$v_{\boldsymbol{q}} = \sum_{i,j} v_{ij} e^{i\boldsymbol{q}\cdot(\boldsymbol{R}_i-\boldsymbol{R}_j)} \tag{2.59}$$

is non-analytic for $\boldsymbol{q} \to 0$, i.e., its value depends on the direction in which $\boldsymbol{q}$ approaches zero. For cubic lattices and $\boldsymbol{q} \to 0$, $v_{\boldsymbol{q}}$ has the form, [64, 65]

$$\lim_{\boldsymbol{q}\to 0} \frac{v_{\boldsymbol{q}}}{nz^{*2}} = \frac{4\pi}{3}\left(1 - 3\frac{q_z^2}{|\boldsymbol{q}|^2}\right) - \eta|\boldsymbol{q}a|^2 + 3\eta(q_z a)^2 \tag{2.60}$$

where n is the number of lattice points per unit volume and η is a dimensionless coefficient that depends on the structure of the lattice ($\eta \simeq 0.084$ for FCC lattices).

We will use the notation,

$$v_0 = \begin{cases} v_0^{\perp} = \frac{4\pi}{3} nz^{*2}, & \boldsymbol{q} \perp \hat{z} \text{ (transverse)} \\ v_0^{\parallel} = -\frac{8\pi}{3} nz^{*2}, & \boldsymbol{q} \parallel \hat{z} \text{ (longitudinal)} \end{cases} \tag{2.61}$$

Our goal is to derive self-consistent equations for the phonon frequencies. These, in turn, will determine the susceptibility and the fluctuations of polarization. To do so, we use linear response theory,

$$\begin{aligned} \langle u_i \rangle_{th} &= \phi(\omega) E_i^{cavity} \\ &= \phi(\omega) \left[\sum_j v_{ij} \langle u_j \rangle_{th} + E_i^{ext}(t) - \lambda \langle u_i \rangle_{th} \right] \end{aligned} \tag{2.62}$$

Here, $\phi(\omega)$ is the susceptibility of the non-interacting problem H_i^0, i.e, a dipole in a local potential $V(u_i) - \lambda u_i^2/2$.

By Fourier transforming (2.62), we obtain the susceptibility of the interacting problem,

$$\chi_{\boldsymbol{q}}(\omega) = \frac{u_{\boldsymbol{q}}}{E_{\boldsymbol{q}}} = \frac{1}{\phi(\omega)^{-1} - (v_{\boldsymbol{q}} - \lambda)} \tag{2.63}$$

We now determine the polarizability of the non-interacting problem.

Equation of motion of a dipole in a local potential $V(u_i) - \lambda u_i^2/2$.

$$M\ddot{u}_i = -\frac{dV(u_i)}{du_i} + \lambda u_i + E_i^{ext}(t) - \Gamma \dot{u}_i \tag{2.64}$$

$$= -\kappa u_i + \lambda u_i - \gamma u_i^3 + \lambda u_i + E_i^{ext}(t) - \Gamma \dot{u}_i. \tag{2.65}$$

Here, $E_i^{ext}(t) = E_i^{ext} e^{i\omega t}$ is an infinitesimal external field. We have added a retarded force which gives rise to damping. The damping constant is Γ.

We now linearize the equation (2.64). We consider fluctuations around the expectation value of u_i,

$$u_i = \langle u_i \rangle_{th}^0 + \eta_i \tag{2.66}$$

Here, $\langle \ldots \rangle_{th}^0$ is the static thermal average with $E_i^{ext} = 0$. η_i are the fluctuations around $\langle u_i \rangle_{th}^0$ with zero average, $\langle \eta_i \rangle_{th}^0 = 0$.

Substitution of Eq. (2.66) into (2.64) gives,

$$\begin{aligned} M\ddot{\eta}_i = &-(\kappa - \lambda)\left(\langle u_i \rangle_{th}^0 + \eta_i\right) \\ &- \gamma\left(\langle u_i \rangle_{th}^{0\ 3} + 3\langle u_i \rangle_{th}^{0\ 2}\eta_i + 3\langle u_i \rangle_{th}^0 \eta_i^2 + \eta_i^3\right) \\ &+ E_i^{ext}(t) - \Gamma\dot{\eta}_i. \end{aligned} \tag{2.67}$$

We now assume quasi-harmonic approximation in the absence of the external ap-

plied field, i.e, $\langle \ddot{u}_i \rangle_{th}^0 = 0, \langle \dot{u}_i \rangle_{th}^0 = 0$ for $E_i^{ext} = 0$

$$\left[(\kappa - \lambda) + \gamma \langle u_i \rangle_{th}^{0\ 2} + 3\gamma \left\langle \eta_i^2 \right\rangle_{th}^0 \right] \langle u_i \rangle_{th}^0 = 0 \tag{2.68}$$

We used $\langle \eta_i \rangle_{th} = 0$ to derive the above result. We now subtract the above equation from (2.67),

$$M\ddot{\eta}_i = -(\kappa - \lambda)\eta_i - \gamma \left[3\langle u_i \rangle_{th}^{0\ 2} \eta_i + 3 \langle u_i \rangle_{th}^0 \left[\eta_i^2 - \left\langle \eta_i^2 \right\rangle_{th}^0 \right] + \eta_i^3 \right] - \Gamma \dot{\eta}_i \tag{2.69}$$

By approximating the fluctuations η_i^2 by their static thermal averages, i.e., $\eta_i^2 \simeq \left\langle \eta_i^2 \right\rangle_{th}^0$, we obtain the equation of motion,

$$M\ddot{\eta}_i = -M\Omega'^2 \eta_i + E_i^{ext}(t) - \Gamma \dot{\eta}_i \tag{2.70}$$

where Ω' is the frequency of the non-interacting problem,

$$M\Omega'^2 \equiv \kappa - \lambda + 3\gamma \left(\left\langle \eta_i^2 \right\rangle_{th}^0 + \langle u_i \rangle_{th}^{0\ 2} \right) \tag{2.71}$$

Eq. (2.70) is the equation of motion of a damped harmonic oscillator with frequency Ω' in a external field $E_i^{ext}(t)$ and damping constant Γ.

We now determine the fluctuations of the non-interacting system, $\left\langle \eta_i^2 \right\rangle_{th}^0$. We fix the fluctuations $\left\langle \eta_i^2 \right\rangle_{th}^0$ to those of a undamped quantum harmonic oscillator with frequency Ω',

$$\left\langle \eta_i^2 \right\rangle_{th}^0 = \left\langle u_i^2 \right\rangle_{th}^0 - \langle u_i \rangle_{th}^{0\ 2} = \frac{\hbar}{2M\Omega'} \coth \left(\frac{\beta \hbar \Omega'}{2} \right). \tag{2.72}$$

We are now ready to determine the susceptibility of the non-interacting system, $\phi(\omega)$. $\phi(\omega)$ is easily obtained from (2.70),

$$\phi(\omega) = \frac{1}{M\Omega'^2 - \omega^2 + i\omega\Gamma} \tag{2.73}$$

where Ω' is given in Eq. (2.71).

We have now determined the susceptibility of the non-interacting problem, $\phi(\omega)$. Substitution of (2.73) into (2.63) gives the susceptibility of the interacting problem,

$$\chi_{\boldsymbol{q}}(\omega) = \frac{1}{M\Omega'^2 - M\omega^2 + i\omega\Gamma - (v_{\boldsymbol{q}} - \lambda)} \tag{2.74}$$

We recast the susceptibility (2.74) as follows,

$$\chi_{\boldsymbol{q}}(\omega) = \frac{1}{M\Omega_{\boldsymbol{q}}^2 - M\omega^2 + i\omega\Gamma} \tag{2.75}$$

where $\Omega_{\boldsymbol{q}}$ is the phonon frequency of the interacting problem,

$$M\Omega_{\boldsymbol{q}}^2 = M\left(\Omega_0^{\perp}\right)^2 + \left(v_0^{\perp} - v_{\boldsymbol{q}}\right) \tag{2.76}$$

and $\Omega_0^{\perp}$ is the $\boldsymbol{q} = 0$ component of the phonon frequency in the direction perpendicular to the polar axis ($\boldsymbol{q} \perp \hat{\boldsymbol{z}}$),

$$M\left(\Omega_0^{\perp}\right)^2 = M\Omega'^2 - \left(v_0^{\perp} - \lambda\right). \tag{2.77}$$

To close the system of equations we must determine the parameter λ. We obtain λ by enforcing the fluctuation dissipation theorem, [75, 76]

$$\left\langle u_i^2 \right\rangle_{th}^0 - \left\langle u_i \right\rangle_{th}^{0\ 2} = \frac{1}{N}\sum_{\boldsymbol{q}} \frac{1}{2\pi}\int_{-\infty}^{\infty} d\omega \coth\left(\frac{\beta\hbar\omega}{2}\right) \mathrm{Im}\left[\chi_{\boldsymbol{q}}(\omega)\right] \tag{2.78}$$

where $\mathrm{Im}\left[\chi_{\boldsymbol{q}}(\omega)\right]$ is the imaginary part of the susceptibility (2.75). The summation over $\boldsymbol{q}$ extends over the first Brillouin zone.

We compute the integral (2.78) in the limit of zero damping. For zero damping, $\mathrm{Im}\left[\chi_{\boldsymbol{q}}(\omega)\right]$ becomes the sum of two Dirac delta functions peaked at $\omega = \pm\Omega_{\boldsymbol{q}}$,

$$\begin{aligned}\lim_{\Gamma\to 0} \mathrm{Im}\left[\chi_{\boldsymbol{q}}(\omega)\right] &= \lim_{\Gamma\to 0} \frac{\omega\Gamma}{M^2\left[\Omega_{\boldsymbol{q}}^2 - \omega^2\right]^2 + (\omega\Gamma)^2} \\ &= \frac{\pi}{2M}\left[\frac{1}{\omega}\,\delta\left(\omega - \Omega_{\boldsymbol{q}}\right) + \frac{1}{\omega}\,\delta\left(\omega + \Omega_{\boldsymbol{q}}\right)\right]\end{aligned} \tag{2.79}$$

Substitution of (2.79) into (2.78) gives,

$$\left\langle u^2 \right\rangle_{th}^0 - \left\langle u \right\rangle_{th}^{0\ 2} = \frac{1}{N} \sum_{\boldsymbol{q}} \frac{\hbar}{2M\Omega_{\boldsymbol{q}}} \coth\left(\frac{\beta\hbar\Omega_{\boldsymbol{q}}}{2}\right). \tag{2.80}$$

where the summation over $\boldsymbol{q}$ extends over the first Brillouin zone.

Equations (2.68) (2.71), (2.72), (2.75), (2.76), (2.77), (2.80) form a closed system of equations that determine the temperature dependence of $\langle u_i \rangle_{th}^0$, Ω', $\left\langle \eta^2 \right\rangle_{th}^0$, λ , $\Omega_{\boldsymbol{q}}$, $\Omega_0^{\perp}$. Here, we will refer to these equations as Onsager equations.

By setting $\lambda = 0$ into Eqs (2.68) (2.71), (2.72), (2.77), we recover the results in the Lorentz field approximation. We run into a contradiction, however, if we set $\lambda = 0$ in the Onsager equations. This is the point of Brout and Thomas: the fluctuation dissipation theorem of statistical mechanics is not satisfied within the Lorentz field approximation. [75, 76]

Our presentation of the model Hamiltonian for ferroelectrics in the Onsager approximation concludes here. In the next section we discuss the onset of the paraelectric-to-ferroelectrics phase transition of conventional ferroelectrics.

Paraelectric Phase and the Onset of the Paraelectric-to-Ferroelectric Transition in the Onsager Approximation

We now discuss the paraelectric phase and the onset of the paraelectric-to-ferroelectric phase transition. Our discussion is done in the classical limit, $\hbar \to 0$. This is justified since transverse optic frequency that drives the ferroelectric transition in conventional ferroelectrics softens at temperatures well above ($\sim 10^2$ K) the temperatures where the zero-point fluctuations become important (~ 0 K).

In the paraelectric phase, $\langle u \rangle_{th} = 0$, and in the classical limit we can eliminate

Ω' and λ from the Onsager equations, Eqs.(2.71), (2.72), (2.75), (2.76), (2.77), (2.80). The resulting system of equations is given as follows,

$$M\Omega_{\boldsymbol{q}}^2 = M\left(\Omega_0^{\perp}\right)^2 + \left(v_0^{\perp} - v_{\boldsymbol{q}}\right) \tag{2.81a}$$

$$M\left(\Omega_0^{\perp}\right)^2 = \kappa + 3\gamma\left\langle\eta_i^2\right\rangle_{th}^0 - v_0^{\perp} \tag{2.81b}$$

$$\left\langle\eta_i^2\right\rangle_{th}^0 = \frac{1}{N}\sum_{\boldsymbol{q}}\frac{k_BT}{M\left(\Omega_0^{\perp}\right)^2 + \left(v_0^{\perp} - v_{\boldsymbol{q}}\right)} \tag{2.81c}$$

where,

$$\lim_{\boldsymbol{q}\to 0}\frac{v_0^{\perp} - v_{\boldsymbol{q}}}{nz^{*2}} = 4\pi\frac{q_z^2}{|\boldsymbol{q}|^2} + \eta|\boldsymbol{q}a|^2 - 3\eta(q_za)^2. \tag{2.82}$$

Here, n is the number of dipoles per unit volume; a is the lattice constant; z^* is the effective charge of the unit cell; and η is a dimensionless coefficient that depends on the lattice structure ($\eta \simeq 0.084$ for FCC lattice).

Eqs. (2.81a)-(2.81c) are the Onsager field equations for a ferroelectric without compositional disorder in the classical limit. Eqs. (2.81b)-(2.81c) determine the temperature dependence of $\boldsymbol{q} = 0$ component of the soft mode frequency $\Omega_0^{\perp}$. Eq. (2.81a) determines the temperature dependence of the $\boldsymbol{q} \neq 0$ component of the soft mode frequency, $\Omega_{\boldsymbol{q}}$.

We now consider the static susceptibility. The $\boldsymbol{q}$ component of the static susceptibility is given by Eq. (2.75),

$$\chi_{\boldsymbol{q}}^{-1} = M\Omega_{\boldsymbol{q}}^2 = M\left(\Omega_0^{\perp}\right)^2 + \left(v_0^{\perp} - v_{\boldsymbol{q}}\right), \tag{2.83}$$

$\chi_{\boldsymbol{q}}$ is non-analytic, i.e., its value depends on the direction in which $\boldsymbol{q}$ approaches zero,

$$\chi_{\boldsymbol{q}=0}^{-1} = \begin{cases} M\left(\Omega_0^{\perp}\right)^2, & \boldsymbol{q} \perp \hat{\boldsymbol{z}} \\ M\left(\Omega_0^{\perp}\right)^2 + 4\pi nz^{*2}, & \boldsymbol{q} \parallel \hat{\boldsymbol{z}} \end{cases} \tag{2.84}$$

This non-analicity is due to the dipole forces.

The susceptibility diverges in direction perpendicular to the polar axis provided there is a soft mode, i.e, $\Omega_0^\perp \to 0$ for $T \to T_c$, where T_c is some critical temperature. We will derive an expression for T_c below.

We now show that dipole forces produce a soft mode. The phonon frequency $\Omega_0^\perp$ is given by Eqs. (2.81b)-(2.81c). Dipole forces produce a lattice instability if the following condition is satisfied,

$$M\left(\Omega_0^\perp\right)^2 = \kappa + 3\gamma \left\langle \eta^2 \right\rangle_{th}^0 - v_0^\perp = 0, \quad T = T_c. \tag{2.85}$$

For $T < T_c$, the lattice becomes unstable against the phonon mode, i.e, $\left(\Omega_0^\perp\right)^2 < 0$, and a structural phase transition must occur. For $T > T_c$, the fluctuations $\left\langle \eta^2 \right\rangle_{th}^0$ increase and stabilize the mode, i.e, $\left(\Omega_0^\perp\right)^2 > 0$.

The limit of stability of the paraelectric phase is the critical temperature T_c. By setting $\Omega_0^\perp = 0$ and $T = T_c$ in Eqs. (2.81b)-(2.81c), we find an expression for T_c,

$$k_B T_c = \frac{v_0^\perp - \kappa}{3\gamma} \times \left[\frac{1}{N}\sum_{\boldsymbol{q}} \frac{1}{\left(v_0^\perp - v_{\boldsymbol{q}}\right)}\right]^{-1}, \quad \text{(Onsager)}. \tag{2.86}$$

Since the term in the square brackets is positive-definite, there is a finite critical temperature provided the $\boldsymbol{q} = 0$ component of the dipole force is greater than the stiffness of the lattice, i.e., there is a paraelectric-to-ferroelectric phase transition provided

$$v_0^\perp - \kappa > 0. \tag{2.87}$$

We contrast the result (2.86) with that of the Lorentz field,

$$k_B T_c = \frac{v_0^\perp - \kappa}{3\gamma} \times v_0^\perp \quad \text{(Lorentz)} \tag{2.88}$$

The term in the square brackets of Eq. (2.86) is less than 1, therefore, T_c in the Onsager approximation is less than that of Lorentz. This is expected since fluctuations are ignored in

the Lorentz approximation. A plot of the critical temperature in the Lorentz and Onsager approximations is shown in Fig. 2.1.

We now derive the temperature dependence of $\Omega_0^\perp$ for $T \gtrsim T_c$. First, we rewrite Eqs. (2.81b) and (2.81c) as follows,

$$M\left(\Omega_0^\perp\right)^2 = 3\gamma k_B \left\{TF[\Omega_0^\perp] - T_c F[0]\right\} \tag{2.89}$$

where,

$$F[\Omega_0^\perp] \equiv \frac{1}{N}\sum_{\boldsymbol{q}} \frac{1}{M\left(\Omega_0^\perp\right)^2 + \left(v_0^\perp - v_{\boldsymbol{q}}\right)}. \tag{2.90}$$

For $\Omega_0^\perp \to 0$ (see Appendix A),

$$F[\Omega_0^\perp] \simeq F[0]\left\{1 - \frac{M\left(\Omega_0^\perp\right)^2}{2B^2Q^2}\ln\left[\frac{(2BQ)^2}{M\left(\Omega_0^\perp\right)^2}\right]\right\}, \tag{2.91}$$

where $B^2 \equiv \eta\, n(z^*a)^2 = (3\eta a^2/(4\pi))v_0^\perp$, $C^2 \equiv 4\pi n(z^*)^2 = 3v_0^\perp$. Q is an upper cut-off wavevector, and $F[0] = (1/N)\sum_{\boldsymbol{q}}\left(v_0^\perp - v_{\boldsymbol{q}}\right)^{-1} \simeq (3\pi)/(4QBC)$. Here, we take the cut-off wavevector Q to be an edge of the FCC Brillouin zone, i.e., $Q = 2\pi/a$. a, n, z^*, η are defined right below Eq. (2.82).

Substitution of (2.91) into (2.89) gives,

$$M\left(\Omega_0^\perp\right)^2\left\{1 + \frac{3\gamma F[0]T_c}{2B^2Q^2}\ln\left[\frac{(2BQ)^2}{M\left(\Omega_0^\perp\right)^2}\right]\right\} = 3\gamma F[0](T - T_c), \quad T \gtrsim T_c \tag{2.92}$$

The solution to this equation is of the form,

$$M\left(\Omega_0^\perp\right)^2 \propto \frac{t}{\ln(1/t)}, \quad t = \frac{T - T_c}{T_c} \ll 1, \quad \text{(Onsager)}, \tag{2.93}$$

to order $\ln\left[\ln(1/t)\right]/\ln(1/t)$.

We contrast the result (2.93) with that of the Lorentz field,

$$M\left(\Omega_0^\perp\right)^2 \propto t, \quad t = \frac{T - T_c}{T_c} \ll 1, \quad \text{(Lorentz)}. \tag{2.94}$$

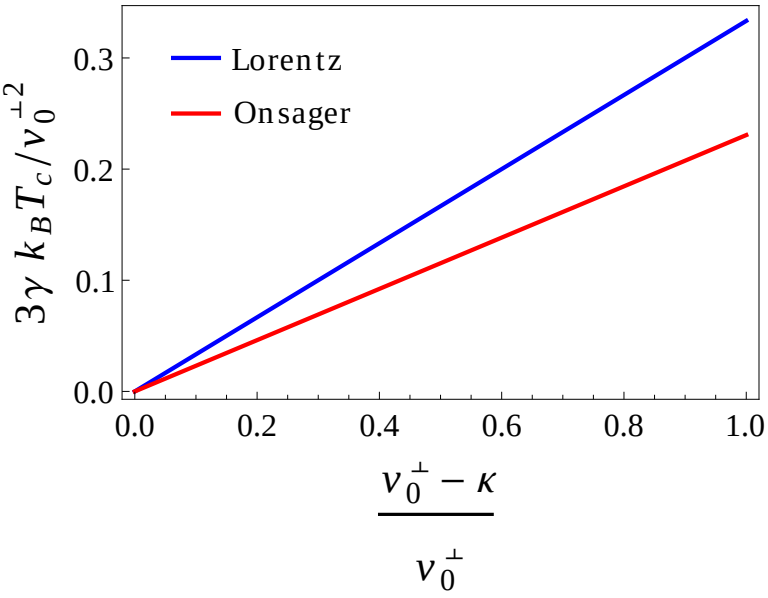

Figure 2.1: Critical temperatures in the Lorentz and Onsager approximations.

We see that the soft mode in the Lorentz field approximation gives Cochran's law, i.e, $M\left(\Omega_0^{\perp}\right)^2 \propto t$ for $t \to 0$. [22, 23] A plot of the temperature dependence of $M\left(\Omega_0^{\perp}\right)^2$ in the Lorentz and Onsager approximations is shown in Fig. 2.2.

Logarithmic corrections such as that of Eq. (2.93) are typical of uniaxial dipolar systems. This is confirmed by renormalization group methods and diagrammatic techniques for uniaxial ferroelectrics which give a logarithmic correction such as that of Eq. (2.93) but with a different power, $M\left(\Omega_0^{\perp}\right)^2 \propto t/(\log(1/t))^{1/3}$. [77, 78] These logarithmic corrections to the Lorentz result (2.94), are difficult to observe and have not been found in conventional ferroelectrics (the transition is of first order [79]). They have been observed, however, in dipolar magnets. [80]

The temperature dependence of the susceptibility in the Onsager model is simply

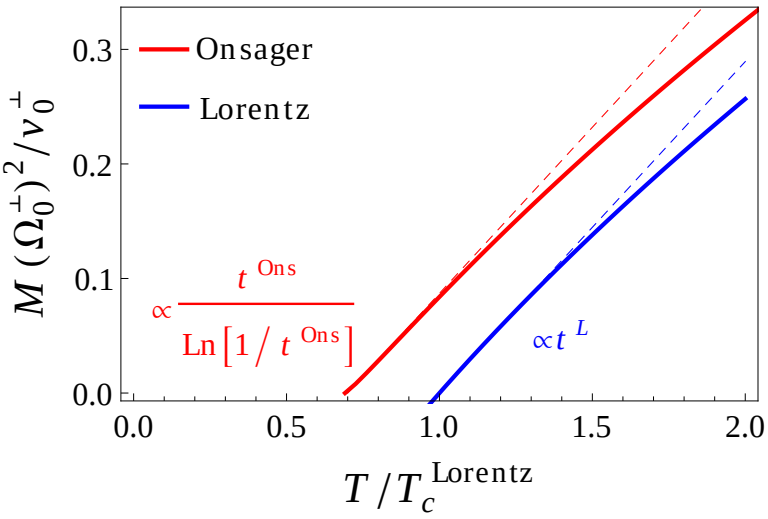

Figure 2.2: Temperature dependence of the transverse optic frequency in the Lorentz and Onsager approximations. Here, $t^{Ons} = (T - T_c^{Ons})/T_c^{Ons}$ and $t^L = (T - T_c^L)/T_c^L$ where T_c^{Ons} and T_c^L are the critical temperatures in the Onsager and Lorentz approximations (see Eqs. (2.86) and (2.88).

given by the inverse phonon frequency, Eq. (2.83). For $T \to T_c$, we obtain the result,

$$\chi_0^{\perp} = \frac{1}{M\left(\Omega_0^{\perp}\right)^2} \propto \frac{1}{t/\ln(1/t)}, \quad t = \frac{T - T_c}{T_c} \ll 1, \tag{2.95}$$

where $\chi_0^{\perp}$ is the $\boldsymbol{q} = 0$ component of the susceptibility in the direction perpendicular to the polar axis (see Eq. (2.83)). From (2.95) we determine Curie-Weiss constant C_{CW} to be determined by the anharmonic coefficient, $C_{CW} \propto 1/\gamma$ ($T_c \propto 1/\gamma$, see Eq. (2.86)). This is typical of displacive ferroelectrics and it is the same result obtained from the Lorentz approximation.

Let us now consider the susceptibility at large temperatures ($T \gg T_c$). For $T \gg T_c$, Eqs. (2.81b), and (2.81c) give the following the temperature behavior for $\Omega_0^{\perp}$,

$$M\left(\Omega_0^{\perp}\right)^2 = \sqrt{3\gamma k_B T}, \quad (T \gg T_c). \tag{2.96}$$

For large temperatures, there is no distinction between the longitudinal and transverse components of the susceptibility (see Eq. (2.84)). Substitution of Eq. (2.96) into (2.83)

gives,

$$\chi_0^{\parallel} \simeq \chi_0^{\perp} = \frac{1}{\sqrt{3\gamma k_B T}}, \quad (T \gg T_c). \tag{2.97}$$

The results (2.96) and (2.97) are identical to those in the Lorentz approximation (see Eqs. (2.52) and (2.53)). This is expected since fluctuations are important only close to the critical point.

The results (2.97) and (2.96) must be taken with caution: for large temperatures ($T \gg T_c$), the anharmonic effects may be more important and invalidate the quasi-harmonic approximation used here.

We conclude our discussion of the paraelectric and onset of the ferroelectric transition in the Onsager approximation here. In the next section we calculate the structure factor for conventional ferroelectrics.

2.4.1 Structure Factor without Random Fields

The dynamical structure factor $S_{\boldsymbol{q}}(\omega)$ for $T > T_c$ is as follows, [81]

$$S_{\boldsymbol{q}}(\omega) = \hbar \coth\left(\frac{\beta\hbar\omega}{2}\right) \mathrm{Im}\left[\chi_{\boldsymbol{q}}(\omega)\right] \tag{2.98}$$

The static structure factor $S_{\boldsymbol{q}}$ is given as follows,

$$S_{\boldsymbol{q}} = \frac{1}{2\pi}\int_{-\infty}^{\infty} d\omega\, S_{\boldsymbol{q}}(\omega) = \frac{\hbar}{2M\Omega_{\boldsymbol{q}}} \coth\left(\frac{\beta\hbar\Omega_{\boldsymbol{q}}}{2}\right) \tag{2.99}$$

In the classical limit ($\hbar \to 0$),

$$S_{\boldsymbol{q}} = \frac{k_B T}{M(\Omega_{\boldsymbol{q}})^2} = \frac{k_B T}{M\left(\Omega_0^{\perp}\right)^2 + \left(v_0^{\perp} - v_{\boldsymbol{q}}\right)} \tag{2.100}$$

where,

$$\lim_{\boldsymbol{q}\to 0} \frac{v_0^{\perp} - v_{\boldsymbol{q}}}{nz^{*2}} = 4\pi\frac{q_z^2}{|\boldsymbol{q}|^2} + \eta|\boldsymbol{q}a|^2 - 3\eta(q_z a)^2. \tag{2.101}$$

Here, n is the number of dipoles per unit volume; a is the lattice constant; z^* is the effective charge of the unit cell. $S_{\boldsymbol{q}}$ is non-analytic since $v_{\boldsymbol{q}}$ is non-analytic.

The component of $S_{\boldsymbol{q}}$ perpendicular to the polar axis ($\boldsymbol{q} \perp \hat{\boldsymbol{z}}$) has the shape of a Lorentzian in the long-wavelength limit,

$$S_{\boldsymbol{q}}^{\perp} = \frac{k_B T}{M\left(\Omega_0^{\perp}\right)^2 + \frac{v_0^{\perp}\eta}{4\pi/3}\left[(q_x a)^2 + (q_y a)^2\right]} \tag{2.102}$$

$S_{\boldsymbol{q}}^{\perp}$ is observed in neutron scattering experiments of conventional ferroelectrics such as $BaTiO_3$. [48]

2.4.2 Correlation Functions of Polarization in Real Space without Random Fields

In this section, we compute the correlation functions of polarization in real space. We do the calculation in the classical limit, $\hbar \to 0$ and in the paraelectric phase ($T > T_c$).

The static correlation functions of polarization are obtained from the structure factor $S_{\boldsymbol{q}}$ of Eq. (2.100). In the paraelectric phase ($T > T_c$),

$$\begin{aligned} \langle u_i u_j \rangle_{th} &= \frac{1}{N}\sum_{\boldsymbol{q}} e^{-i\boldsymbol{q}\cdot\boldsymbol{R}_{ij}} S_{\boldsymbol{q}} \\ &= \frac{1}{N}\sum_{\boldsymbol{q}} e^{-i\boldsymbol{q}\cdot\boldsymbol{R}_{ij}} \frac{k_B T}{\left(\chi_0^{\perp}\right)^{-1} + \left(v_0^{\perp} - v_{\boldsymbol{q}}\right)} \end{aligned} \tag{2.103}$$

where where $\left(\chi_0^{\perp}\right)^{-1} = M\left(\Omega_0^{\perp}\right)^2$ and

$$\lim_{\boldsymbol{q}\to 0} \frac{v_{\boldsymbol{q}}}{n z^{*2}} = \frac{4\pi}{3}\left(1 - 3\frac{q_z^2}{|\boldsymbol{q}|^2}\right) - \eta|\boldsymbol{q}a|^2 + 3\eta(q_z a)^2 \tag{2.104}$$

where n is the number of lattice points per unit volume and η is a dimensionless coefficient that depends on the structure of the lattice ($\eta \simeq 0.084$ for FCC lattices).

Close to the critical point ($T \gtrsim T_c$), the correlation functions of polarization for the uniaxial dipolar system are anisotropic and decay as power laws for large distances,

(see Appendix B)

$$\langle u_i u_j \rangle_{th} = \begin{cases} \frac{4\pi}{3}\frac{k_B T}{v_0^\perp} \times \frac{16\pi^3}{v_{BZ}} \times \frac{(\bar{\chi}_0^\perp)^2}{|\boldsymbol{R}_{ij}|^3}, & |\boldsymbol{R}_{ij}| \to \infty,\ \boldsymbol{R}_{ij} \parallel \hat{\boldsymbol{z}}, \\ -\frac{4\pi}{3}\frac{k_B T}{v_0^\perp} \times \frac{\pi^{3/2}}{v_{BZ}} \frac{\left(\bar{\chi}_0^\perp\right)^{1/2}}{|\boldsymbol{R}_{ij}|^3}, & |\boldsymbol{R}_{ij}| \to \infty,\ \boldsymbol{R} \perp \hat{\boldsymbol{z}}. \end{cases} \tag{2.105}$$

where $\left(\bar{\chi}_0^\perp\right)^{-1} = (4\pi/3)\left(\chi_0^\perp\right)^{-1}/v_0^\perp \to 0$ is a dimensionless susceptibility; and v_{BZ} is the volume of the Brillouin zone of the FCC or BCC lattice. This is in sharp contrast with short-range forces where the correlation functions are isotropic and decay exponentially, $\langle S_i S_j \rangle_{th} \sim (1/|\boldsymbol{R}_{ij}|)\exp\left[-|\boldsymbol{R}_{ij}|/\xi\right]$, where $\xi \propto \chi^{1/2}$ is the correlation length.

At the critical point ($T = T_c$) the correlation functions for the uniaxial dipolar system decay as power laws for large distances,

$$\langle u_i u_j \rangle_{th} = \frac{4\pi}{3}\frac{k_B T}{v_0^\perp} \times \frac{\pi^2}{v_{BZ}\eta a^2}\frac{1}{|\boldsymbol{R}|_{ij}}, \quad |\boldsymbol{R}|_{ij} \to \infty,\ \boldsymbol{R} \parallel \hat{\boldsymbol{z}}. \tag{2.106}$$

We now discuss the near-neighbor correlations. The results presented here are meant to give a qualitative description of the behavior of the correlations since our calculation uses $v_{\boldsymbol{q}}$ in the long-wavelength limit (see Eq. (2.104)). $v_{\boldsymbol{q}}$ differs from (3.16) as $\boldsymbol{q}$ approached the edge of the Brillouin zone. The results are shown in Fig. 2.3. For short distances, the longitudinal component ($\boldsymbol{R}_{ij} \parallel \hat{\boldsymbol{z}}$) is positive (see Fig. 2.3 (a)) whereas the transverse component ($\boldsymbol{R}_{ij} \perp \hat{\boldsymbol{z}}$) is negative (see Fig. 2.3 (b)). The longitudinal component is significantly greater than the transverse component, particularly close to T_c. Thus, even though the transverse correlations prefer antiferroelectric order, the system orders ferroelectrically since the (ferroelectric) longitudinal correlations are stronger than the transverse component.

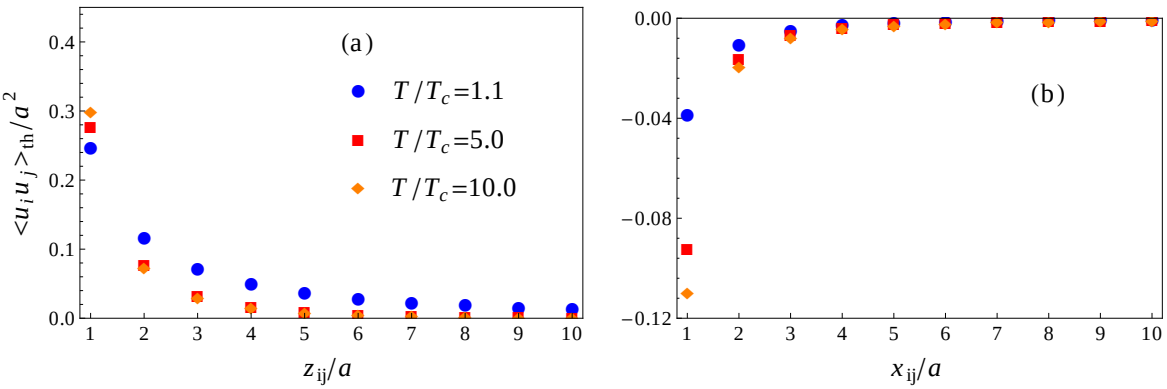

Figure 2.3: Near-neighbor correlation functions of polarization for a ferroelectric without disorder in the paraelectric phase. The longitudinal component, $\boldsymbol{R}_{ij} \parallel \hat{\boldsymbol{z}}$, (a) is positive and the transverse, $\boldsymbol{R}_{ij} \perp \hat{\boldsymbol{z}}$, (b) is negative. The longitudinal component is significantly greater than the transverse component. Here, circles, squares, and rhombohedrons are for $T/T_c = 10.0, 5.0, 1.1$, respectively. The lattice is FCC.

Chapter 3

Theory of Relaxor Ferroelectrics

In this chapter, we present our model for relaxor ferroelectrics. First, we introduce a model Hamiltonian in terms of polarizable unit cells with local forces, dipolar forces and compositional disorder. Second, we derive an effective Hamiltonian within the Onsager approximation. Third, we study the thermodynamics of the model within the Onsager approximation and discuss the onset of the diffuse phase transition. A comparison to experiments is provided.

3.1 Model Hamiltonian

We consider a simplified model of an uniaxial ferroelectric with compositional disorder in which the displacements of the ions in the unit cell i are described by a local displacement field $\boldsymbol{u}_i$ along the polar axis (here, arbitrarily chosen to be the z-axis). $\boldsymbol{u}_i$ is a linear combination of the displacements of the individual ions taking part in the soft transverse optic mode, the condensation of which leads to the distorted structure in the absence of disorder. [61, 62, 63] The cell at site i experiences a local random field h_i with

probability $\mathcal{P}(h_1, ..., h_N)$. The local random field arise from strong compositional disorder. For instance, the random distribution over the B-site, different ionic radii and different valencies of Mg^{+2}, Nb^{+5} in PMN, generate strong local random fields.

We consider the following model Hamiltonian,

$$H = \sum_i \left[\frac{\Pi_i^2}{2M} + V(u_i) \right] - \frac{1}{2} \sum_{i,j} v_{ij} u_i u_j - \sum_i E_i^{ext} u_i - \sum_i h_i u_i. \tag{3.1}$$

Here, u_i is the displacement associated with the transverse optic mode such that $z^* u_i$ is the dipole moment of the unit cell at site $\boldsymbol{R}_i$ and z^* is the effective charge of the unit cell. $\Pi_i = M\dot{u}_i$ is the conjugate momentum of the displacement associated with the the dipole u_i; M is an effective mass; and E_i^{ext} is an external applied field. The h_i's are local random electric fields with a probability distribution $\mathcal{P}(h_1, ..., h_N)$. We assume the h_i's are independent random variables with zero mean and variance Δ^2,

$$\langle h_i \rangle_c = \int dh_1 \cdots dh_N h_i \mathcal{P}(h_1, ..., h_N) = 0, \quad \langle h_i h_j \rangle_c = \int dh_1 \cdots dh_N h_i h_j \mathcal{P}(h_1, ..., h_N) = \Delta^2 \delta_{ij} \tag{3.2}$$

where δ_{ij} is the Kronecker delta.

$V(u_i)$ is an anharmonic potential,

$$V(u_i) = \frac{\kappa}{2} u_i^2 + \frac{\gamma}{4} u_i^4, \tag{3.3}$$

where κ, γ are positive constants.

v_{ij} is the dipole interaction,

$$v_{ij}/z^{*2} = \begin{cases} 3\frac{(z_i - z_j)^2}{|\boldsymbol{R}_i - \boldsymbol{R}_j|^5} - \frac{1}{|\boldsymbol{R}_i - \boldsymbol{R}_j|^3}, & \boldsymbol{R}_i \neq \boldsymbol{R}_j \\ 0, & \boldsymbol{R}_i = \boldsymbol{R}_j, \end{cases} \tag{3.4}$$

where a is the lattice constant.

The Fourier transform of the dipole interaction,

$$v_{\boldsymbol{q}} = \sum_{i,j} v_{ij} e^{i\boldsymbol{q}\cdot(\boldsymbol{R}_i - \boldsymbol{R}_j)} \tag{3.5}$$

is non-analytic for $\boldsymbol{q} \to 0$, i.e., its value depends on the direction in which $\boldsymbol{q}$ approaches zero. For cubic lattices and $\boldsymbol{q} \to 0$, $v_{\boldsymbol{q}}$ has the form, [64, 65]

$$\lim_{\boldsymbol{q}\to 0} \frac{v_{\boldsymbol{q}}}{nz^{*2}} = \frac{4\pi}{3}\left(1 - 3\frac{q_z^2}{|\boldsymbol{q}|^2}\right) - \eta|\boldsymbol{q}a|^2 + 3\eta(q_z a)^2 \tag{3.6}$$

where n is the number of lattice points per unit volume and η is a dimensionless coefficient that depends on the structure of the lattice ($\eta \simeq 0.084$ for FCC lattices).

We will use the notation,

$$v_0 = \begin{cases} v_0^{\perp} = \frac{4\pi}{3} nz^{*2}, & \boldsymbol{q} \perp \hat{z} \text{ (transverse)} \\ v_0^{\parallel} = -\frac{8\pi}{3} nz^{*2}, & \boldsymbol{q} \parallel \hat{z} \text{ (longitudinal)} \end{cases} \tag{3.7}$$

Disorder in the relaxors is quenched, therefore, the average over compositional disorder must be performed after the thermal averages. Here, we will use the notation,

$$\langle(\dots)\rangle_c = \int dh_1 \dots dh_N \mathcal{P}(h_1, ..., h_N)(\dots) \tag{3.8}$$

to denote average over compositional disorder.

Several simplifications are made in writing the Hamiltonian (3.1): we ignore (i) the full cubic symmetry typical of perovskite relaxor ferroelectrics (ii) coupling of the transverse optic mode to the transverse acoustic mode (see Ref. [11, 12].); (iii) coupling to strain; (iv) short-range interactions between unit cells; and (v) disorder in the dipolar bonds v_{ij}. For conventional ferroelectrics, it is well known what (i)-(iv) do to the minimal model of ferroelectricity (see Sec. 2.1). For relaxor ferroelectrics, it is not clear at the current state of research: there is no satisfactory theoretical description of the relaxors (see Sec. 1.4).

Inclusion of (i)-(iv) in our model, Eq. (3.1), is beyond the scope of the present work, which is to study the effect of quenched random fields in the minimal model for conventional ferroelectrics. Disorder in the dipolar bonds v_{ij} is expected due to compositional disorder in B-site of the relaxor unit cell. Here, we assume its effect is secondary in describing the broad region of fluctuations, as suggested by the line shape of the elastic diffuse scattering measured with neutrons (see Sec. 1.3.3). In the conclusions we discuss some of the possible consequences of incorporating (i)-(v) in the model Hamiltonian (3.1).

Despite the simplifications mentioned above, we show that the Hamiltonian (3.1) gives a fairly good description of the diffuse phase transition observed the relaxors.

The Hamiltonian (2.1) presents several difficulties: (i) long ranged anisotropic dipolar forces; (ii) compositional disorder; and (iii) anharmonic local forces.

To handle the dipolar forces, we adhere to the Onsager field approximation described in Sec. 2.2. This approximation is essential to describe the fluctuations of polarization in the relaxors. As discussed in Secs. 1.3 and 2.2, compositional disorder in the relaxors extends the region of critical fluctuations over a broad range of temperatures, which, together with the dipolar forces, become significant down to zero temperature. [74] It is then essential that any theory of relaxor ferroelectrics accounts for the fluctuations of polarization at all temperatures. The Lorentz field approximation violates the fluctuation dissipation theorem of statistical mechanics and, consequently, fails to account for such fluctuations. On the other hand, the Onsager approximation is the simplest necessary correction to the Lorentz field which accounts for the fluctuations and guarantees the fluctuation dissipation theorem. [75, 76]

To handle compositional disorder, we use a self-consistent approach used to study

two and three dimensional magnets with quenched random fields. [52]. The basic idea is to relate the local polarization to the random fields and to the susceptibility averaged over compositional disorder. [52] This self-consistent method gives a lower critical dimension of three for the random field Ising model, although there is no consensus on the lower critical dimension d_l of the random field Ising model: the Imry and Ma criterion based on domain-wall arguments favor $d_l = 2$ [82], whereas ϵ-expansion and supersymmetry arguments favor $d_l = 3$ [51, 83, 84, 85]. More complex arguments favor $d_l = 2$. [86] We point out, however, that these results do not apply to the model considered here nor to the relaxors in general. This is because (i) relaxors are not uniaxial systems but have cubic symmetry and (ii) the dominant forces are not isotropic and short-ranged but anisotropic and long-ranged. The great advantage of the self-consistent approach is its simplicity and that it gives a fairly reasonable agreement with the observed critical fluctuations (Lorentzian plus Lorentzian squared) in systems with isotropic short-range forces and compositional disorder. [13, 14, 15, 16, 52].

To handle the local anharmonic forces, we use the quasi-harmonic approximation, similar to that of conventional displacive ferroelectrics (see Sec. 2.1). The basic idea is to assume that the local potential $V(u_i)$ of Eq. (3.3) is slightly anharmonic so the equations of motion can be linearized after configurational average has been taken. This reduces the problem to that of a harmonic oscillator with a renormalized phonon frequency which is determined self-consistently. We justify the use of a quasi-harmonic assumption in the relaxors since (i) the observed Curie-Weiss constant is very large (see, for instance, Fig. 1.6 (b)) and (ii) the observed shape of the probability density of the displacements of the ions is a Gaussian centered at the equilibrium lattice point for temperatures above the Burns

temperature (see Sec. 1.2). [26, 27] The details of the quasi-harmonic approximation are presented in Sec. 3.2.

3.2 Model for Relaxor Ferroelectrics in the Onsager Approximation

We now study the thermodynamics of the model Hamiltonian (3.1) in the Onsager field approximation.

We first write the exact Hamiltonian (3.1) in the Onsager approximation. The derivation of the effective Hamiltonian in the Onsager approximation is almost identical to that of conventional ferroelectrics (see Sec. 2.2), except that one incorporates the random field h_i.

The Hamiltonian (3.1) in the Onsager approximation is a sum of single cell Hamiltonians $H_i^{Onsager}$,

$$H = \sum_i H_i^{Onsager} = \sum_i \left(H_i^0 - h_i u_i - E_i^{cavity} u_i \right). \tag{3.9}$$

H_i^0 is the non-interacting part of the Hamiltonian,

$$H_i^0 = \frac{\Pi_i^2}{2M} + V(u_i) - \frac{\lambda}{2} u_i^2, \tag{3.10}$$

where u_i is the displacement along the z-axis of the unit cell at site $\boldsymbol{R}_i$; and $\langle u_i \rangle_{th}$ its thermal average. $\Pi_i = M\dot{u}_i$ is the conjugate momentum of the displacement associated with the the displacement u_i; M is an effective mass. $V(u_i)$ is an anharmonic potential,

$$V(u_i) = \frac{\kappa}{2} u_i^2 + \frac{\gamma}{4} u_i^4, \tag{3.11}$$

where $\kappa,\ \gamma$ are positive constants.

h_i of Eq. (3.9) is a local random electric field with zero mean and variance Δ^2,

$$\langle h_i \rangle_c = 0, \quad \langle h_i h_j \rangle_c = \Delta^2 \delta_{ij}. \tag{3.12}$$

Here, δ_{ij} is the Kronecker delta.

E_i^{cavity} in Eq. (3.9) is Onsager's cavity field,

$$E_i^{cavity} = \sum_j v_{ij} \langle u_j \rangle_{th} - \lambda \langle u_i \rangle_{th} + E_i^{ext}. \tag{3.13}$$

v_{ij} is the dipole interaction,

$$v_{ij}/z^{*2} = \begin{cases} 3\frac{(z_i - z_j)^2}{|\boldsymbol{R}_i - \boldsymbol{R}_j|^5} - \frac{1}{|\boldsymbol{R}_i - \boldsymbol{R}_j|^3}, & \boldsymbol{R}_i \neq \boldsymbol{R}_j \\ 0, & \boldsymbol{R}_i = \boldsymbol{R}_j, \end{cases} \tag{3.14}$$

where z^* is the effective charge of the unit cell; a is the lattice constant.

The Fourier transform of the dipole interaction,

$$v_{\boldsymbol{q}} = \sum_{i,j} v_{ij} e^{i\boldsymbol{q}\cdot(\boldsymbol{R}_i - \boldsymbol{R}_j)} \tag{3.15}$$

is non-analytic for $\boldsymbol{q} \to 0$, i.e., its value depends on the direction in which $\boldsymbol{q}$ approaches zero. For cubic lattices and $\boldsymbol{q} \to 0$, $v_{\boldsymbol{q}}$ has the form, [64, 65]

$$\lim_{\boldsymbol{q}\to 0} \frac{v_{\boldsymbol{q}}}{nz^{*2}} = \frac{4\pi}{3}\left(1 - 3\frac{q_z^2}{|\boldsymbol{q}|^2}\right) - \eta|\boldsymbol{q}a|^2 + 3\eta(q_z a)^2 \tag{3.16}$$

where n is the number of lattice points per unit volume and η is a dimensionless coefficient that depends on the structure of the lattice ($\eta \simeq 0.084$ for FCC lattices).

We will use the notation,

$$v_0 = \begin{cases} v_0^{\perp} = \frac{4\pi}{3} nz^{*2}, & \boldsymbol{q} \perp \hat{z} \text{ (transverse)} \\ v_0^{\parallel} = -\frac{8\pi}{3} nz^{*2}, & \boldsymbol{q} \parallel \hat{z} \text{ (longitudinal)} \end{cases} \tag{3.17}$$

The Hamiltonian in the Onsager approximation, Eq. (3.9), is the sum of single cell Hamiltonians $H_i^{Onsager}$ in which a dipole experiences a a local potential $V(u_i) - (\lambda/2)u_i^2$; a random field h_i; and a cavity field E_i^{cavity}.

The Hamiltonian (3.9) has several advantages: (i) it has reduced the many-body problem (3.1) to a single-body problem; and (ii) it incorporates fluctuations of polarization through the parameter λ, which are essential for the relaxors (see Secs. 1.3 and 2.2). Eq. (3.9) is the starting point of our calculations.

Our goal is to derive self-consistent equations for the phonon frequencies. These, in turn, will determine the susceptibility and the fluctuations of polarization. To do so, we use linear response theory,

$$\begin{aligned} \langle u_i \rangle_{th} &= \phi_{h_i}(\omega) E_i^{cavity} \\ &= \phi_{h_i}(\omega) \left[\sum_j v_{ij} \langle u_j \rangle_{th} + E_i^{ext}(t) - \lambda \langle u_i \rangle_{th} \right] \end{aligned} \tag{3.18}$$

Here, $\phi_{h_i}(\omega)$ is the susceptibility of the non-interacting problem with a random field, $H_i^0 - u_i h_i$.

We first take configurational average and assume decoupling effects of the random fields h_i on $\phi_{h_i}(\omega)$ and $\langle u_i \rangle_{th}$.

$$\langle \langle u_i \rangle_{th} \rangle_c = \langle \phi_{h_i}(\omega) \rangle_c \left[\sum_j v_{ij} \left\langle \langle u_j \rangle_{th} \right\rangle_c + E_i^{ext}(t) - \lambda \left\langle \langle u_i \rangle_{th} \right\rangle_c \right] \tag{3.19}$$

By Fourier transforming,

$$\chi_{\boldsymbol{q}}(\omega) = \frac{u_{\boldsymbol{q}}}{E_{\boldsymbol{q}}} = \frac{1}{\langle \phi_{h_i}(\omega) \rangle_c^{-1} + (v_{\boldsymbol{q}} - \lambda)} \tag{3.20}$$

We now determine the polarizability of the non-interacting problem with a random field. The equation of motion of a dipole in a local potential $V(u_i) - \lambda u_i^2/2$ and in a local

random field h_i is as follows,

$$M\ddot{u}_i = -\frac{dV(u_i)}{du_i} + \lambda u_i + h_i + E_i^{ext}(t) - \Gamma\dot{u}_i$$
$$= -\kappa u_i + \lambda u_i - \gamma u_i^3 + \lambda u_i + h_i + E_i^{ext}(t) - \Gamma\dot{u}_i. \tag{3.21}$$

Here, $E_i^{ext}(t) = E_i^{ext}e^{i\omega t}$ is an infinitesimal external field. We have added a retarded force which gives rise to damping. The damping constant is Γ.

We now linearize the equation (3.21). We consider fluctuations σ_i around the expectation value of u_i,

$$u_i = \left\langle \langle u_i \rangle_{th}^0 \right\rangle_c + \sigma_i \tag{3.22}$$

Here, $\left\langle \langle \ldots \rangle_{th}^0 \right\rangle_c$ denotes thermal and compositional average with $E_i^{ext}(t) = 0$. σ_i are the fluctuations around $\left\langle \langle u_i \rangle_{th}^0 \right\rangle_c$ with zero average in the absence of the external field, i.e., $\left\langle \langle \sigma_i \rangle_{th}^0 \right\rangle_c = 0$ for $E_i^{ext}(t) = 0$. Substitution of (3.22) into (3.21) gives,

$$M\ddot{\sigma}_i = -(\kappa - \lambda)\left(\left\langle \langle u_i \rangle_{th}^0 \right\rangle_c + \sigma_i\right)$$
$$-\gamma\left(\left\langle \langle u_i \rangle_{th}^0 \right\rangle_c^3 + 3\left\langle \langle u_i \rangle_{th}^0 \right\rangle_c^2 \sigma_i + 3\left\langle \langle u_i \rangle_{th}^0 \right\rangle_c \sigma_i^2 + \sigma_i^3\right)$$
$$+ h_i + E_i^{ext}(t) - \Gamma\dot{\sigma}_i. \tag{3.23}$$

We now assume quasi-harmonic approximation in the absence of the external applied field, i.e, $\langle\langle\ddot{\sigma}_i\rangle_{th}\rangle_c = 0, \langle\langle\dot{\sigma}_i\rangle_{th}\rangle_c = 0$ for $E_i^{ext} = 0$

$$\left[(\kappa - \lambda) + \gamma\left\langle \langle u_i \rangle_{th}^0 \right\rangle_c^2 + 3\gamma\left\langle \langle \sigma_i^2 \rangle_{th}^0 \right\rangle_c\right]\left\langle \langle u_i \rangle_{th}^0 \right\rangle_c = 0 \tag{3.24}$$

Here, $\left\langle \langle \ldots \rangle_{th}^0 \right\rangle_c$ denotes thermal and compositional average with $E_i^{ext}(t) = 0$. Here, we used $\left\langle \langle \sigma_i \rangle_{th}^0 \right\rangle_c = 0$.

We now subtract the above equation from (3.23),

$$M\ddot{\sigma}_i = -(\kappa - \lambda)\sigma_i - \gamma\left[3\left\langle \langle u_i \rangle_{th}^0 \right\rangle_c^2 \sigma_i + 3\left\langle \langle \sigma_i \rangle_{th}^0 \right\rangle_c\left[\sigma_i^2 - \left\langle \langle \sigma_i^2 \rangle_{th}^0 \right\rangle_c\right] + \sigma_i^3\right] + h_i + E_i^{ext}(t) - \Gamma\dot{\sigma}_i \tag{3.25}$$

By approximating the fluctuations σ_i^2 to their static average, $\sigma_i^2 \simeq \left\langle \langle \sigma_i^2 \rangle_{th}^0 \right\rangle_c$ in (3.25), we obtain the equation of motion,

$$M\ddot{\sigma}_i = -M\Omega'^2 \sigma_i + h_i + E_i^{ext}(t) - \Gamma \dot{\sigma}_i \tag{3.26}$$

where,

$$M\Omega'^2 \equiv \kappa - \lambda + 3\gamma \left(\left\langle \langle \sigma_i^2 \rangle_{th}^0 \right\rangle_c + \left\langle \langle u_i \rangle_{th}^0 \right\rangle_c^2 \right) \tag{3.27}$$

Eq. (3.26) is the equation of motion of a damped harmonic oscillator with frequency Ω' in a external field $E_i^{ext}(t)$.

We now determine the fluctuations $\left\langle \langle \sigma_i^2 \rangle_{th}^0 \right\rangle_c$ of the non-interacting system in random field.

First, we determine the fluctuations of the non-interacting system from those of an undamped quantum harmonic oscillator with frequency Ω' in a random field h_i. For a fixed realization of disorder, the fluctuations are independent of the field h_i,

$$\langle u_i^2 \rangle_{th}^0 - \langle u_i \rangle_{th}^{0\ 2}, = \frac{\hbar}{2M\Omega'} \coth\left(\frac{\beta\hbar\Omega'}{2}\right) \tag{3.28}$$

Therefore, upon taking configurational average,

$$\left\langle \langle u_i^2 \rangle_{th}^0 \right\rangle_c - \left\langle \langle u_i \rangle_{th}^{0\ 2} \right\rangle_c = \frac{\hbar}{2M\Omega'} \coth\left(\frac{\beta\hbar\Omega'}{2}\right). \tag{3.29}$$

We leave $\left\langle \langle u_i \rangle_{th}^{0\ 2} \right\rangle_c$ unspecified for now. The fluctuations $\left\langle \langle \sigma_i \rangle_{th}^0 \right\rangle_c$ of the non-interacting problem are given as follows,

$$\begin{aligned} \langle \langle \sigma_i^2 \rangle_{th} \rangle_c &= \left\langle \langle u_i^2 \rangle_{th}^0 \right\rangle_c - \left\langle \langle u_i \rangle_{th}^0 \right\rangle_c^2 \\ &= \frac{\hbar}{2M\Omega'} \coth\left(\frac{\beta\hbar\Omega'}{2}\right) + \left\langle \langle u_i \rangle_{th}^{0\ 2} \right\rangle_c - \left\langle \langle u_i \rangle_{th}^0 \right\rangle_c^2 \end{aligned} \tag{3.30}$$

We are now ready to determine the susceptibility $\langle \phi_{h_i}(\omega) \rangle_c$ of the non-interacting system in a random field. $\langle \phi_{h_i}(\omega) \rangle_c$ is easily obtained from (3.26),

$$\langle \phi_{h_i}(\omega) \rangle_c = \frac{1}{M\Omega'^2 - \omega^2 + i\omega\Gamma} \tag{3.31}$$

where Ω' is given in Eq. (3.27).

We have now determined the susceptibility $\langle \phi_{h_i}(\omega) \rangle_c$ of the non-interacting problem in a random field.

$$\chi_{\boldsymbol{q}}(\omega) = \frac{1}{M\Omega'^2 - M\omega^2 + i\omega\Gamma - (v_{\boldsymbol{q}} - \lambda)} \tag{3.32}$$

We recast the susceptibility (3.32) as follows,

$$\chi_{\boldsymbol{q}}(\omega) = \frac{1}{M\Omega_{\boldsymbol{q}}^2 - M\omega^2 + i\omega\Gamma} \tag{3.33}$$

where we identify $\Omega_{\boldsymbol{q}}$ as the phonon frequency of the interacting problem,

$$M\Omega_{\boldsymbol{q}}^2 = M\left(\Omega_0^{\perp}\right)^2 + \left(v_0^{\perp} - v_{\boldsymbol{q}}\right) \tag{3.34}$$

and $\Omega_0^{\perp}$ is the $\boldsymbol{q} = 0$ component of the phonon frequency in the direction perpendicular to the polar axis ($\boldsymbol{q} \perp \hat{\boldsymbol{z}}$),

$$M\left(\Omega_0^{\perp}\right)^2 = M\Omega'^2 - \left(v_0^{\perp} - \lambda\right). \tag{3.35}$$

We now determine the parameter λ. We obtain λ by enforcing the fluctuation dissipation theorem, [75, 76]

$$\left\langle \langle u_i^2 \rangle_{th}^0 \right\rangle_c - \left\langle \langle u_i \rangle_{th}^{0\ 2} \right\rangle_c = \frac{1}{N} \sum_{\boldsymbol{q}} \frac{1}{2\pi} \int_{-\infty}^{\infty} d\omega \coth\left(\frac{\beta\hbar\omega}{2}\right) \mathrm{Im}\left[\chi_{\boldsymbol{q}}(\omega)\right] \tag{3.36}$$

where $\mathrm{Im}\left[\chi_{\boldsymbol{q}}(\omega)\right]$ is the imaginary part of the susceptibility (3.33). The summation over $\boldsymbol{q}$ extends over the first Brillouin zone.

We compute the integral (3.36) in the limit of zero damping. For zero damping, $\mathrm{Im}\left[\chi_{\boldsymbol{q}}(\omega)\right]$ becomes the sum of two Dirac delta functions peaked at $\omega = \pm\Omega_{\boldsymbol{q}}$,

$$\begin{aligned}\lim_{\Gamma\to 0}\mathrm{Im}\left[\chi_{\boldsymbol{q}}(\omega)\right] &= \lim_{\Gamma\to 0}\frac{\omega\Gamma}{M^2\left[\Omega_{\boldsymbol{q}}^2-\omega^2\right]^2+(\omega\Gamma)^2}\\ &= \frac{\pi}{2M}\left[\frac{1}{\omega}\,\delta\left(\omega-\Omega_{\boldsymbol{q}}\right)+\frac{1}{\omega}\,\delta\left(\omega+\Omega_{\boldsymbol{q}}\right)\right]\end{aligned} \tag{3.37}$$

Substitution of (3.37) into (3.36) gives,

$$\left\langle\left\langle u^2\right\rangle_{th}^0\right\rangle-\left\langle\left\langle u\right\rangle_{th}^{0\ 2}\right\rangle_c=\frac{1}{N}\sum_{\boldsymbol{q}}\frac{\hbar}{2M\Omega_{\boldsymbol{q}}}\coth\left(\frac{\beta\hbar\Omega_{\boldsymbol{q}}}{2}\right). \tag{3.38}$$

where the summation over $\boldsymbol{q}$ extends over the first Brillouin zone.

To close the system of equations the polarization $\langle u_i\rangle_{th}^0$ must itself be related to the random fields through the susceptibility (3.33). For a fixed realization of disorder, [52]

$$\langle u_i\rangle_{th}^0=\sum_j\langle\chi_{ij}\rangle_c\,h_j, \tag{3.39}$$

where $\langle\chi_{ij}\rangle_c$ is the susceptibility averaged over compositional disorder with Fourier transform $\chi_{\boldsymbol{q}}=\sum_{ij}\langle\chi_{ij}\rangle_c\,e^{i\boldsymbol{q}\cdot R_{ij}}$ where $\chi_{\boldsymbol{q}}$ is given by (3.33).

Since $\langle h_j\rangle_c=0$ and $\langle h_ih_j\rangle_c=\Delta^2\delta_{ij}$ by definition (see Eq. (3.12)), the order parameter vanishes and only quadratic terms in h differ from zero,

$$\left\langle\langle u\rangle_{th}^0\right\rangle_c=0,\quad\left\langle\langle u\rangle_{th}^{0\ 2}\right\rangle_c=\frac{\Delta^2}{N}\sum_{\boldsymbol{q}}\chi_{\boldsymbol{q}}^2, \tag{3.40}$$

where $\chi_{\boldsymbol{q}}$ is given by (3.33).

We use (3.27), (3.29), (3.30), (3.35), (3.38), (3.40) to eliminate λ and Ω'. The

resulting system of equations is the following,

$$M\Omega_{\boldsymbol{q}}^2 = M\left(\Omega_0^{\perp}\right)^2 + \left(v_0^{\perp} - v_{\boldsymbol{q}}\right), \tag{3.41a}$$

$$M\left(\Omega_0^{\perp}\right)^2 = \kappa + 3\gamma\left\langle\left\langle\sigma_i^2\right\rangle_{th}^0\right\rangle_c - v_0^{\perp}, \tag{3.41b}$$

$$\left\langle\left\langle\sigma_i^2\right\rangle_{th}^0\right\rangle_c = \left\langle\left\langle u_i^2\right\rangle_{th}^0\right\rangle_c \tag{3.41c}$$

$$\left\langle\left\langle u^2\right\rangle_{th}^0\right\rangle_c - \left\langle\left\langle u\right\rangle_{th}^{0\ 2}\right\rangle_c = \frac{1}{N}\sum_{\boldsymbol{q}}\frac{\hbar}{2M\Omega_{\boldsymbol{q}}}\coth\left(\frac{\beta\hbar\Omega_{\boldsymbol{q}}}{2}\right), \tag{3.41d}$$

$$\left\langle\left\langle u_i\right\rangle_{th}^{0\ 2}\right\rangle_c = \frac{1}{N}\sum_{\boldsymbol{q}}\frac{\Delta^2}{\left(M\Omega_{\boldsymbol{q}}^2\right)^2}. \tag{3.41e}$$

Equations (3.41a)-(3.41e) are the Onsager field equations of our model. Equations (3.41b)-(3.41e) determine the temperature dependence of the $\boldsymbol{q} = 0$ component of the phonon frequency $\Omega_0^{\perp}$. The temperature dependence of the $\boldsymbol{q} \neq 0$ component is determined by Eq. (3.41a). We recover the results for the uniaxial ferroelectric without compositional disorder in the paraelectric phase by setting $\Delta = 0$.

Our presentation of our model for the relaxors concludes here. In the next section we present and discuss the results obtained from our model.

3.2.1 Soft Mode

Here, we present the results for the calculated soft mode frequency from our model for the relaxors.

The results for the $\boldsymbol{q} = 0$ component of the phonon frequency, $\Omega_0^{\perp}$, are shown in Fig. 3.1 (a). For no disorder ($\Delta = 0$, gray dashed line), ${\Omega_0^{\perp}}^2 \sim T^{1/2}$ for high temperatures ($T \gg T_c$, not show in figure) and vanishes as $t/\ln(1/t)$, $t = (T - T_c)/T_c$ for $T \to T_c$. For finite disorder ($\Delta > 0$, blue,red and orange lines), ${\Omega_0^{\perp}}^2 \sim T^{1/2}$ for high temperatures ($T > T_c$, not shown in figure). As temperature decreases, ${\Omega_0^{\perp}}^2$ decreases approximately with linear dependence, remains finite at T_c, and it is fairly constant as it

approaches $T = 0$. At $T = 0$, $\Omega_0^{\perp}$ is finite for arbitrary small disorder Δ, as shown in Fig. 3.1 (b) (the integral in (3.41e) diverges logarithmically for $\Omega_0^{\perp} \to 0$, see Appendix A). Since ${\Omega_0^{\perp}}^2$ is positive at all temperatures, there is no lattice instability, the lattice remains cubic down to $T = 0$, and there is no long-range ferroelectric order at any temperature.

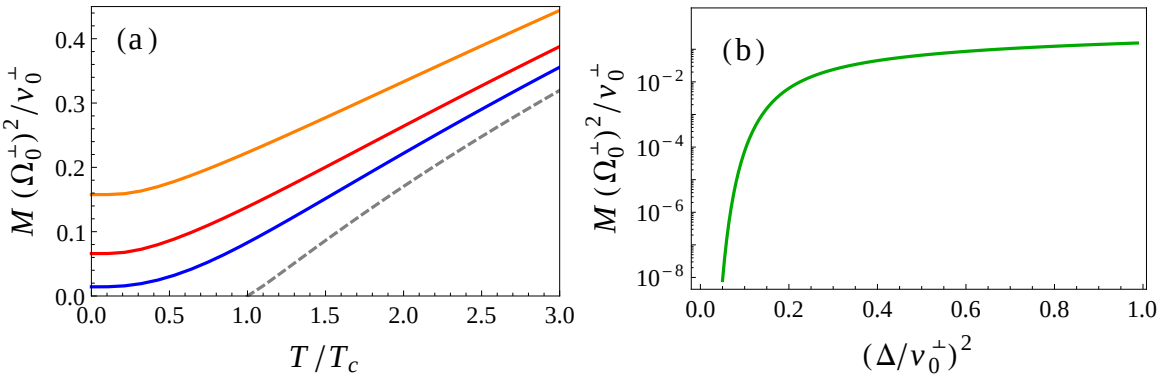

Figure 3.1: Temperature dependence of the phonon frequencies. (a) Blue, red, and orange lines are the phonon frequencies for a ferroelectric with compositional disorder $(\Delta^2/{v_0^{\perp}}^2 = 0.25, 0.50, 1.0)$ Gray dashed line is the phonon frequency without compositional disorder ($\Delta = 0$). (b) Log-linear plot of $\Omega_0^{\perp}$ against disorder. For arbitrary small compositional disorder the phonon frequencies remain finite down to $T = 0\,\mathrm{K}$. Here, $(v_0^{\perp} - \kappa)/v_0^{\perp} = 0.40$, $\gamma a^2/v_0^{\perp} = 0.10$, and $\hbar/(M v_0^{\perp} a^4)^{1/2} = 1.0$.

We contrast our results to those of the random field Ising model in 3 dimensions, i.e., isotropic short-range forces with random fields. The theoretical studies that favor the lower critical dimension $d_l = 3$, predict a finite correlation length at $T = 0$ for arbitrary small disorder Δ, thus, long-range order is absent. [51, 52, 83, 84, 85]. The theoretical studies that favor the lower critical dimension $d_l = 2$, predict a divergent correlation length at a finite temperature, therefore, there is long-range order. [82, 86].

We conclude our discussion of the phonon frequencies for an uniaxial ferroelectric with random fields here. In the next section, we present the calculation of the structure factor and compare it to that measured by neutron scattering experiments.

3.2.2 Structure Factor with Random Fields

In this section, we compute the dynamic and static structure factors.

The dynamical structure factor $S_{\boldsymbol{q}}(\omega)$ is as follows, [81]

$$S_{\boldsymbol{q}}(\omega) = S^{inel}_{\boldsymbol{q}}(\omega) + (2\pi)\delta(\omega)S^{el}_{\boldsymbol{q}}. \tag{3.42}$$

where $S^{inel}_{\boldsymbol{q}}(\omega)$ is the inelastic component of the structure factor,

$$S^{inel}_{\boldsymbol{q}}(\omega) = \hbar \coth\left(\frac{\beta\hbar\omega}{2}\right) \mathrm{Im}\left[\chi_{\boldsymbol{q}}(\omega)\right] \tag{3.43}$$

and $S^{el}_{\boldsymbol{q}}$ is the elastic component of the structure factor,

$$S^{el}_{\boldsymbol{q}} = \mathcal{FT}\left[\left\langle \langle u_i \rangle^2_{th} \right\rangle_c\right] = \frac{\Delta^2}{\left(M\,\Omega^2_{\boldsymbol{q}}\right)^2}, \quad M\,\Omega^2_{\boldsymbol{q}} = M\,\left(\Omega^{\perp}_0\right)^2 + (v^{\perp}_0 - v_{\boldsymbol{q}}) \tag{3.44}$$

where $\mathcal{FT}$ stands for Fourier transform. The phonon frequencies $\Omega^{\perp}_0$ are obtained from the Onsager equations (3.41).

The static structure factor $S_{\boldsymbol{q}}$ is obtained by integrating over the frequencies,

$$S_{\boldsymbol{q}} = \frac{1}{2\pi}\int_{-\infty}^{\infty} d\omega\, S_{\boldsymbol{q}}(\omega) = \frac{\hbar}{2M\Omega_{\boldsymbol{q}}} \coth\left(\frac{\beta\hbar\Omega_{\boldsymbol{q}}}{2}\right) + \frac{\Delta^2}{\left(M\Omega^2_{\boldsymbol{q}}\right)^2} \tag{3.45}$$

Since $v_{\boldsymbol{q}}$ is non-analytic for $\boldsymbol{q} \to 0$, the value of $S_{\boldsymbol{q}}$ depends on the direction in which $\boldsymbol{q}$ approaches zero. For systems without disorder, the observed static structure factor corresponds to its transverse component, i.e, $\boldsymbol{q}$ perpendicular to the polar axis $\hat{\boldsymbol{z}}$. For the relaxors, we will show that this is the component that is being observed.

The transverse component of $S_{\boldsymbol{q}}$ ($\boldsymbol{q} \perp \hat{\boldsymbol{z}}$) is as follows,

$$S^{\perp}_{\boldsymbol{q}} = \frac{\hbar}{2M\Omega^{\perp}_{\boldsymbol{q}}} \coth\left(\frac{\beta\hbar\Omega^{\perp}_{\boldsymbol{q}}}{2}\right) + \frac{\Delta^2}{\left(M(\Omega^{\perp}_{\boldsymbol{q}})^2\right)^2} \tag{3.46}$$

where,

$$M(\Omega^{\perp}_{\boldsymbol{q}})^2 = \lim_{\boldsymbol{q}\to 0, \boldsymbol{q}\perp\hat{\boldsymbol{z}}} M\Omega^2_{\boldsymbol{q}} = M(\Omega^{\perp}_0)^2 + \frac{3}{4\pi} v^{\perp}_0 \eta \left[(q_x a)^2 + (q_y a)^2\right] \tag{3.47}$$

Fig. 3.2 shows the temperature dependence of the $\boldsymbol{q} = 0$ transverse component of the structure factor $S_0^\perp$ of Eq. (3.46). For no compositional disorder ($\Delta = 0$), $S_0^\perp$ is small for large temperatures ($T \gg T_c$); it increases very rapidly for $T \to T_c$; and it diverges at T_c. For finite compositional disorder ($\Delta > 0$), $S_0^\perp$ is small for large temperatures ($T \gg T_c$); it increases at about $T \simeq T_c$; and it saturates at low temperatures ($T \ll T_c$).

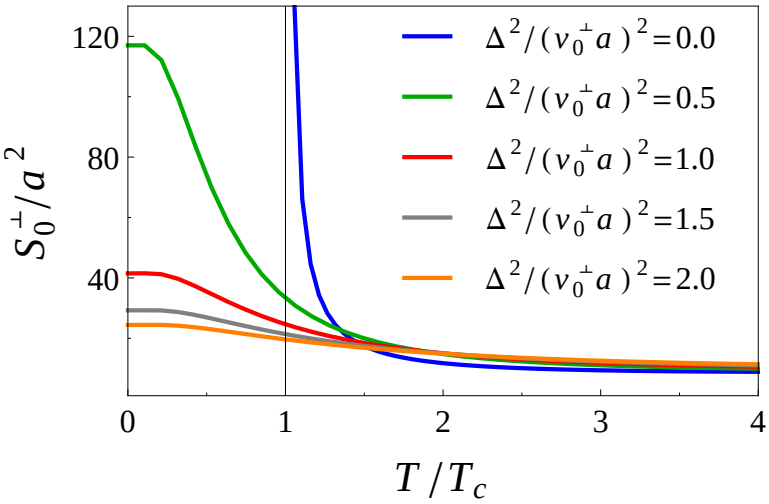

Figure 3.2: Temperature dependence of $\boldsymbol{q} = 0$ transverse component of the elastic structure factor. Here, $(v_0^\perp - \kappa)/v_0^\perp = 0.40$, $\gamma a^2/v_0^\perp = 0.10$, and $\hbar/(M v_0^\perp a^4)^{1/2} = 1.0$.

Fig. 3.3 shows the wave-vector dependence of the transverse component of the structure factor $S_{\boldsymbol{q}}^\perp$ along the $(q_x, 0, 0)$ direction of the FCC Brillouin zone. For no compositional disorder ($\Delta = 0$, Fig. 3.3 (a)), $S_{\boldsymbol{q}}^\perp$ is a Lorentzian of width $M\left(\Omega_0^\perp\right)^2$ (see Eq. (2.102)). For $T > T_c$, $S_{\boldsymbol{q}}^\perp$ has finite width ($M\left(\Omega_0^\perp\right)^2 > 0$) and is maximum at $(0, 0, 0)$. For $T \to T_c$, the width of $S_{\boldsymbol{q}}^\perp$ decreases ($M\left(\Omega_0^\perp\right)^2 \to 0$), and is zero at T_c ($M\left(\Omega_0^\perp\right)^2 = 0$). For finite compositional disorder ($\Delta^2/(v_0^\perp a)^2 = 0.5$, Fig. 3.3 (b)), $S_{\boldsymbol{q}}^\perp$ is given by Eq. (3.46). For $T > T_c$, $S_{\boldsymbol{q}}^\perp$ has finite width ($M\left(\Omega_0^\perp\right)^2 > 0$) and is maximum at $(0, 0, 0)$. For $T \to T_c$, the width of $S_{\boldsymbol{q}}^\perp$ decreases and remains finite at $T = T_c$. For $T < T_c$, the width of $S_{\boldsymbol{q}}^\perp$ decreases and remains finite at $T = 0$ ($M\left(\Omega_0^\perp\right)^2 > 0$ at $T = 0$). Similar temperature dependence

is obtained for increasing disorder ($\Delta^2/(v_0^\perp a)^2 = 1.0$, Fig. 3.3 (c)) except that the overall $S_{\boldsymbol{q}}^\perp$ decreases. $S_{\boldsymbol{q}}^\perp$ has the same behavior along the $(0, q_y, 0)$ direction of the FCC Brillouin zone.

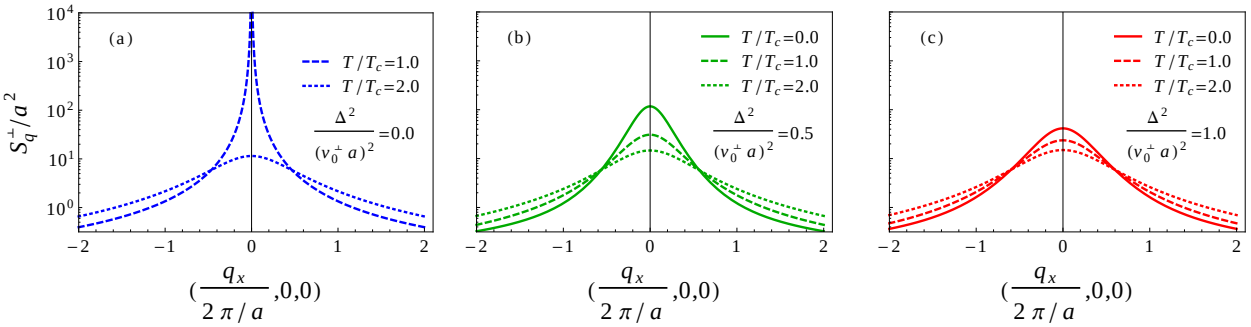

Figure 3.3: Log-linear plot of the structure factor in the transverse direction ($\boldsymbol{q} \perp \hat{\boldsymbol{z}}$). Here, $(v_0^\perp - \kappa)/v_0^\perp = 0.40$, $\gamma a^2/v_0^\perp = 0.10$, and $\hbar/(M v_0^\perp a^4)^{1/2} = 1.0$.

3.2.3 Correlation Functions of Polarization in Real Space with Random Fields

In this section we compute the correlation functions of polarization in real space.

The static correlation functions of polarization are obtained from the structure factor $S_{\boldsymbol{q}}$ of Eq. (3.45),

$$\begin{aligned}\left\langle \langle u_i u_j \rangle_{th} \right\rangle_c &= \frac{1}{N} \sum_{\boldsymbol{q}} e^{-i\boldsymbol{q}\cdot\boldsymbol{R}_{ij}} S_{\boldsymbol{q}} \\ &= \frac{1}{N} \sum_{\boldsymbol{q}} e^{-i\boldsymbol{q}\cdot\boldsymbol{R}_{ij}} \left[\frac{\hbar}{2M\Omega_{\boldsymbol{q}}} \coth\left(\frac{\beta\hbar\Omega_{\boldsymbol{q}}}{2}\right) + \frac{\Delta^2}{\left(M\Omega_{\boldsymbol{q}}^2\right)^2} \right] \end{aligned} \tag{3.48}$$

where

$$M\Omega_{\boldsymbol{q}}^2 = M\left(\Omega_0^\perp\right)^2 + \left(v_0^\perp - v_{\boldsymbol{q}}\right), \tag{3.49}$$

and

$$\lim_{\boldsymbol{q}\to 0} \frac{v_{\boldsymbol{q}}}{nz^{*2}} = \frac{4\pi}{3}\left(1 - 3\frac{q_z^2}{|\boldsymbol{q}|^2}\right) - \eta|\boldsymbol{q}a|^2 + 3\eta(q_z a)^2 \tag{3.50}$$

where n is the number of lattice points per unit volume and η is a dimensionless coefficient that depends on the structure of the lattice ($\eta \simeq 0.084$ for FCC lattices).

We first consider the correlation functions of polarization at large distances ($|\boldsymbol{R}_{ij}| \gg a$). For low temperatures ($T \to 0$) and arbitrarily small but finite disorder ($0 < \Delta/v_0^{\perp} \ll 1$), the phonon frequencies are small but finite, $M\left(\Omega_0^{\perp}\right)^2/v_0^{\perp} \ll 1$ down to $T = 0$. Therefore, the correlation functions are dominated by the second term in the square brackets of (3.48),

$$\left\langle\langle u_i u_j\rangle_{th}\right\rangle_c \simeq \frac{1}{N}\sum_{\boldsymbol{q}} e^{-i\boldsymbol{q}\cdot\boldsymbol{R}_{ij}} \frac{\Delta^2}{\left[\left(\chi_0^{\perp}\right)^{-1} + \left(v_0^{\perp} - v_{\boldsymbol{q}}\right)\right]^2}, \quad T \to 0, \quad (0 < \Delta/(v_0^{\perp} a) \ll 1), \tag{3.51}$$

where $\left(\chi_0^{\perp}\right)^{-1} = M\left(\Omega_0^{\perp}\right)^2$ is $\boldsymbol{q} = 0$ component of the susceptibility in the transverse direction ($\boldsymbol{q} \perp \hat{\boldsymbol{z}}$) For large distances, Eq. (3.51) gives correlation functions that are anisotropic and that decay as power laws,

$$\left\langle\langle u_i u_j\rangle_{th}\right\rangle_c = \begin{cases} \left(\frac{4\pi}{3}\right)^2 \frac{\Delta^2}{\left(v_0^{\perp}\right)^2} \times \frac{32\pi^3}{v_{BZ}} \frac{\left(\bar{\chi}_0^{\perp}\right)^3}{|\boldsymbol{R}|_{ij}^3}, & |\boldsymbol{R}_{ij}| \to \infty,\ \boldsymbol{R}_{ij} \parallel \hat{\boldsymbol{z}} \text{ (longitudinal)}, \\ -\left(\frac{4\pi}{3}\right)^2 \frac{\Delta^2}{\left(v_0^{\perp}\right)^2} \times \frac{1}{2}\frac{\pi^{3/2}}{v_{BZ}} \frac{\left(\bar{\chi}_0^{\perp}\right)^{3/2}}{|\boldsymbol{R}_{ij}|^3}, & |\boldsymbol{R}_{ij}| \to \infty,\ \boldsymbol{R}_{ij} \perp \hat{\boldsymbol{z}} \text{ (transverse)}, \end{cases} \tag{3.52}$$

where $\left(\bar{\chi}_0^{\perp}\right)^{-1} = (4\pi/3)\left(\chi_0^{\perp}\right)^{-1}/v_0^{\perp} \to 0$ is a dimensionless susceptibility; and v_{BZ} is the volume of the Brillouin zone of the FCC or BCC lattice.

We contrast the result (3.52) with the correlations of (i) uniaxial ferroelectric without random fields; and (ii) short-range forces with random fields, i.e., random field Ising model in three dimensions. For an uniaxial ferroelectric without random fields and above T_c (see Eq. (2.105)), the correlation functions exhibit the same anisotropy, power law decay, and longitudinal to transverse ratio of ${\chi_0^{\perp}}^{3/2}$ as those of Eq. (3.48). The longitudinal to transverse ratio of ${\chi_0^{\perp}}^{3/2}$ indicates the correlations are mostly concentrated along the polar axis. For short-range forces with random fields, the correlations are isotropic and decay

exponentially, $\left\langle \langle S_i S_j \rangle_{th} \right\rangle_c \sim \Delta^2 \exp\left[-|\boldsymbol{R}_{ij}|/\xi\right]$ where $\xi \sim \exp\left[1/\Delta^2\right]$ is the correlation length at $T = 0$. [13, 51]

We now discuss the near-neighbor correlations with compositional disorder. The results presented here are meant to give a qualitative qualitative description of the behavior of the correlations since our calculation uses $v_{\boldsymbol{q}}$ in the long-wavelength limit (see Eq. (3.50)). $v_{\boldsymbol{q}}$ differs from (3.50) as $\boldsymbol{q}$ approached the edge of the Brillouin zone. The results are shown in Fig. 3.4. We first describe the correlations without compositional disorder ($\Delta = 0$) and in the longitudinal direction ($\boldsymbol{R}_{ij} \parallel \hat{\boldsymbol{z}}$).

For high temperatures ($T \gg T_c$), the longitudinal correlations are positive and strong in the first few near-neighbors and become weak for larger distances (see Fig. 3.4 (a)). Close to the critical point ($T \gtrsim T_c$), the correlations are strong in the first few neighbors and become weak but slowly decaying ($\propto r^{-3}$, see Eq. (2.105)) for larger distances. (see Fig. 3.4 (b)). The correlations in the transverse direction ($\boldsymbol{R}_{ij} \perp \hat{\boldsymbol{z}}$) are negative and follow similar behavior than those along the longitudinal direction, except that they are significantly weaker (see Figs. 3.4 (d)-(e)). We now describe the correlations with compositional disorder ($\Delta > 0$) and in the longitudinal direction. For high temperatures ($T > T_c$), the longitudinal correlations do not vary significantly from those without compositional disorder (see Fig. 3.4 (a)). Close to the critical point ($T \gtrsim T_c$), the longitudinal correlations are slightly stronger than those without compositional disorder for the first few nearest-neighbors (see Fig. 3.4 (b)). Beyond the first few nearest-neighbors, the longitudinal correlations become weaker than those without compositional disorder (see Fig. 3.4 (b)). As temperature decreases below T_c, the longitudinal correlations with compositional disorder grow in the immediate vicinity of the unit cell and become weak beyond a few unit

cells. (see Fig. 3.4 (c)). We recall that for arbitrarily small but finite compositional disorder and low temperatures ($T \simeq 0\,\mathrm{K}$), the correlation functions decay as power laws ($\propto r^{-3}$, see Eq. (3.52)) for large distances. Similar behavior is obtained for the correlations in the transverse direction, however, they are significantly smaller than their longitudinal counterparts. (see Fig. 3.4 (d)-(f)).

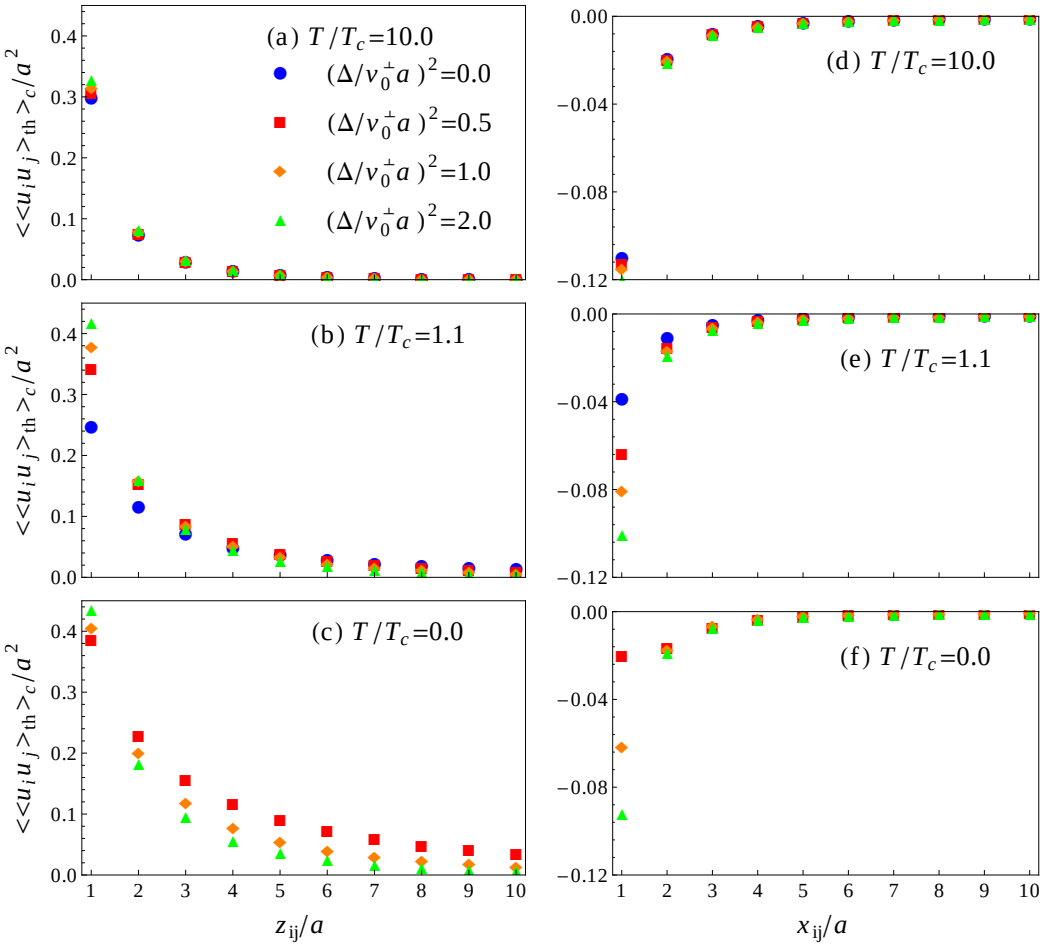

Figure 3.4: Near-neighbor correlation functions of polarization for a ferroelectric with disorder in the longitudinal ($\boldsymbol{R}_{ij} \parallel \hat{\boldsymbol{z}}$, (a)-(c)) and transverse ($\boldsymbol{R}_{ij} \perp \hat{\boldsymbol{z}}$, (d)-(f)) directions. Here, $(v_0^{\perp} - \kappa)/v_0^{\perp} = 0.40$, $\gamma a^2/v_0^{\perp} = 0.10$, and $\hbar/(M v_0^{\perp} a^4)^{1/2} = 1.0$. Lattice is FCC.

3.2.4 Dielectric Response with Random Fields

We now discuss the dynamic dielectric response of our model. In section 3.2, we derived the susceptibility for a damped anharmonic oscillator, with a Dirac delta damping function (see Eq. (3.21)),

$$\int_0^t \Gamma\delta(t-t')\dot{u}(t')\,dt' = \Gamma\dot{u}(t), \quad t > t'. \tag{3.53}$$

where Γ is the damping constant. Here, we will consider for now a damping function $G(t-t')$ of unspecified form,

$$\int_0^t G(t-t')\dot{u}(t')\,dt', \quad t > t'. \tag{3.54}$$

instead of the instantaneous damping function (3.53).

The derivation of the susceptibility for the general damping (3.54), is similar to that of the instantaneous damping (3.53) (see Sec. 3.2). Thus, we skip the derivation and state the final result.

The susceptibility for an anharmonic oscillator with damping function $G(t-t')$, Eq. (3.54), is given as follows,

$$\chi_{\boldsymbol{q}}^{-1}(\omega) = M\Omega_{\boldsymbol{q}}^2 - M\omega^2 + i\omega G(\omega). \tag{3.55}$$

Here, $\Omega_{\boldsymbol{q}}$ is the phonon frequency,

$$M\Omega_{\boldsymbol{q}}^2 = M\left(\Omega_0^{\perp}\right)^2 - (v_0^{\perp} - v_{\boldsymbol{q}}), \tag{3.56}$$

and $G(\omega)$ is the Fourier transform of $G(t)$

$$G(\omega) = \int_{-\infty}^{\infty} dt e^{-i\omega t} G(t)H(t), \tag{3.57}$$

where $H(t)$ is the unitary step function,

$$H(t) = \begin{cases} 1, & t > 0, \\ 0, & t < 0. \end{cases} \tag{3.58}$$

Since $\boldsymbol{v_q}$ is non-analytic for $\boldsymbol{q} \to 0$, the susceptibility (3.55) depends on the shape of the sample. To avoid this shape dependence, the susceptibility is defined as the response to the macroscopic field, which differs from the external field by the depolarizing field, [87, 88]

$$\tilde{\chi}_{\boldsymbol{q}}^{-1}(\omega) = \chi_{\boldsymbol{q}}^{-1}(\omega) - D_{\boldsymbol{q}}, \tag{3.59}$$

where $\tilde{\chi}_{\boldsymbol{q}}(\omega)$ is the shape-independent susceptibility. $D_{\boldsymbol{q}}$ is the depolarizing factor,

$$D_{\boldsymbol{q}} = \lim_{\boldsymbol{q}\to 0} 4\pi n z^{*2} \frac{q_z^2}{|\boldsymbol{q}|^2}, \tag{3.60}$$

where n is the number of unit cells per unit volume and z^* is the effective charge. Using (3.59) and (3.60) we obtain the shape independent susceptibility,

$$\tilde{\chi}_{\boldsymbol{q}}^{-1}(\omega) = M\tilde{\Omega}_{\boldsymbol{q}}^2 - M\omega^2 + i\omega G(\omega). \tag{3.61}$$

where,

$$M\tilde{\Omega}_{\boldsymbol{q}}^2 = M\left(\Omega_0^{\perp}\right)^2 - (\tilde{v}_0 - \tilde{v}_{\boldsymbol{q}}). \tag{3.62}$$

and $\tilde{v}_{\boldsymbol{q}} \equiv v_{\boldsymbol{q}} + D_{\boldsymbol{q}}$. Defined this way, $\tilde{v}_{\boldsymbol{q}}$ is analytic for $\boldsymbol{q} \to 0$ and $\tilde{v}_0 = (4\pi/3)nz^{*2}$.

The real part of the shape independent susceptibility $\tilde{\chi}_{\boldsymbol{q}}$ is as follows,

$$\mathrm{Re}[\tilde{\chi}_{\boldsymbol{q}}(\omega)] = \frac{M\tilde{\Omega}_{\boldsymbol{q}}^2 + \omega \mathrm{Im}[G(\omega)]}{\left(M\tilde{\Omega}_{\boldsymbol{q}}^2 + \omega \mathrm{Im}[G(\omega)]\right)^2 + \left(\omega \mathrm{Re}[G(\omega)]\right)^2}, \tag{3.63}$$

where $\mathrm{Re}[G(\omega)], \mathrm{Im}[G(\omega)]$ are the real and imaginary parts of $G(\omega) = \mathrm{Re}[G(\omega)] - i\,\mathrm{Im}[G(\omega)]$.

Here, we made the approximation that $\tilde{\Omega}_{\boldsymbol{q}}^2 \gg \omega^2$. This is justified since measurements of the dielectric susceptibility are done at low frequencies compared to that of

phonons (phonon energies are of the order of about 1 meV whereas the the energies associated with the measurements of the dielectric constant are of the order of about 10^{-3} meV, at most.) The approximation $\tilde{\Omega}_{\boldsymbol{q}}^2 \gg \omega^2$ means the kinetic energy of the unit cell is small, i.e., $\Pi_i^2 \simeq 0$.

We now obtain an equation for the temperature $T_{\max}$ where the susceptibility is maximum. The susceptibility is a maximum for,

$$\left.\frac{d\tilde{\chi}_{\boldsymbol{q}}(\omega)}{dT}\right|_{T_{\max}} = \left.\frac{d\tilde{\chi}_{\boldsymbol{q}}(\omega)}{d(M(\tilde{\Omega}_{\boldsymbol{q}})^2)} \times \frac{d(M(\tilde{\Omega}_{\boldsymbol{q}})^2)}{dT}\right|_{T_{\max}} = 0. \tag{3.64}$$

Here, we used the chain rule and the fact that $\tilde{\chi}_{\boldsymbol{q}}(\omega)$ depends on T only through $M(\tilde{\Omega}_{\boldsymbol{q}})^2)$. In general, $\left.\frac{d(M(\tilde{\Omega}_{\boldsymbol{q}})^2)}{dT}\right|_{T_{\max}} > 0$ for $T > 0$, thus, the above equation vanishes for $\frac{d\tilde{\chi}_{\boldsymbol{q}}(\omega)}{d(M(\tilde{\Omega}_{\boldsymbol{q}})^2)} = 0$. This gives $M(\tilde{\Omega}_{\boldsymbol{q}})^2\Big|_{T_{\max}} = \omega\left(\pm\mathrm{Re}[G(\omega)] - \mathrm{Im}[G(\omega)]\right)$. $\mathrm{Re}[G(\omega)],\ \mathrm{Im}[G(\omega)] > 0$ for physical functional forms of the damping function $G(t)$ (e.g., Dirac delta function or exponential decay) Since $M(\tilde{\Omega}_{\boldsymbol{q}})^2 > 0$ for finite disorder, only the "+" gives sensible answers, i.e., $T_{\max} > 0$. Therefore, the equation for the temperature $T_{\max}$ where the susceptibility is maximum is given as follows,

$$M\left[\tilde{\Omega}_{\boldsymbol{q}}(T_{\max})\right]^2 = \omega\left(\mathrm{Re}[G(\omega)] - \mathrm{Im}[G(\omega)]\right). \tag{3.65}$$

$M\left[\tilde{\Omega}_{\boldsymbol{q}}(T_{\max})\right]^2 > 0$ for finite disorder. The maximum of the dynamic susceptibility is given by the difference in the real and imaginary parts of the damping function.

Using Eq. (3.65) we find the maximum of the real part of the susceptibility is given as follows,

$$\left.\mathrm{Re}[\tilde{\chi}_{\boldsymbol{q}}(\omega)]\right|_{T_{\max}} = \frac{1}{2\omega\mathrm{Re}[G(\omega)]}. \tag{3.66}$$

The shape independent dielectric constant is given as follows,

$$\epsilon(\omega) = 1 + 4\pi n z^{*2}\tilde{\chi}_0(\omega) = 1 + 4\pi \times \frac{\tilde{v_0}}{4\pi/3}\tilde{\chi}_0(\omega), \tag{3.67}$$

where $\tilde{\chi}_0(\omega)$ is given in Eq. (3.59).

Figure 3.5 shows the temperature and frequency dependence of the real part of the shape-independent susceptibility $\mathrm{Re}[\tilde{\chi}_0(\omega)]$ with $G(\omega)$ purely real and constant (this corresponds to an instantaneous damping function $G(t) = \Gamma\delta(t - t')$ where Γ is a damping constant). For no compositional disorder ($\Delta = 0$), the static susceptibility $\mathrm{Re}[\tilde{\chi}_0(0)]$ follows the Curie-Weiss law with logarithmic corrections close to T_c, i.e., $\mathrm{Re}[\tilde{\chi}_0(0)] \propto \log(1/t)/t$ for $t = (T - T_c)/T_c \to 0$ (see gray dashed line in inset of Fig. 3.5 and Sec. 2.4). The Curie-Weiss constant C_{CW} is inversely proportional to the anharmonic coefficient γ (see Sec. 2.4). For finite compositional disorder ($\Delta > 0$), $\chi_0(\omega)$ follows the Curie-Weiss law for temperatures above the Burns temperature T_B with Curie-Weiss temperature $T_{CW} < T_B$ and Curie-Weiss constant $C_{CW} \propto \gamma^{-1}$ (see orange line in inset of Fig. 3.5). For $T < T_{CW}$, $\mathrm{Re}[\tilde{\chi}_0(0)]$ grows and reaches a maximum at $T = 0$. The dynamic susceptibility $\mathrm{Re}[\tilde{\chi}_0(\omega)]$ follows the same temperature behavior as that of its static component $\mathrm{Re}[\tilde{\chi}_0(0)]$ for $T > T_B$. For $T < T_B$, $\mathrm{Re}[\tilde{\chi}_0(\omega)]$ increases and reaches a maximum at $T_{\max}$. The maximum of $\mathrm{Re}[\tilde{\chi}_0(\omega)]$ and $T_{\max}$ are given by Eqs. (3.66) and (3.65), respectively. For $T < T_{\max}$, $\mathrm{Re}[\tilde{\chi}_0(\omega)]$ decreases and remains finite at $T = 0$.

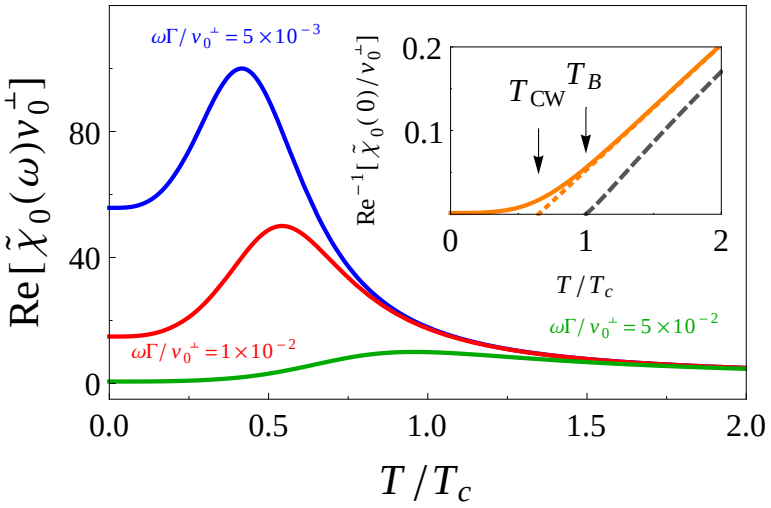

Figure 3.5: Real part of the shape-independent dynamic susceptibility. Inset: inverse of the real part of the shape-independent static susceptibility without compositional disorder ($\Delta = 0$, gray dashed line) and with compositional disorder ($\Delta^2/(v_0^{\perp}a)^2 = 0.15$, solid orange line). Deviations from Curie-Weiss law indicated by orange, dashed line. T_{CW} and T_B are the Curie-Weiss and Burns temperatures, respectively. Here, $(v_0^{\perp} - \kappa)/{v_0^{\perp}}^2 = 0.40$ and $\gamma a^2/v_0^{\perp} = 0.10$.

Figure 3.6 shows the dependence of the Curie-Weiss (T_{CW}) and Burns (T_B) temperatures on compositional disorder Δ. We first describe T_{CW}. For no compositional disorder ($\Delta = 0$), $T_{CW} = T_c$, where T_c is the critical temperature of the ferroelectric without disorder. For finite disorder ($\Delta > 0$), T_{CW} decreases approximately linearly with Δ^2. We now describe T_B. For no compositional disorder ($\Delta = 0$), $T_B = T_c$. For finite disorder ($\Delta > 0$), T_B decreases with Δ^2.

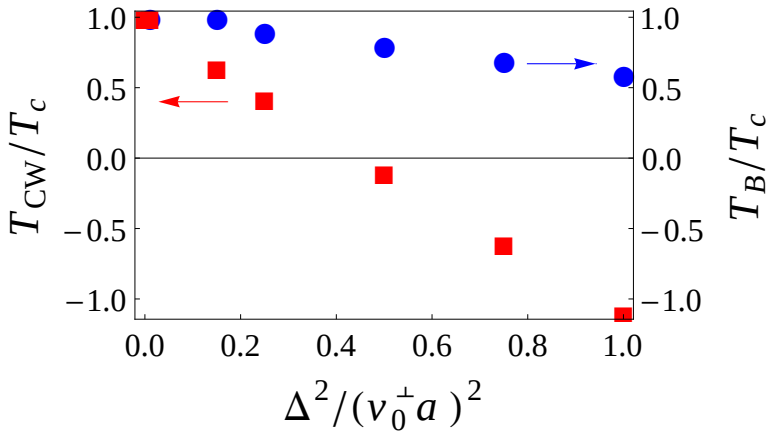

Figure 3.6: Curie-Weiss (T_{CW}) and Burns (T_B) temperatures. Here, $(v_0^{\perp} - \kappa)/{v_0^{\perp}}^2 = 0.40$ and $\gamma a^2/v_0^{\perp} = 0.10$.

Figure 3.7 shows the frequency and disorder dependence of $T_{\max}$ obtained from Eq. (3.65) with with $G(\omega)$ purely real and constant (this corresponds to an instantaneous damping function $G(t) = \Gamma\delta(t - t')$ where Γ is a damping constant). $T_{\max}$ increases with frequency and decreases with increasing disorder.

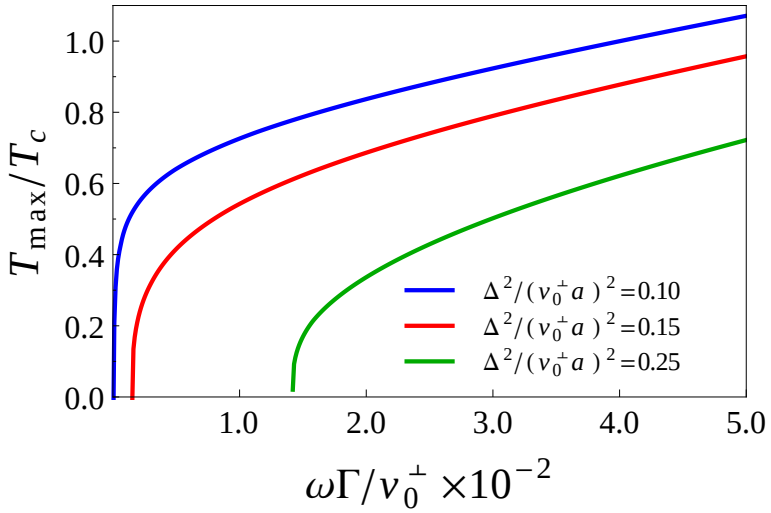

Figure 3.7: Frequency and compositional disorder dependence of $T_{\max}$. Here, $(v_0^{\perp} - \kappa)/{v_0^{\perp}}^2 = 0.40$ and $\gamma a^2/v_0^{\perp} = 0.10$.

3.3 Comparison to Experiments

In this section, we compare the calculated elastic structure factor $S_{\boldsymbol{q}}$ and dynamic dielectric constant $\epsilon(\omega)$ to those observed for the relaxors. The observed behavior of $S_{\boldsymbol{q}}$ and $\epsilon(\omega)$ in the relaxors was discussed in Sec. 1.3.

Our model parameters are (i) the lattice stiffness κ; (ii) the anharmonic coefficient γ; (iii) the effective charge of the unit cell z^* (absorbed in $v_0^\perp \equiv 4\pi n z^{*2}/3$); (iv) the variance of the quenched random fields Δ; and (v) the damping constant Γ.

We first compare to the elastic structure factor to that observed by neutron scattering experiments. The results for the temperature dependence of the structure factor $S_{\boldsymbol{q}}^\perp$ at $q_x^2 + q_y^2 = 0.05\,\mathrm{rlu}$ are shown in Fig. 3.8. For temperatures above about $T_c = 465\,\mathrm{K}$, $S_{\boldsymbol{q}}^\perp$ is very small. At $465\,\mathrm{K}$ $S_{\boldsymbol{q}}^\perp$ starts increasing and keeps on growing down to $100\,\mathrm{K}$. As temperature keeps decreasing, $S_{\boldsymbol{q}}^\perp$ remains fairly constant down to $T = 0\,\mathrm{K}$. The red dots and blue squares in Fig. 3.8 correspond to the neutron scattering data for PMN in the vicinity of the (110) and (100) Bragg peaks. [11, 12, 53]

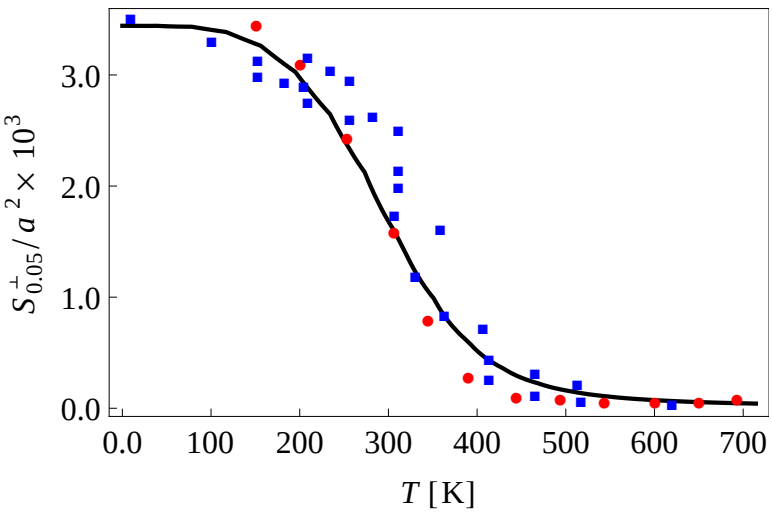

Figure 3.8: Structure factor $S_{\boldsymbol{q}}$. Black solid line corresponds to the present model. Red dots and blue squares correspond to the neutron experimental data taken in the vicinity ($q = 0.05\,\mathrm{rlu}$) of the (110) and (100) Bragg peaks. Data taken from Refs. [11, 12, 53]

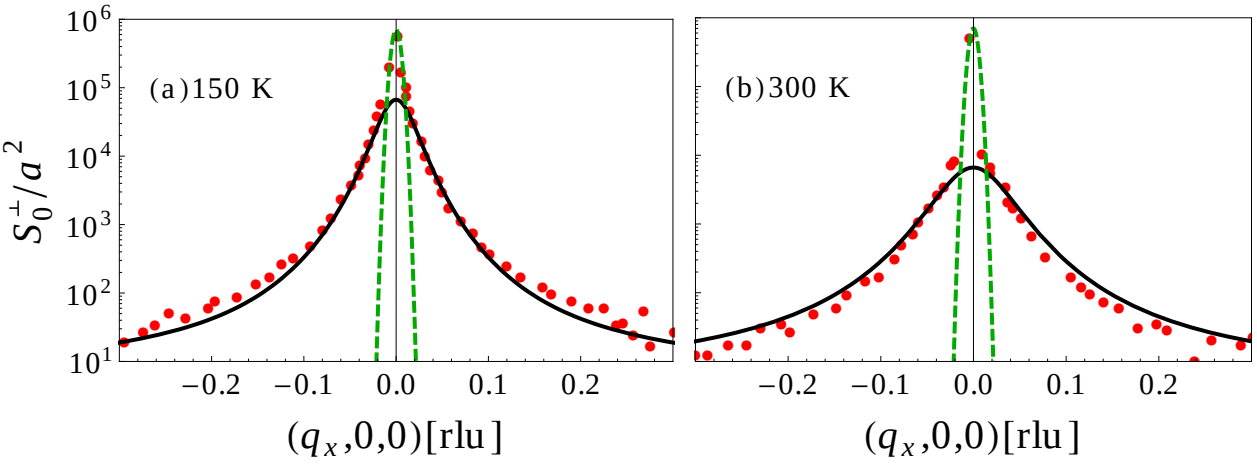

Figure 3.9: Log-linear plot of the wavevector distribution of the structure factor $S_{\boldsymbol{q}}^{\perp}$. Solid black line corresponds to the present model. Red dots correspond to the neutron experimental data around the (110) Bragg peak. Green dashed line is a Gaussian Bragg peak of width given by the experimental resolution ($\simeq 0.01$ rlu). Data taken from Refs. [11, 12]

The results for the wavevector distribution of the structure factor $S_{\boldsymbol{q}}^{\perp}$ for $T = 150\,\mathrm{K}$ and $T = 300\,\mathrm{K}$ are shown in Fig. 3.9 (black, solid line). The red dots and blue squares correspond to the neutron scattering data for PMN in the vicinity of the (110) and (100) Bragg peaks. [11, 12] The thin-gray line is a Gaussian Bragg peak of width given by the experimental resolution ($\simeq 0.01$ rlu). For long wavelengths ($|\boldsymbol{q}a| \to 0$), the diffuse scattering is dominated by the second term in the square brackets of (3.46). For short wavelengths ($|\boldsymbol{q}a| \gg 1$), the diffuse scattering is dominated by the first term in the square brackets of (3.46).

We now compare the dielectric constant (3.67) to that of the relaxors. Fig. 3.10 (a) shows the observed dielectric constant for PMN (dots, squares, and rhombohedrons) compared to that of our model (solid lines). Here, we chose $G(\omega)$ to be purely real and constant (this corresponds to an instantaneous damping function $G(t) = \Gamma\delta(t-t')$ where Γ is a fitting constant). For $T > T_B \simeq 600\,\mathrm{K}$, the calculated $\epsilon(\omega)$ follows the Curie-Weiss law with

a Curie-Weiss constant $C_{\rm CW} \propto \gamma^{-1} \sim 10^5\,{\rm K}$ and a Curie-Weiss temperature $T_{\rm CW} \simeq 450\,K$. For $T < T_B$, $\epsilon(\omega)$ reaches a maximum $\epsilon_{\rm max}(\omega)$ at $T_{\rm max}$ given by Eqs. (3.66)-(3.65). $\epsilon_{\rm max}(\omega)$ shifts towards higher temperatures as frequency increases. $\epsilon(\omega)$ then decreases upon further cooling. The calculated values of $\epsilon_{\rm max}(\omega)$ tend to be much lower than those of experiments, and the calculated values for $T_{\rm max}$ tend to be higher (see Fig. 3.10 (a)). This is because our choice of the instantaneous damping is too simplistic. We noticed better agreement with the observed $\epsilon_{\rm max}(\omega)$ and $T_{\rm max}$ if we let the damping constant Γ to decrease with frequency (see Fig. 3.10 (b)). This suggests a damping function $G(t)$ with a finite relaxation time. The simplest possible damping function with a finite relaxation time that can be handled analytically is exponential, i.e., $G(t) = (\Gamma/\tau){\rm Exp}(-t/\tau)$, where τ is the relaxation time. This, however, did not give much improvement with respect to that of instantaneous damping (see Fig. 3.10 (a)). We believe more complicated forms of the damping function are needed to obtain quantitative agreement for $\epsilon_{\rm max}(\omega)$ and $T_{\rm max}$. This is beyond the scope of the present work. We emphasize, however, that the dielectric constant (3.67) gives a broad region of fluctuations with a large Curie-Weiss constant proportional to the anharmonic coefficient γ^{-1}, as expected for displacive systems.

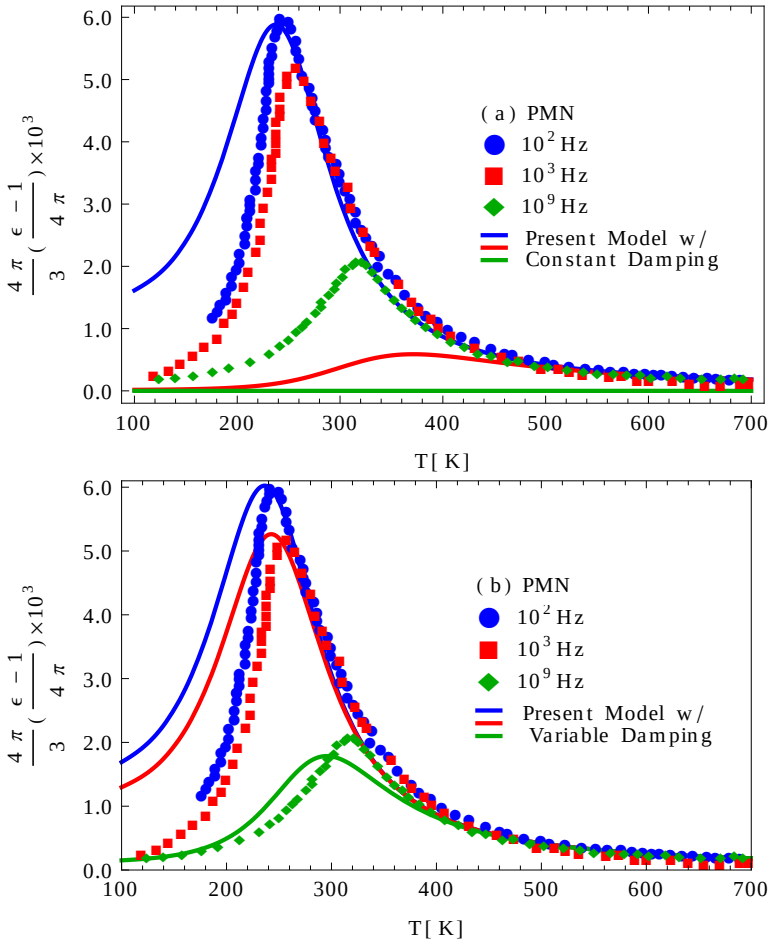

Figure 3.10: Comparison between observed and calculated dynamic dielectric constant for PMN. Dots, squares and rhombohedrons correspond to experimental data. Solid lines to our model. For (a), $(v_0^\perp - \kappa)/v_0^\perp = 0.01$, $\gamma a^2/v_0^\perp = 5.8 \times 10^{-5}$, $\hbar/(M v_0^\perp a^4)^{1/2} = 10^2$, $\Delta^2/{v_0^\perp}^2 = 1.75$, and $\Gamma/v_0^\perp = 8.5 \times 10^{-7}$ s for all frequencies. For (b), $(v_0^\perp - \kappa)/v_0^\perp = 0.01$, $\gamma a^2/v_0^\perp = 5.8 \times 10^{-5}$, $\hbar/(M v_0^\perp a^4)^{1/2} = 10^2$, $\Delta^2/{v_0^\perp}^2 = 1.75$, and $\Gamma/v_0^\perp = 8.5 \times 10^{-7}$ s ($\omega = 10^2$ Hz), 8.5×10^{-8} s ($\omega = 10^3$ Hz), 2.8×10^{-13} s ($\omega = 10^9$ Hz). Experimental data taken from Ref. [29].

Chapter 4

Conclusions

In this chapter we present the main conclusions of this work and discuss some of the simplifications made in our model.

Our main conclusions are the following:

1. any theory of relaxor ferroelectricity must go beyond the Lorentz approximation to account for the broad region in temperature of critical fluctuations. Here, we used the Onsager approximation which is the simplest correction to the Lorentz field that guarantees the fluctuation dissipation theorem of statistical mechanics.

2. arbitrarily small compositional disorder together with dipolar forces extend the region of critical fluctuations down to absolute zero temperature.

3. the correlation functions of polarization are highly anisotropic and slowly varying with a power law component.

4. the elastic diffuse scattering observed in the relaxors is the onset of a transition from a paraelectric to a random field state without long range order. This is not a true

phase transition since no symmetries are broken.

5. the Curie-Weiss constant of the relaxors is proportional to the inverse of the anharmonic coefficient γ, just like in ferroelectrics.

6. the temperature where the dielectric response is maximum, $T_{\max}$ is determined by the soft mode frequency, the damping function, and the frequency of the applied field.

We now discuss some of the simplifications in our model. We ignored:

1. the full cubic symmetry typical of perovskite relaxor ferroelectrics. Soft modes in cubic systems are degenerate, for instance, they are triply degenerate in the absence of dipolar forces since there are three equivalent axes (in the presence of dipolar forces this degeneracy is lifted into two degenerate transverse mode and a single degenerate longitudinal mode). Here, we considered an uniaxial relaxor, therefore there is only a single soft optic mode.

   Cubic symmetry may vary the temperature dependence of the soft mode frequencies since the dynamical matrices will be necessarily different. We point out, however, that mean field models for conventional cubic and uniaxial ferroelectrics predict the same temperature dependence for the soft mode frequencies: $\Omega^2 \propto T - T_c$ for $T \to T_c$. [63]

   We cannot draw any conclusions regarding whether long-range order is absent in cubic systems for arbitrary small compositional disorder. Previous theoretical studies [51, 52, 82] are based on isotropic short ranged forces and not on anisotropic long-ranged dipole forces. An exception is the SRBRF model in which cubic symmetry and random fields are considered with infinite ranged interactions. The SRBRF model predicts no long-range ferroelectric order for arbitrary small random fields. [9] We emphasize that

whether or not long-range order is absent for arbitrary small random fields in cubic systems is a question of theoretical interest, not of the relaxors in particular. Long-range order will always be absent for strong compositional disorder .

2. coupling of the transverse optic mode to the transverse acoustic mode. Neutron scattering experiments [11, 12] showed that coupling of the transverse optic and transverse acoustic modes is important to describe quantitatively the observed dispersion relations for large wave vectors ($\gtrsim 0.1$ r.l.u. for PMN at 670 K). For small wave vectors ($\lesssim 0.1$ r.l.u. for PMN 670 K), the coupling is not important, at least above the Burns temperature $T_B \simeq 620$ K

3. coupling to strain. Relaxor ferroelectrics undergo structural phase transitions, e.g., PMN exhibits a first order cubic-to-rhombohedral phase transition in the presence of large static fields. Coupling of the soft mode coordinates to strain is important in models of conventional ferroelectricity to (i) predict the observed sequence of structural phase transitions, e.g., BTO goes through a sequence of cubic-to-tetragonal-to-orthorhombic-to-rhombohedral phase transitions as temperature is lowered; (ii) to predict that all these phase changes are of first order (models with quartic anharmonicities such as the one considered here can only predict second order phase transitions). [63, 68, 69, 70, 71] We expect to describe the observed structural phase changes in the relaxors by including coupling to strain and cubic symmetry in our model.

4. Short-range interactions between unit cells. Short-range interactions are most likely not as relevant to the relaxors as they are in conventional ferroelectrics, at least as far as the absence of long-range order is concerned. In conventional ferroelectrics, nearest-

neighbor short-range interactions can modify the long-range ferroelectric order. In the relaxors, we have shown that random fields destroy the long-range ferroelectric order for arbitrarily small compositional disorder. Inclusion of short-range forces will not modify this result. Short-range forces will probably vary the values of the Burns temperature T_B, and the temperature $T_{\max}$ where the dielectric constant peaks.

5. disorder in the dipolar bonds v_{ij}. Disorder v_{ij} is present in the relaxors since the B-side of the perovskite unit cell is disordered. However, we expect the effects of disorder in the bonds to be smaller compared to those of the random fields: in systems with both random-bonds and random-fields (such as the relaxors), the contributions to the free energy from the random-fields are linear in the order parameter while the contributions from the random-bonds are quadratic. Moreover, the non-Lorentzian shape observed in the elastic diffuse scattering is characteristic of a random field transition, not a random-bond transition.

Bibliography

[1] G. Schmidt, H. Arndt, J. Voncieminski, T. Petzsche, H. Voigt, and N. Krainik, Krist. Tech. **15**, 1415 (1980).

[2] A. J. Bell, J. Phys.: Condens. Matter **5**, 8773 (1993).

[3] A. Safari and E. K. Akdogan, editors, *Piezoelectric and Acoustic Materials for Transducer Applications*, Springer, 2008.

[4] N. Setter and L. E. Cross, J. Appl. Phys. **51**, 4356 (1980).

[5] G. A. Smilenskii and A. I. Agranovskaia, Sov. Phys. Tech. Phys. **3**, 1380 (1958).

[6] R. Roy, J. Am. Ceram. Soc. **37**, 581 (1954).

[7] R. A. Cowley, S. N. Gvasaliya, S. G. Lushnikov, B. Roessli, and G. M. Rotaru, Advances in Physics **60**, 229 (2011).

[8] V. Westphal, W. Kleemann, and M. D. Glinchuk, Phys. Rev. Lett. **68**, 847 (1992).

[9] R. Pirc and R. Blinc, Phys. Rev. B **60**, 13470 (1999).

[10] R. Pirc, R. Blinc, and V. Bobnar, Phys. Rev. B **63**, 054203 (2001).

[11] S. N. Gvasaliya, B. Roessli, R. A. Cowley, P. Huber, and S. G. Lushnikov, J. Phys.: Condens. Matter **17**, 4343 (2005).

[12] R. A. Cowley, S. N. Gvasaliya, and B. Roessli, Ferroelectrics **378**, 53 (2009).

[13] R. J. Birgeneau, H. Yoshizawa, R. A. Cowley, G. Shirane, and H. Ikeda, Phys. Rev. B **28**, 1438 (1983).

[14] M. Hagen, R. A. Cowley, S. K. Satija, H. Yoshizawa, G. Shirane, R. J. Birgeneau, and H. J. Guggenheim, Phys. Rev. B **28**, 2602 (1983).

[15] R. A. Cowley, H. Yoshizawa, G. Shirane, and R. J. Birgeneau, Z. Phys. B **58**, 15 (1985).

[16] H. Yoshizawa, G. S. R. A. Cowley, R. J. Birgeneau, H. J. Guggenheim, and H. Ikeda, Phys. Rev. Lett. **48**, 438 (1982).

[17] F. Jona and G. Shirane, *Ferroelectric Crystals*, Dover Publications, 1993.

[18] P. W. Anderson, *Qualitative Considerations on the Statistics of the Phase Transition of $BaTiO_3$ type Ferroelectrics*, Akad. Nauk SSSR Fizicheskii Inst., 1960, Reprinted in: P. W. Anderson, *A Career in Theoretical Physics*, (World Scientific Publishing Co., New Jersey, 1994).

[19] D. M. N. Ashcroft, *Solid State Physics*, Thompson Learning Inc., 1976.

[20] J. Harada, J. D. Axe, and G. Shirane, Phys. Rev. B **4**, 155 (1971).

[21] D. Viehland, S. J. Jang, L. E. Cross, and M. Wuttig, Phys. Rev. B **46**, 8003 (1992).

[22] W. Cochran, Phys. Rev. Lett. **3**, 412 (1960).

[23] W. Cochran, Adv. Phys. **9**, 387 (1960).

[24] M. Born and H. Kun, *Dynamical Theory of Crystal Lattices*, Oxford University Press, 1985.

[25] P. Bonneau, P. Garnier, G. Calvarin, E. Husson, J. Gavarri, A. Hewat, and A. Morell, J. Solid State Chem. **91**, 350 (1991).

[26] A. Cervellino, S. Gvasaliya, O. Zaharko, B. Roessli, R. C. G. Rotaru, S. Lushnikov, T. Shaplygina, and M. Fernandez-Diaz, J. Appl. Cryst. **44**, 603 (2011).

[27] S. Vakhrushev and N. Okuneva, AIP Conference Proceedings **626**, 117 (2002).

[28] G. Samara, J. Phys.: Condens. Matter **15**, R367 (2003).

[29] V. Bovtun, S. Kamba, A. Pashkin, M. Savinov, P. Samoukhina, J. Petzelt, I. P. Bykov, and M. D. Glinchuk, Ferroelectrics **298**, 23 (2004).

[30] J. P. Remeika and A. M. Glass, Mater. Res. Bull. **5**, 37 (1970).

[31] N. Goldenfeld, *Lectures on Phase Transitions and the Renormalization Group*, Westview Press, 1992.

[32] E. V. Colla, E. Y. Koroleva, N. M. Okuneva, and S. B. Vakhrusev, J. Phys.:Condens. Matter **4**, 3671 (1992).

[33] A. E. Glazounov and A. K. Tagantsev, Appl. Phys. Lett. **73**, 856 (1998).

[34] A. A. Bokov and Z.-H. Ye, J. Mater. Sci. **41**, 31 (2006).

[35] K. H. Fischer, Phys. Stat. Sol. (b) **116**, 357 (1983).

[36] R. Sommer, N. K. Yushin, and J. J. van der Klink, Phys. Rev. B **48**, 13230 (1993).

[37] X. Zhao, X. T. W. Qu, A. A. Bokov, and Z. Ye, Phys. Rev. B **75**, 104106 (2007).

[38] G. Shirane, J. D. Axe, J. Harada, and J. P. Remeika, Phys. Rev. B **2**, 155 (1970).

[39] J. Harada, J. D. Axe, and G. Shirane, Acta. Cryst. A **26**, 608 (1970).

[40] G. Shirane, Rev. Mod. Phys. **46**, 437 (1974).

[41] J. Hlinka, J. Petzelt, S. Kamba, D. Noujni, and T. Ostapchuk, Phase Transitions **79**, 41 (2006).

[42] P. M. Gehring, Z.-G. Y. S. Wakimoto, and G. Shirane, Phys. Rev. Lett. **87**, 277601 (2001).

[43] H. L. C. Stock, D. Viehland, J. Li, I. Swainson, R. Birgeneau, and G. Shirane, J. Phys. Soc.Jpn. **74**, 3002 (2005).

[44] P. M. Gehring, H. Hiraka, C. Stock, S.-H. Lee, W. Chen, Z.-G. Ye, S. B. Vakhrushev, , and Z. Chowdhuri, Phys. Rev. B **79**, 224109 (2009).

[45] J. Hlinka and M. Kempa, Phase Transitions **81**, 491 (2008).

[46] J. Hlinka, S. Kamba, J. Petzelt, C. A. Randall, , and S. J. Zhang, Phys. Rev. Lett. **91**, 107602 (2003).

[47] S. Wakimoto, C. Stock, R. Birgeneau, Z. Ye, W. Chen, W. L. Buyers, P. Gehring, and G. Shirane, Phys. Rev. B **65**, 172105 (2002).

[48] Y. Yamada, G. Shirane, and A. Linz, Phys. Rev. **177**, 848 (1969).

[49] M. E. Lines, Phys. Rev. B **5**, 3690 (1972).

[50] G. M. Rotaru, S. N. Gvasaliya, B. Roessli, S. Kojima, S. G. Lushnikov, and P. Günter, Appl. Phys. Lett. **93**, 032903 (2008).

[51] D. Mukamel and E. Pytte, Phys. Rev. B **25**, 4779 (1982).

[52] I. Vilfan and R. A. Cowley, J. Phys. C: Solid State Phys. **18**, 5055 (1985).

[53] S.-H. L. H. Hiraka, P. M. Gehring, G. Xu, and G. Shirane, Phys. Rev. B **70**, 184105 (2004).

[54] J. D. R. Blinc, A. Gregorovič, B. Zalar, C. Filipič, Z. Kutnjak, A. Levstik, and R. Pirc, Phys. Rev. Lett. **83**, 424 (1999).

[55] C. Boulesteix, F. Varnier, A. Llebaria, and E. Husson, J. Solid State Chem. **108**, 141 (1994).

[56] R. Blinc, R. Pirc, V. Bobnar, and A. Gregovič, AIP Conference Proceedings: Fundamentals of Physics of Ferroelectrics **582**, 97 (2001).

[57] P. W. Anderson, Ceramic Abstracts **10**, 187b (1951), Reprinted in: P. W. Anderson, *A Career in Theoretical Physics*, (World Scientific Publishing Co., New Jersey, 1994).

[58] A. F. Devonshire, Phil. Mag. **40**, 1040 (1949).

[59] A. F. Devonshire, Phil. Mag. **42**, 1065 (1951).

[60] A. F. Devonshire, Adv. Phys. **3**, 85 (1954).

[61] H. Thomas, Structural phase transitions and soft modes, in *Proceedings of the NATO Advanced Study Institute*, Universitetsforlaget, 1971.

[62] M. A. Moore and H. C. W. L. Williams, J. Phys. C: Solid State Phys. **5**, 3168 (1972).

[63] E. Pytte, Phys. Rev. B **5**, 3758 (1972).

[64] A. Aharony and M. E. Fisher, Phys. Rev. B **8**, 3323 (1973).

[65] M. H. Cohen and F. Keffer, Phys. Rev. **99**, 1128 (1955).

[66] R. Blinc and B. Žekš, *Soft Modes in Ferroelectrics and Antiferroelectrics*, North-Holland Publishing Co., 1974.

[67] W. Zhong, D. Vanderbilt, and K. M. Rabe, Phys. Rev. B **52**, 6301 (1995).

[68] R. Cohen, Nature **358**, 136 (1992).

[69] R. D. King-Smith and D. Vanderblilt, Phys. Rev. B **49**, 5829 (1994).

[70] R. D. King-Smith and D. Vanderblilt, Phil. Trans. R. Soc. Lond. A **354**, 2897 (1996).

[71] U. V. Waghmare and K. M. Rabe, Phys. Rev. B **55**, 6161 (1997).

[72] M. E. Lines and A. M. Glass, *Principles and Applications of Ferroelectrics and Related Materials*, Clarendon Press, 1977.

[73] M. E. Lines, Phys. Rev. B **9**, 950 (1974).

[74] L. Onsager, J. Am. Chem. Soc. **58**, 1486 (1936).

[75] R. Brout and H. Thomas, Phys. **3**, 317 (1967).

[76] H. Thomas and R. Brout, J. Appl. Phys. **39**, 624 (1968).

[77] A. I. Larkin and D. E. Khmel'nitskiĭ, Sov. Phys. JETP **29**, 1123 (1969).

[78] T. Nattermann, Ferroelectrics **9**, 229 (1975).

[79] R. A. Cowley, Integrated Ferroelectrics **133**, 109 (2012).

[80] G. Ahlers, A. Kornblit, and H. J. Guggenheim, Phys. Rev. Lett. **34**, 1227 (1975).

[81] W. Marshall and S. W. Lovesey, *Theory of Thermal Neutron Scattering: the Use of Neutrons for the Investigation of Condensed Matter*, Clarendon Press, 1971.

[82] Y. Imry and S. k. Ma, Phys. Rev. Lett. **35**, 1399 (1975).

[83] G. Grinstein, Phys. Rev. Lett. **37**, 944 (1976).

[84] A. Aharony, Y. Imry, and S. k. Ma, Phys. Rev. Lett. **37**, 1364 (1976).

[85] G. Parisi and N. Sourlas, Phys. Rev. Lett. **43**, 744 (1979).

[86] J. Z. Imbrie, Phys. Rev. Lett. **53**, 1747 (1984).

[87] P. Levy, Phys. Rev. **170**, 595 (1968).

[88] H. Horner, Phys. Rev. **172**, 535 (1968).

[89] S. Vakhrushev, R. Burkovsky, S. Shapiro, and A. Ivanov, Phys. Solid State **52**, 889 (2010).

[90] G. M. Meyer and R. A. Cowley, Ferroelectrics **11**, 479 (1976).

[91] J. M. Luttinger and L. Tisza, Phys. Rev. **70**, 954 (1946).

Appendix A

Calculation of some integrals.

Consider the integrals,

$$F(z) = \frac{\int_0^{2\pi} d\phi \int_0^{Q} dq \int_0^{\pi} d\theta \frac{q^2 \sin\theta}{z^2+B^2q^2+(C^2-3B^2q^2)\cos^2\theta}}{\int_0^{2\pi} d\phi \int_0^{Q} dq \int_0^{\pi} d\theta q^2 \sin\theta}, \tag{A.1}$$

$$G(z) = \frac{\int_0^{2\pi} d\phi \int_0^{Q} dq \int_0^{\pi} d\theta \frac{q^2 \sin\theta}{[z^2+B^2q^2+(C^2-3B^2q^2)\cos^2\theta]^2}}{\int_0^{2\pi} d\phi \int_0^{Q} dq \int_0^{\pi} d\theta q^2 \sin\theta}, \tag{A.2}$$

where Q is an cut-off wavevector. We wish to calculate $F(z)$ and $G(z)$ for $z \to 0$. The calculation of $F(z)$ was done in Ref. [90]. Here, we reproduce it for the sake of completeness.

We first compute $F(z)$ for $z \to 0$. We define $X = QB/z$ and integrate (A.1) over θ,

$$F(z) = \frac{3z^2}{Q^3B^3C} \int_0^{X} dx \frac{x^2}{\sqrt{(1+x^2)\,(1-3x^2/(C/z)^2)}} \arctan\left[(C/z)\sqrt{\frac{1-3x^2/(C/z)^2}{1+x^2}}\right] \tag{A.3}$$

For $C \gg z$ and $C \gg BQ$ we obtain,

$$F(z) = \frac{3\pi}{4QBC}\left[1 - \frac{z^2}{B^2Q^2}\ln\left(\frac{2BQ}{z}\right)\right] \tag{A.4}$$

Eq. (A.4) gives $F(z)$ for $z \to 0$.

We now compute $G(z)$ for $z \to 0$. The calculation of $G(z)$ for $z \to 0$ is straightforward by noticing that $G(z) = -\frac{dF(z)}{dz^2}$. Therefore,

$$G(z) = \frac{3\pi}{4Q^3B^3C} \ln\left(\frac{2BQ}{z}\right), \tag{A.5}$$

to order $\mathcal{O}(z^4)$. Eq. (A.5) gives $G(z)$ for $z \to 0$ and is the final result of this appendix.

Appendix B

Calculation of correlation functions in real space for uniaxial dipole system

The purpose of this appendix is to calculate the correlation functions in real space for an uniaxial dipole ferroelectric with and without quenched random fields.

B.0.1 Correlations without random fields

In the absence of compositional disorder, the correlation functions of polarization for the uniaxial dipole problem between unit cells at the origin $\mathbf{0}$ and at position $\boldsymbol{R}$ are given as follows,

$$\langle u_{\mathbf{0}} u_{\boldsymbol{R}} \rangle_{th} = \frac{k_B T}{N} \sum_{\boldsymbol{q}} \frac{e^{i\boldsymbol{q}\cdot\boldsymbol{R}}}{\chi_0^{\perp -1} + \left(v_0^{\perp} - v_{\boldsymbol{q}}\right)}. \tag{B.1}$$

where $v_{\boldsymbol{q}}$ is the $\boldsymbol{q}$ component of the Fourier transform of the dipole interaction and $v_0^{\perp}$ is the $\boldsymbol{q} = 0$ component of $v_{\boldsymbol{q}}$ in the transverse direction ($\boldsymbol{q} \perp \hat{\boldsymbol{z}}$).

We are interested in the correlations at large distances ($|\boldsymbol{R}| \to \infty$). For large distances, the most significant contributions are from the long-wavelength limit ($|\boldsymbol{q}| \to 0$) for which $v_{\boldsymbol{q}}$ takes the form,

$$\lim_{\boldsymbol{q}\to 0} \frac{v_{\boldsymbol{q}}}{nz^{*2}} = \frac{4\pi}{3}\left(1 - 3\frac{q_z^2}{|\boldsymbol{q}|^2}\right) - \eta|\boldsymbol{q}a|^2 + 3\eta(q_z a)^2 \tag{B.2}$$

where n is the number of lattice points per unit volume and η is a dimensionless coefficient that depends on the structure of the lattice ($\eta \simeq 0.084$ for FCC lattices).

We calculate the correlations in the continuum limit: $(1/N)\sum_{\boldsymbol{q}} \to (1/v_{BZ})\int d^3\boldsymbol{q}$, where v_{BZ} is the volume of the Brillouin zone of the FCC or BCC lattice.

In the continuum and long-wavelength limits, Eq. (B.1) takes the form,

$$\langle u_{\boldsymbol{0}} u_{\boldsymbol{R}}\rangle_{th} = \frac{4\pi}{3}\frac{k_B T}{v_0^{\perp}} I(\boldsymbol{R}) \tag{B.3}$$

where,

$$I(\boldsymbol{R}) = \frac{1}{v_{BZ}}\int d^3\boldsymbol{q} \frac{e^{i\boldsymbol{q}\cdot\boldsymbol{R}}}{(\bar{\chi}_0^{\perp})^{-1} + 4\pi q_z^2/|\boldsymbol{q}|^2 + \eta|\boldsymbol{q}a|^2 - 3\eta(q_z a)^2}, \tag{B.4}$$

and $(\bar{\chi}_0^{\perp})^{-1} \equiv (4\pi/3)(\chi_0^{\perp})^{-1}/v_0^{\perp}$ is a dimensionless susceptibility.

Our goal is to calculate $I(\boldsymbol{R})$ of Eq. (B.4).

Before we proceed with the details of the calculation, we point out that the correlation functions of polarization for an uniaxial dipolar system were computed in Ref. [49]. However, the calculation of Ref. [49] presents some problems: (i) it assumes that the simple cubic lattice has a ferroelectric ground state, i.e., it assumes $(\chi_q^{\perp})^{-1} \to 0$ at the zone center ($\boldsymbol{q} = 0$). This is incorrect since Luttinger and Tisza [91] showed that the ground state of an infinite simple cubic lattice of dipoles has an antiferroelectric ground state, i.e, $(\chi_q^{\perp})^{-1} \to 0$ at the zone boundary ($\boldsymbol{q} > 0$); (ii) it ignores the $3\eta(q_z a)^2$ term in the denominator of (B.4) without justification. Here, we calculate the correlation functions of

polarization for a FCC and a BCC lattice, which have ferroelectric ground states [91] and keep the $3\eta(q_z a)^2$ term in the denominator of (B.4). The methods used in Ref. [49] to calculate the correlation functions of polarization still hold in our case and will be followed here.

Longitudinal Correlations ($\boldsymbol{R} \parallel \hat{\boldsymbol{z}}$).

Let us consider the integral,

$$I_z = \frac{1}{v_{BZ}} \int\int\int dq_x\, dq_y\, dq_z \frac{e^{i|\boldsymbol{R}|q_z}}{(\bar{\chi}_0^{\perp})^{-1} + 4\pi(q_z^2/|\boldsymbol{q}|^2) + \eta|\boldsymbol{q}a|^2 - \alpha(q_z a)^2}, \tag{B.5}$$

where $|\boldsymbol{R}| \to \infty$, $|\boldsymbol{q}|^2 = q_x^2 + q_y^2 + q_z^2$, $\alpha \equiv 3\eta$, and the integration is over all space. By transforming I_z to cylindrical coordinates $\rho,\ q_z,\ \theta$ we obtain,

$$I_z = \frac{2\pi}{v_{BZ}} \int d\rho\rho \int dq_z \frac{e^{i|\boldsymbol{R}|q_z}(\rho^2 + q_z^2)}{(\bar{\chi}_0^{\perp})^{-1}(\rho^2 + q_z^2) + 4\pi q_z^2 + \eta a^2(\rho^2 + q_z^2) - \alpha a^2(\rho^2 + q_z^2)q_z^2}. \tag{B.6}$$

We first integrate over q_z. We replace the integral over q_z by an integral taken for complex q_z from $-\infty$ to ∞ along the real axis and a semicircle at infinity in the positive half-plane. The poles of the integrand in Eq. (B.6) are the following,

$$q_z^2 = \frac{1}{2}\frac{\alpha - 2\eta}{\alpha - \eta}\rho^2 + \frac{1}{2}\frac{c}{\alpha - \eta}\left(1 \pm \sqrt{1 + \frac{2\alpha c - 16\pi a^2(\alpha - \eta)}{c^2}\rho^2 + \frac{(\alpha a)^2}{c^2}\rho^4}\right), \tag{B.7}$$

where $c = 4\pi + (\bar{\chi}_0^{\perp})^{-1}$.

The dominant contributions to I_z as $|\boldsymbol{R}| \to \infty$ are those in the long-wavelength limit $q_z \to 0$. They correspond to solutions to (B.7) for which $q_z \to 0$. Eq. (B.7) has solutions as $q_z \to 0$ only for the upper sign and for $\rho \to 0$. By expanding (B.7) for $\rho \ll 1$, we obtain,

$$q_z = i\sqrt{\frac{(\bar{\chi}_0^{\perp})^{-1}\rho^2}{c} + \frac{16\pi\eta a^2 + \pi\alpha a^2 \bar{\chi}_0^{-1}}{c^3}\rho^4} \tag{B.8}$$

We now calculate the integral in (B.6) using the theorem of residues,

$$I_z = \frac{2\pi}{v_{BZ}} \frac{(2\pi)(4\pi)}{2c^2} \int_0^\infty d\rho\, \rho^2 \frac{e^{-|\boldsymbol{R}|\rho\sqrt{p}}}{\sqrt{p}}, \tag{B.9}$$

where,

$$p = \frac{(\bar{\chi}_0^\perp)^{-1}}{c} + \frac{16\pi\eta a^2 + \pi\alpha a^2 (\bar{\chi}_0^\perp)^{-1}}{c^3}\rho^2. \tag{B.10}$$

Here, we neglected terms $\rho^4 e^{-|\boldsymbol{R}|\rho p^{1/2}}$ in the numerator ((B.9) is dominated by contributions as $\rho \to 0$).

For $(\bar{\chi}_0^\perp)^{-1} \neq 0$, (B.9) gives to lowest order,

$$\begin{aligned} I_z &= \frac{8\pi^3}{v_{BZ}} \times \frac{1}{c^{3/2}} \int_0^\infty d\rho \rho^2 \sqrt{\bar{\chi}_0^\perp} \exp\left(-\frac{|\boldsymbol{R}|\rho}{\sqrt{c\,\bar{\chi}_0^\perp}}\right) \\ &= \frac{8\pi^3}{v_{BZ}} \times \frac{2(\bar{\chi}_0^\perp)^2}{|\boldsymbol{R}|^3} \\ &= \frac{16\pi^3}{v_{BZ}} \times \frac{(\bar{\chi}_0^\perp)^2}{|\boldsymbol{R}|^3}, \quad ((\bar{\chi}_0^\perp)^{-1} \neq 0, |\boldsymbol{R}| \to \infty) \end{aligned} \tag{B.11}$$

For $(\bar{\chi}_0^\perp)^{-1} = 0$ ($T = T_c$), (B.9) gives the following result,

$$\begin{aligned} I_z &= \frac{1}{v_{BZ}} \times \frac{\pi^{3/2}}{(\eta a^2)^{1/2}} \int_0^\infty d\rho\, \rho \exp\left[-|\boldsymbol{R}|\rho^2 (\eta a^2/4\pi)^{1/2}\right] \\ &= \frac{1}{v_{BZ}} \times \frac{\pi^2}{\eta a^2 |\boldsymbol{R}|} \\ &= \frac{\pi^2}{v_{BZ}\eta a^2} \frac{1}{|\boldsymbol{R}|}, \quad ((\bar{\chi}_0^\perp)^{-1} = 0, \quad |\boldsymbol{R}| \to \infty). \end{aligned} \tag{B.12}$$

Substitution of Eq. (B.11) into (B.3) gives the longitudinal component of the correlation function without compositional disorder for $T \gtrsim T_c$,

$$\langle u_{\boldsymbol{0}} u_{\boldsymbol{R}} \rangle_{th} = \frac{4\pi}{3} \frac{k_B T}{v_0^\perp} \times \frac{16\pi^3}{v_{BZ}} \times \frac{(\bar{\chi}_0^\perp)^2}{|\boldsymbol{R}|^3}, \quad |\boldsymbol{R}| \to \infty, \ \boldsymbol{R} \parallel \hat{\boldsymbol{z}}. \tag{B.13}$$

Substitution of Eq. (B.12) into (B.3) gives the longitudinal component of the correlation function without compositional disorder for $T = T_c$,

$$\langle u_{\boldsymbol{0}} u_{\boldsymbol{R}} \rangle_{th} = \frac{4\pi}{3} \frac{k_B T}{v_0^\perp} \times \frac{\pi^2}{v_{BZ}\eta a^2} \frac{1}{|\boldsymbol{R}|}, \quad |\boldsymbol{R}| \to \infty, \ \boldsymbol{R} \parallel \hat{\boldsymbol{z}}. \tag{B.14}$$

We now compute the correlations in the transverse direction.

Transverse Correlations ($\boldsymbol{R} \perp \hat{\boldsymbol{z}}$).

Let us now consider the integral,

$$I_x = \frac{1}{v_{BZ}} \int\int\int dq_x\, dq_y\, dq_z \frac{e^{i|\boldsymbol{R}|q_x}}{(\bar{\chi}_0^{\perp})^{-1} + 4\pi q_z^2/|\boldsymbol{q}|^2 + \eta|\boldsymbol{q}a|^2 - \alpha(q_z a)^2}, \tag{B.15}$$

where $|\boldsymbol{q}|^2 = q_x^2 + q_y^2 + q_z^2$, $\boldsymbol{R} \to \infty$ and the integral is taken over all space. We first compute the integral over q_x by replacing it by an integral over the complex plane q_x from $-\infty$ to ∞ along the real axis and around the semicircle at infinity in the positive half-plane. The poles are the following,

$$q_x^2 = -\left[q_y^2 - \left(\frac{\alpha}{2\eta} - 1\right) q_z^2 + \frac{(\bar{\chi}_0^{\perp})^{-1}}{2\eta a^2}\right] \pm \sqrt{\left(\frac{(\bar{\chi}_0^{\perp})^{-1} - \alpha a^2 q_z^2}{2\eta a^2}\right)^2 + \left(\frac{4\pi^2}{\eta a^2}\right)^2}. \tag{B.16}$$

For $|\boldsymbol{R}| \to \infty$, the most dominant contribution to (B.15) is from $q_x \to 0$. Eq. (B.16) has $q_x \to 0$ solutions for $\chi_0^{-1} \neq 0$ only from the upper sign and for $q_y \to 0,\ q_z \to 0$,

$$q_x^2 = -q_y^2 - q_z^2 - \frac{4\pi}{(\bar{\chi}_0^{\perp})^{-1}} q_z^2 + \mathcal{O}(q_z^4). \tag{B.17}$$

We make the observation that the lower sign can also take arbitrarily small values as $x \sim i(\bar{\chi}_0^{\perp})^{-1/2}$ for which the correlations would go as $\exp\left[-(|\boldsymbol{R}|/a)(\bar{\chi}_0^{\perp})^{-1/2}\right]$. These correlations are small compared to those from (B.17), which will be shown to go as $1/|\boldsymbol{R}|^3$) for finite $(\bar{\chi}_0^{\perp})^{-1}$ as $|\boldsymbol{R}| \to \infty$. The exponential correlations may become the dominant for $(\bar{\chi}_0^{\perp})^{-1} \to 0$, $T \to T_c^+$.

For $(\bar{\chi}_0^{\perp})^{-1} > 0$, we obtain for I_x the following result,

$$I_x = -\frac{4\pi^2(\bar{\chi}_0^{\perp})^2}{v_{BZ}} \int_{-\infty}^{\infty}\int_{-\infty}^{\infty} dq_y\, dq_z \frac{q_z^2 \exp\left[-|\boldsymbol{R}|\sqrt{q_x^2 + g q_z^2}\right]}{\sqrt{q_x^2 + g q_z^2}} \tag{B.18}$$

where $g = 1 + 4\pi\bar{\chi}_0^{\perp}$. We now integrate by using polar coordinates $\rho^2 = q_y^2 + g q_z^2$, $\tan\theta =$

$\sqrt{g}q_z/q_y$. The result is as follows,

$$\begin{aligned} I_x &= -\frac{4\pi^2(\bar{\chi}_0^{\perp})^2}{v_{BZ}}\frac{1}{g^{3/2}}\int_0^{2\pi} d\theta \sin^2\theta \int_0^{\infty} d\rho\rho^2 \exp\left[-|\boldsymbol{R}|\rho\right] \\ &= -\frac{4\pi^2(\bar{\chi}_0^{\perp})^2}{v_{BZ}}\frac{1}{g^{3/2}} \times \pi \times \frac{2}{|\boldsymbol{R}|^3} \\ &= -\frac{8\pi^3}{v_{BZ}}\frac{(\bar{\chi}_0^{\perp})^2}{g^{3/2}}\frac{1}{|\boldsymbol{R}|^3}. \end{aligned} \tag{B.19}$$

For $4\pi\bar{\chi}_0^{\perp} \gg 1$, we obtain,

$$I_x \simeq -\frac{\pi^{3/2}}{v_{BZ}}\frac{\left(\bar{\chi}_0^{\perp}\right)^{1/2}}{R^3}, \quad ((\bar{\chi}_0^{\perp})^{-1} \neq 0, |\boldsymbol{R}| \to \infty) \tag{B.20}$$

Substitution of Eq. (B.20) into (B.3) gives the transverse component of the correlation functions without compositional disorder for $T \gtrsim T_c$,

$$\langle u_{\boldsymbol{0}} u_{\boldsymbol{R}} \rangle_{th} = -\frac{4\pi}{3}\frac{k_B T}{v_0^{\perp}} \times \frac{\pi^{3/2}}{v_{BZ}}\frac{\left(\bar{\chi}_0^{\perp}\right)^{1/2}}{|\boldsymbol{R}|^3}, \quad |\boldsymbol{R}| \to \infty, \ \boldsymbol{R} \perp \hat{\boldsymbol{z}}. \tag{B.21}$$

The calculation of the correlation functions without compositional disorder concludes here.

B.0.2 Correlations with random fields

In the presence of compositional disorder and low temperatures, the correlation functions of polarization between a unit cells at the origin $\boldsymbol{0}$ and at a position $\boldsymbol{R}$, are given as follows,

$$\langle \langle u_{\boldsymbol{0}} u_{\boldsymbol{R}} \rangle_{th} \rangle_c = \frac{\Delta^2}{N}\sum_{\boldsymbol{q}} \frac{e^{i\boldsymbol{q}\cdot\boldsymbol{R}}}{\left[\left(\chi_0^{\perp}\right)^{-1} + \left(v_0^{\perp} - v_{\boldsymbol{q}}\right)\right]^2}. \tag{B.22}$$

where $v_{\boldsymbol{q}}$ is the $\boldsymbol{q}$ component of the Fourier transform of the dipole interaction and $v_0^{\perp}$ is the $\boldsymbol{q} = 0$ component of $v_{\boldsymbol{q}}$ in the transverse direction ($\boldsymbol{q} \perp \hat{\boldsymbol{z}}$).

We are interested in the correlations at large distances ($|\boldsymbol{R}| \to \infty$). For large distances, the most significant contributions are from the long-wavelength limit ($|\boldsymbol{q}| \to 0$)

for which $v_{\boldsymbol{q}}$ takes the form,

$$\lim_{\boldsymbol{q}\to 0}\frac{v_{\boldsymbol{q}}}{nz^{*2}}=\frac{4\pi}{3}\left(1-3\frac{q_z^2}{|\boldsymbol{q}|^2}\right)-\eta|\boldsymbol{q}a|^2+3\eta(q_za)^2 \tag{B.23}$$

where n is the number of lattice points per unit volume and η is a dimensionless coefficient that depends on the structure of the lattice ($\eta\simeq 0.084$ for FCC lattices).

We now take the continuum limit $(1/N)\sum_{\boldsymbol{q}}\to(1/v_{BZ})\int d^3\boldsymbol{q}$, where v_{BZ} is the volume of the Brillouin zone of the FCC or BCC lattice.

In the continuum and long-wavelength limits, Eq. (B.22) takes the form,

$$\langle\langle u_{\boldsymbol{0}}u_{\boldsymbol{R}}\rangle_{th}\rangle_c=\left(\frac{4\pi}{3}\right)^2\frac{\Delta^2}{\left(v_0^\perp\right)^2}\times\frac{1}{v_{BZ}}\int d^3\boldsymbol{q}\frac{e^{i\boldsymbol{q}\cdot\boldsymbol{R}}}{\left[(\bar{\chi}_0^\perp)^{-1}+4\pi q_z^2/|\boldsymbol{q}|^2+\eta|\boldsymbol{q}a|^2-\alpha(q_za)^2\right]^2}, \tag{B.24}$$

where $\alpha\equiv 3\eta$. The calculation of the correlation functions with compositional disorder is straightforward if one notices that,

$$-\frac{\partial I(\boldsymbol{R})}{\partial(\bar{\chi}_0^\perp)^{-1}}=\frac{1}{v_{BZ}}\int d^3\boldsymbol{q}\frac{e^{i\boldsymbol{q}\cdot\boldsymbol{R}}}{\left[(\bar{\chi}_0^\perp)^{-1}+4\pi q_z^2/|\boldsymbol{q}|^2+\eta|\boldsymbol{q}a|^2-\alpha(q_za)^2\right]^2} \tag{B.25}$$

where $I(\boldsymbol{R})$ is given in Eq. (B.4). Therefore,

$$\langle\langle u_{\boldsymbol{0}}u_{\boldsymbol{R}}\rangle_{th}\rangle_c=-\left(\frac{4\pi}{3}\right)^2\frac{\Delta^2}{\left(v_0^\perp\right)^2}\times\frac{\partial I(\boldsymbol{R})}{\partial(\bar{\chi}_0^\perp)^{-1}}. \tag{B.26}$$

Direct substitution of Eqs. (B.11) and (B.20) into (B.26) gives for the longitudinal and transverse components of the correlation functions with compositional disorder,

$$\langle\langle u_{\boldsymbol{0}}u_{\boldsymbol{R}}\rangle_{th}\rangle_c=\begin{cases}\left(\frac{4\pi}{3}\right)^2\frac{\Delta^2}{\left(v_0^\perp\right)^2}\times\frac{32\pi^3}{v_{BZ}}\frac{(\bar{\chi}_0^\perp)^3}{|\boldsymbol{R}|^3}, & |\boldsymbol{R}|\to\infty,\ \boldsymbol{R}\parallel\hat{\boldsymbol{z}},\\ -\left(\frac{4\pi}{3}\right)^2\frac{\Delta^2}{\left(v_0^\perp\right)^2}\times\frac{1}{2}\frac{\pi^{3/2}}{v_{BZ}}\frac{(\bar{\chi}_0^\perp)^{3/2}}{|\boldsymbol{R}|^3}, & |\boldsymbol{R}|\to\infty,\ \boldsymbol{R}\perp\hat{\boldsymbol{z}}.\end{cases} \tag{B.27}$$

The calculation of the correlation functions of polarization with compositional disorder concludes here.

Appendix C

Derivation of Clausius-Mossotti and Onsager Formulas

The purpose of this appendix is to derive the Clausius-Mossotti and Onsager formulas using, respectively, the Lorentz and Onsager approximations, The derivations presented here are not new (see Ref. [75, 76]) but they are given here for the sake of completeness.

C.1 Clausius-Mossotti Formula

Consider a system of permanent dipoles $\boldsymbol{p}_i = p\boldsymbol{u}_i$. p is the magnitude of the dipole and $\boldsymbol{u}_i$ is the direction of the dipole at site i. $\boldsymbol{u}_i$ is a vector of magnitude one, $|\boldsymbol{u}_i| = 1$.

The Hamiltonian is as follows,

$$\begin{aligned} H &= -\frac{1}{2}\sum_{i,j} \boldsymbol{u}_i \cdot \boldsymbol{v}_{ij} \cdot \boldsymbol{u}_j - \sum_i \boldsymbol{u}_i \cdot \boldsymbol{E}_i^{ext} \\ &= -\frac{1}{2}\sum_{i,j}\sum_{\alpha,\alpha'} u_i^{\alpha} v_{ij}^{\alpha\alpha'} u_j^{\alpha'} - \sum_i \sum_{\alpha} u_i^{\alpha} E_i^{ext\ \alpha}. \end{aligned} \tag{C.1}$$

where the sum over i, j is over all dipole sites and the sum over α, α' is over the x, y, z components of the vector $\boldsymbol{u}_i$.

Here, $v_{ij}^{\alpha\alpha'}$ is the dipolar tensor,

$$v_{ij}^{\alpha\alpha'} = \begin{cases} \frac{p^2}{|\boldsymbol{r}_{ij}|^5}\left[3r_{ij}^{\alpha}r_{ij}^{\alpha'} - |\boldsymbol{r}_{ij}|^2\delta_{\alpha\alpha'}\right], & \boldsymbol{r}_{ij} \neq 0, \\ 0, & \boldsymbol{r}_{ij} = 0, \end{cases} \tag{C.2}$$

where $\boldsymbol{r}_{ij} = \boldsymbol{r}_i - \boldsymbol{r}_j$ is the distance between sites i, j; r_{ij}^{α} are the $\alpha = x, y, z$ components of $\boldsymbol{r}_{ij}$.

In the Lorentz approximation, the local field of the Hamiltonian (C.1) is replaced by the Lorentz field (see Sec. 2.2). The Hamiltonian (C.1) then becomes,

$$H = -\sum_i \boldsymbol{u}_i \cdot \boldsymbol{E}_i^{Lorentz} \tag{C.3}$$

where $\boldsymbol{E}_i^{Lorentz}$ is the Lorentz field at site i,

$$\boldsymbol{E}_i^{Lorentz} = \sum_j \boldsymbol{v}_{ij} \cdot \langle \boldsymbol{u}_i \rangle_{th} + \boldsymbol{E}_i^{ext}, \tag{C.4}$$

The thermal average of $\boldsymbol{u}_i$ is given as follows,

$$\langle \boldsymbol{u}_i \rangle_{th} = \frac{\mathrm{Tr}_{\boldsymbol{u}_i}\, e^{-\beta \boldsymbol{u}_i \cdot \boldsymbol{E}_i^{Lorentz}} \boldsymbol{u}_i}{\mathrm{Tr}_{\boldsymbol{u}_i}\, e^{-\beta \boldsymbol{u}_i \cdot \boldsymbol{E}_i^{Lorentz}}} \tag{C.5}$$

where $\boldsymbol{E}_i^{Lorentz}$ is given in Eq. (C.4).

From (C.5) we compute the susceptibility $\chi_{ij}^{\alpha\alpha'}$,

$$\chi_{ij}^{\alpha\alpha'} = n\frac{\partial \langle u_i^{\alpha} \rangle_{th}}{\partial E_i^{ext\,\alpha'}}\bigg|_{\boldsymbol{E}_i^{ext}=0} = n\beta p^2 \left(\delta_{ij}\,\delta_{\alpha\alpha'} + \sum_k \sum_{\alpha''} v_{ik}^{\alpha\alpha''}\chi_{kj}^{\alpha''\alpha'}\right) \tag{C.6}$$

where $\delta_{ij},\ \delta_{\alpha\alpha'}$ are Kronecker deltas. Here, we have assumed there is no long-range order, $\langle u_i \rangle_{th} = 0$ for $\boldsymbol{E}_i^{ext} = 0$.

We now Fourier transform (C.6),

$$\chi_{\boldsymbol{q}}^{\alpha\alpha'} = \beta n p^2 \left(\delta_{\alpha\alpha'} + \sum_{\alpha''} v_{\boldsymbol{q}}^{\alpha\alpha''}\chi_{\boldsymbol{q}}^{\alpha''\alpha'}\right) \tag{C.7}$$

where

$$\chi_{\boldsymbol{q}}^{\alpha\alpha'} = \sum_{ij} \chi_{ij}^{\alpha\alpha'} e^{\boldsymbol{q}\cdot\boldsymbol{r}_{ij}}, \quad v_{\boldsymbol{q}}^{\alpha\alpha'} = \sum_{ij} v_{ij}^{\alpha\alpha'} e^{\boldsymbol{q}\cdot\boldsymbol{r}_{ij}},$$

We solve Eq (C.7) by going into diagonal representation,

$$\bar{\chi}_{\boldsymbol{q}}^{\alpha} = \frac{\beta n p^2}{3 - \beta \bar{v}_{\boldsymbol{q}}^{\alpha}} \tag{C.8}$$

where $\bar{\chi}_{\boldsymbol{q}}^{\alpha}, \bar{v}_{\boldsymbol{q}}^{\alpha}$ are the eigenvalues of the susceptibility and dipolar tensors, respectively.

$\bar{\chi}_{\boldsymbol{0}}^{\alpha}$ of Eq. (C.8) depends on the shape of the sample since $v_{\boldsymbol{q}}^{\alpha}$ is non-analytic for $\boldsymbol{q} \to 0$. To avoid the shape dependence, χ_0^{α} is defined as the response to the macroscopic field, which differs from the external field by the depolarizing field,

$$\tilde{\chi}_0^{\alpha} = \frac{\beta n p^2}{3 - \beta \tilde{\omega}_0^{\alpha}}. \tag{C.9}$$

Here, $\tilde{\omega}_0^{\alpha}$ are the eigenvalues of the shape-independent tensor, $\boldsymbol{\omega}_0 = \boldsymbol{v}_0 + \boldsymbol{D}$, where $\boldsymbol{D}$ is the depolarizing tensor,

$$D^{\alpha\alpha'} = \lim_{\boldsymbol{q}\to 0} 4\pi n p^2 \frac{q_\alpha q_{\alpha'}}{|\boldsymbol{q}|^2}.$$

Defined this way, $\tilde{\chi}_0^{\alpha}$ is independent of the shape of the sample.

Eq. (C.9) is the Lorentz equation which determined the temperature dependence of the χ_0^{α}.

To get the Clausius-Mossotti formula, we make the approximation that $v_{\boldsymbol{q}}^{\alpha}$ is constant throughout the Brillouin zone,

$$\begin{aligned} v_{\boldsymbol{q}}^1 = v_{\boldsymbol{q}}^2 = \frac{4\pi}{3} n p^2, \quad &\text{(eigenvector perpendicular to } \boldsymbol{q}) \\ v_{\boldsymbol{q}}^3 = -\frac{8\pi}{3} n p^2, \quad &\text{(eigenvector parallel to } \boldsymbol{q}). \end{aligned} \tag{C.10}$$

Here, the constants are such that the eigenvalues agree with the simple cubic values for $|\boldsymbol{q}| \ll 1$. The eigenvalues of $\boldsymbol{\omega}$ are,

$$w_0^1 = w_0^2 = w_0^3 = \frac{4\pi}{3} n p^2 \tag{C.11}$$

Substitution of Eqs. (C.10), (C.11) into Eq. (C.9) gives the Lorentz formula for the dielectric constant $\epsilon = 1 + 4\pi\tilde{\chi}_0$,

$$\frac{\epsilon - 1}{\epsilon + 2} = \frac{4\pi}{3}\frac{np^2}{3k_BT}. \tag{C.12}$$

This concludes our derivation of the Clausius-Mossotti formula.

C.2 Onsager Formula

In the Onsager approximation, the local field of the Hamiltonian (C.1) is replaced by the Onsager field (see Sec. 2.2). The Hamiltonian (C.1) then becomes,

$$H = -\sum_i \boldsymbol{u}_i \cdot \boldsymbol{E}_i^{cavity} \tag{C.13}$$

where $\boldsymbol{E}_i^{cavity}$ is the cavity field,

$$\boldsymbol{E}_i^{cavity} = \boldsymbol{E}_i^{Lorentz} - \left\langle \boldsymbol{E}_i^{reaction} \right\rangle_{th}, \tag{C.14}$$

$\boldsymbol{E}_i^{Lorentz}$ is the Lorentz field at site i,

$$\boldsymbol{E}_i^{Lorentz} = \sum_j \boldsymbol{v}_{ij} \cdot \langle \boldsymbol{u}_i \rangle_{th} + \boldsymbol{E}_i^{ext}, \tag{C.15}$$

and $\left\langle \boldsymbol{E}_i^{reaction} \right\rangle_{th}$ is thermal average of the reaction field $\boldsymbol{E}_i^{reaction}$ at site i,

$$\boldsymbol{E}_i^{reaction} = \lambda \boldsymbol{u}_i. \tag{C.16}$$

The coefficient of proportionality λ is temperature dependent. In writing Eq. (C.13), we ignored the constant term $-(\lambda/2)p^2$.

The thermal average of $\boldsymbol{u}_i$ is given as follows,

$$\langle \boldsymbol{u}_i \rangle_{th} = \frac{\mathrm{Tr}_{\boldsymbol{u}_i}\, e^{-\beta \boldsymbol{u}_i \cdot \boldsymbol{E}_i^{cavity}} \boldsymbol{u}_i}{\mathrm{Tr}_{\boldsymbol{u}_i}\, e^{-\beta \boldsymbol{u}_i \cdot \boldsymbol{E}_i^{cavity}}} \tag{C.17}$$

where $\boldsymbol{E}_i^{cavity}$ is given in Eq. (C.14).

We now compute the susceptibility from (C.17). The derivation follows that of the the Clausius-Mossotti formula (see Sec. C.1), except that one carries the parameter λ. The result is the following,

$$\bar{\chi}^{\alpha}_{\boldsymbol{q}} = \frac{\beta n p^2}{3 - \beta\left[\bar{v}^{\alpha}_{\boldsymbol{q}} - \lambda\right]} \tag{C.18}$$

where $\bar{\chi}^{\alpha}_{\boldsymbol{q}}, \bar{v}^{\alpha}_{\boldsymbol{q}}$ are the eigenvalues of the susceptibility and dipolar tensors, respectively.

We now determine the parameter λ. λ is determined by the fluctuation dissipation theorem in the paraelectric phase,

$$\left\langle p^{\alpha}_i p^{\alpha'}_j \right\rangle = p^2 \left\langle u^{\alpha}_i u^{\alpha'}_j \right\rangle = \frac{1}{nN} \sum_{\boldsymbol{q}} \beta^{-1}\, \chi^{\alpha\alpha'}_{\boldsymbol{q}}\, e^{i\boldsymbol{q}\cdot\boldsymbol{r}_{ij}} \tag{C.19}$$

where the summation over $\boldsymbol{q}$ is over the first Brillouin zone. We now set $\alpha = \alpha'$ and $i = j$ in (C.19) and sum over α,

$$1 = \frac{1}{N} \sum_{\boldsymbol{q}} \sum_{\alpha} \frac{1}{3 - \beta\left[\bar{v}^{\alpha}_{\boldsymbol{q}} - \lambda\right]}. \tag{C.20}$$

Here, we used the definition $|\boldsymbol{u}_i|^2 = \sum_{\alpha} (u^{\alpha}_i)^2 = 1$ and the property that the trace is invariant under a change of representation.

$\bar{\chi}^{\alpha}_{\boldsymbol{0}}$ of Eq. (C.18) depends on the shape of the sample since $v^{\alpha}_{\boldsymbol{q}}$ is non-analytic for $\boldsymbol{q} \to 0$. To avoid the shape dependence, χ^{α}_0 is defined as the response to the macroscopic field, which differs from the external field by the depolarizing field,

$$\tilde{\chi}^{\alpha}_0 = \frac{\beta n p^2}{3 - \beta(\tilde{\omega}^{\alpha}_0 - \lambda)}. \tag{C.21}$$

Here, $\tilde{\omega}^{\alpha}_0$ are the eigenvalues of the shape-independent tensor, $\boldsymbol{\omega}_0 = \boldsymbol{v}_0 + \boldsymbol{D}$, where $\boldsymbol{D}$ is the depolarizing tensor,

$$D^{\alpha\alpha'} = \lim_{\boldsymbol{q}\to 0} 4\pi n p^2 \frac{q_{\alpha} q_{\alpha'}}{|\boldsymbol{q}|^2}$$

Defined this way, $\tilde{\chi}^{\alpha}_0$ is independent of the shape of the sample.

Eqs. (C.20), (C.21) are the Onsager equations. The temperature dependence of λ is determined from Eq. (C.20). The temperature dependence of the χ_0^α follows from Eq. (C.21).

To get the Onsager formula, we make the approximation that $v_{\boldsymbol{q}}^\alpha$ is constant throughout the Brillouin zone,

$$\begin{aligned} v_{\boldsymbol{q}}^1 = v_{\boldsymbol{q}}^2 &= \frac{4\pi}{3} np^2, \quad \text{(eigenvector perpendicular to } \boldsymbol{q}) \\ v_{\boldsymbol{q}}^3 &= -\frac{8\pi}{3} np^2, \quad \text{(eigenvector parallel to } \boldsymbol{q}). \end{aligned} \tag{C.22}$$

Here, the constants are such that the eigenvalues agree with the simple cubic values for $|\boldsymbol{q}| \ll 1$. The eigenvalues of $\boldsymbol{\omega}$ are,

$$w_0^1 = w_0^2 = w_0^3 = \frac{4\pi}{3} np^2 \tag{C.23}$$

Substitution of Eqs. (C.22), (C.23) into Eqs. (C.20), (C.21) and elimination of λ gives the Onsager formula for the dielectric constant $\epsilon = 1 + 4\pi\tilde{\chi}_0$,

$$\epsilon - 1 = \frac{\epsilon}{2\epsilon + 1} \frac{4\pi np^2}{k_B T}. \tag{C.24}$$

This concludes our derivation of the Onsager formula.